

# The role of a peroxisomal NAD<sup>+</sup> carrier in plants



Inaugural-Dissertation

zur Erlangung des Doktorgrades  
der Mathematisch-Naturwissenschaftlichen Fakultät  
der Heinrich-Heine Universität Düsseldorf

vorgelegt von

**Kristin Bernhardt**

aus Düsseldorf

Düsseldorf, September 2012

aus dem Institut für Biochemie der Pflanzen  
der Heinrich-Heine Universität Düsseldorf

Gedruckt mit der Genehmigung der  
Mathematisch-Naturwissenschaftlichen Fakultät der  
Heinrich-Heine Universität Düsseldorf

Referent: Prof. Dr. Andreas Weber  
Korreferent: Prof. Dr. Rüdiger Simon

Tag der mündlichen Prüfung: 17. Oktober 2012

*Gib jedem Tag die Chance, der schönste deines Lebens zu werden.*

Mark Twain



---

## Table of contents

<b>1</b>	<b>Introduction .....</b>	<b>1</b>
1.1	Importance of peroxisomes.....	1
1.1.1	Discovery and characteristics of peroxisomes.....	1
1.1.2	Peroxisomal functions.....	1
1.1.3	Peroxisome biogenesis.....	2
1.2	Peroxisomal protein import .....	2
1.2.1	Import of peroxisomal matrix proteins.....	2
1.2.2	Import of peroxisomal membrane proteins .....	3
1.3	Peroxisomal metabolism in plants .....	4
1.3.1	Fatty acid degradation via peroxisomal $\beta$ -oxidation.....	5
1.3.2	Photorespiration.....	6
1.3.3	Hydrogen peroxide detoxification .....	7
1.4	NAD <sup>+</sup> biosynthesis and degradation .....	8
1.5	Supplying peroxisomes with cofactors.....	9
1.5.1	Permeability of the peroxisomal membrane for cofactors.....	9
1.5.2	Peroxisomal members of the mitochondrial carrier family .....	10
1.5.3	Peroxisomal NAD <sup>+</sup> and CoA carrier .....	11
1.6	Goals of this thesis.....	12
<b>2</b>	<b>Material and Methods .....</b>	<b>13</b>
2.1	Consumables and chemicals .....	13
2.2	General methods .....	13
2.2.1	Cloning.....	13
2.2.2	Protein biochemistry .....	14
2.2.3	<i>In silico</i> expression and co-expression analysis .....	15
2.3	Plant work .....	15
2.3.1	Plant lines .....	15
2.3.2	Plant growth conditions.....	16
2.3.3	Arabidopsis transformation .....	16
2.3.4	Arabidopsis mutant lines generating by crossing .....	17

---

2.3.5	Verifying of T-DNA insertion lines .....	17
2.3.6	Plant membrane isolation of etiolated seedlings .....	18
2.3.7	PXN-specific polyclonal antibody generation.....	18
2.3.8	Silencing of gene expression using artificial microRNA and small interfering RNA.....	19
2.3.9	Generation of PXN over-expression lines.....	20
2.3.10	PXN promoter GUS analysis .....	20
2.3.11	Transient expression of YFP fusions in tobacco.....	20
2.3.12	Fatty acid analysis .....	22
2.3.13	Staining of lipid bodies.....	22
2.3.14	Transmission electron microscope pictures.....	22
2.3.15	NAD <sup>+</sup> level measurement of Arabidopsis seedlings.....	22
2.4	Biochemistry of recombinant protein.....	22
2.4.1	Two-step protein expression using wheat germ extract .....	22
2.4.2	One-step protein expression using wheat germ extract .....	24
2.4.3	Protein expression in yeast.....	25
2.4.4	Site-directed mutagenesis of PXN S155 and PXN loop deletion.....	25
2.4.5	Reconstitution of recombinant protein into liposomes and transport activity measurements using radioactive labelled substrates .....	27
2.5	PEX19 interaction studies.....	27
2.6	Accession numbers.....	27
<b>3</b>	<b>Results .....</b>	<b>28</b>
3.1	Homology among At2g39970 and other members of the mitochondrial carrier family .....	28
3.2	Biochemistry of recombinant PXN protein .....	30
3.2.1	NAD <sup>+</sup> transport activity of recombinant PXN protein.....	30
3.2.2	Comparison of peroxisomal, chloroplastic, and mitochondrial NAD <sup>+</sup> carrier...	34
3.2.3	NAD <sup>+</sup> uptake activity of recombinant PNC1-His and PNC2 protein.....	36
3.3	PXN antibody generation .....	38
3.4	PXN expression and co-expression analysis.....	39
3.4.1	<i>In silico</i> PXN expression analysis .....	39

---

---

3.4.2	<i>In silico</i> co-expression analysis .....	40
3.4.3	PXN promoter-GUS analysis .....	41
3.5	<i>pxn</i> T-DNA insertion lines .....	42
3.5.1	Genotype of Arabidopsis <i>pxn</i> mutant lines .....	42
3.5.2	PXN protein level of <i>pxn</i> mutant lines .....	43
3.5.3	PXN complementation lines.....	44
3.6	The impact of PXN on $\beta$ -oxidation .....	45
3.6.1	Seedling establishment of <i>pxn</i> mutants .....	45
3.6.2	Sensitivity to the root growth inhibitor 2,4-DB of <i>pxn</i> seedlings .....	46
3.6.3	Impact of PXN on fatty acid degradation during seedling establishment.....	47
3.6.4	Germination efficiency of <i>pxn</i> seeds .....	48
3.7	Role of PXN during oxidative stress .....	50
3.7.1	Response to H <sub>2</sub> O <sub>2</sub> , 3-aminotriazole, and methylviologen.....	50
3.7.2	PXN Expression level in response to low pH.....	52
3.7.3	Response to <i>Pseudomonas syringae</i> .....	52
3.8	Redundant systems for supplementing peroxisomes with NAD <sup>+</sup> .....	53
3.8.1	NAD <sup>+</sup> level of <i>pxn</i> seedlings.....	53
3.8.2	PNC gene silencing using siRNAi approach in <i>pxn</i> mutants .....	54
3.8.3	Redox equivalent exchange by the malate/oxaloacetate shuttle .....	55
3.9	Function of the unique loop region of PXN .....	56
3.9.1	Impact of the loop region and phosphorylation site S155 on peroxisomal targeting .....	57
3.9.2	Impact of the loop region and phosphorylation site S155 on transport activity... .....	58
3.10	The role of PEX19 in peroxisomal membrane protein targeting .....	60
3.10.1	<i>In vitro</i> PEX19 pull-down assay .....	61
3.10.2	<i>In vivo</i> PEX19 mis-localization assay .....	62
3.10.3	<i>In silico</i> analysis of PEX19 binding sites.....	63
<b>4</b>	<b>Discussion.....</b>	<b>64</b>
4.1	PXN is the first characterized peroxisomal NAD <sup>+</sup> carrier of plants.....	64
4.1.1	PXN catalyzed <i>in vitro</i> the uptake of NAD <sup>+</sup> , NADH and CoA.....	64

---

---

4.1.2	Putative <i>in vivo</i> functions of PXN.....	66
4.1.3	Phosphorylation of S155 regulates PXN activity .....	68
4.2	<i>pxn</i> mutant plants are delayed in fatty acid degradation during seedling establishment.....	69
4.3	Putative role of PXN in jasmonic acid and auxin biosynthesis.....	71
4.4	PXN expression is altered during oxidative stress.....	72
4.5	Is PXN required for the photorespiratory C <sub>2</sub> cycle? .....	74
4.6	Redundant systems for PXN function .....	74
4.6.1	PNC1 and PNC2 are candidates for a redundant system for PXN.....	74
4.6.2	Malate/oxaloacetate shuttle redundancy to the PXN mediated NAD <sup>+</sup> /NADH transport.....	76
4.6.3	NAD <sup>+</sup> is imported by cofactor-bound enzymes .....	78
4.7	Peroxisomal members of the MCF are targeted to peroxisomes via PEX19.....	78
<b>5</b>	<b>Summary.....</b>	<b>80</b>
5.1	Summary.....	80
5.2	Zusammenfassung .....	82
<b>6</b>	<b>References.....</b>	<b>84</b>
<b>7</b>	<b>Appendix.....</b>	<b>103</b>
7.1	Supplemental figures and tables.....	103
7.2	Abbreviations .....	106
7.3	Companies, websites and used softwares.....	109
7.4	Figures .....	111
7.5	Tables .....	112
7.6	Vector and construct maps .....	114
7.6.1	Plasmids used for cloning.....	114
7.6.2	Plasmid used for gene silencing .....	115
7.6.3	Plasmid used for PXN over-expression .....	115
7.6.4	Plasmid used for PXN promoter GUS analysis .....	116
7.6.5	Plasmids used for co-localization .....	116
7.6.6	Plasmids used for <i>in vitro</i> two-step WGE expression .....	117
7.6.7	Plasmids used for <i>in vitro</i> one-step WGE expression.....	118

---



7.7	List of publications .....	119
7.8	Curriculum vitae .....	120
<b>8</b>	<b>Acknowledgement .....</b>	<b>121</b>

# 1 Introduction

## 1.1 Importance of peroxisomes

### 1.1.1 Discovery and characteristics of peroxisomes

Peroxisomes were first termed as “microbodies” by Rhodin in 1954 (Rhodin, 1954). 1966 De Duve and Baudhuin renamed these organelles “peroxisomes” because of their high content of hydrogen peroxide (H<sub>2</sub>O<sub>2</sub>) and the association with oxidases (De Duve and Baudhuin, 1966). Peroxisomes were the last discovered cell compartment in eukaryotes (Brown, 1866; Schimper, 1883; Ernster and Schatz, 1981). Organelles like peroxisomes, chloroplasts, mitochondria, nuclei, and endoplasmic reticulum (ER) are specialized compartments inside eukaryotic cells that consist of separate enzymes and metabolites for specific metabolic pathways (Bowsher and Tobin, 2001). Peroxisomes are small organelles with a size of 0.1 - 1 μM and are surrounded by a single lipid bilayer (Schrader and Fahimi, 2008). In contrast to plastids and mitochondria, peroxisomes are devoid of DNA and any translation machinery (Schrader and Fahimi, 2008).

### 1.1.2 Peroxisomal functions

Peroxisomes are highly dynamic organelles and harbour many different metabolic pathways. Common peroxisomal functions in mammals, plants, and fungi are fatty acid β-oxidation (section 1.3.1) and reactive oxygen species (ROS) detoxification (section 1.3.3; Gabaldon, 2010; Islinger *et al.*, 2012). Biotin biosynthesis takes place in peroxisomes of plants and fungi (Islinger *et al.*, 2012). Special functions of human peroxisomes are the fatty acid α-oxidation and biosynthesis of ether phospholipids (Wanders and Waterham, 2006). A defect in human peroxisomal function leads to serious illness or death, like the Zellweger syndrome and neonatal adrenoleukodystrophy (NALD; Wanders, 2004). Plant peroxisomal pathways are the glyoxylate cycle, photorespiration (section 1.3.2), the metabolism of branched amino acids and the biosynthesis of phytohormones like jasmonic acid (JA), auxin, and salicylic acid (SA; Hu *et al.*, 2012). Plant peroxisomes play a major role during germination, seedling establishment, senescence, photorespiration, oxidative stress, and pathogen defence (Hu *et al.*, 2012). Plants with impaired or blocked peroxisomal function are often embryo lethal or have a severe photorespiratory or β-oxidation phenotype (Somerville and Ogren, 1980; Hayashi *et al.*, 1998; Sparkes *et al.*, 2003; Fan *et al.*, 2005; Nito *et al.*, 2007).

### **1.1.3 Peroxisome biogenesis**

The current state of all eukaryotic organisms concerning peroxisome biogenesis is controversially discussed in two models (reviewed in (Platta and Erdmann, 2007b; Hu *et al.*, 2012). The first model is the “ER vesiculation model”. Pre-peroxisomal vesicles are derived from the ER and deliver phospholipids and some peroxisomal membrane proteins (PMPs) to produce new peroxisomes (Mullen and Trelease, 2006; Schluter *et al.*, 2006; Tabak *et al.*, 2008; Hu *et al.*, 2012). The second model is the “growth and division model” (Lazarow and Fujiki, 1985; Hu *et al.*, 2012). The existing peroxisomes elongate and undergo fission to result in an increased number of peroxisomes (Lazarow and Fujiki, 1985; Hu *et al.*, 2012). In mammals and yeast, a “ER semi-autonomous model” exists with both, peroxisomes derived from the ER and by division (Hu *et al.*, 2012). In plants, no direct evidence for *de novo* synthesis of peroxisomes via the ER exists, suggesting an “ER semi-autonomous peroxisome maturation and replication model” (Mullen and Trelease, 2006; Hu *et al.*, 2012). ER and peroxisomes share membrane components and a number of PMPs, which are originated from the ER and then fused with pre-existing peroxisomes derived from divided peroxisomes. However, no “new” plant peroxisomes are originated directly from the ER (Mullen and Trelease, 2006; Hu *et al.*, 2012).

## **1.2 Peroxisomal protein import**

Peroxisomal membrane and matrix proteins are nuclear encoded and post-translationally imported into peroxisomes (Brown and Baker, 2008). More than 30 so-called peroxin (PEX) proteins, a common class of conserved genes, are involved in peroxisomal protein import, membrane biogenesis and organelle proliferation (Platta and Erdmann, 2007b).

### **1.2.1 Import of peroxisomal matrix proteins**

The import machinery of peroxisomal matrix proteins is well studied and conserved in all eukaryotic organisms (Lanyon-Hogg *et al.*, 2010; Ma *et al.*, 2011). Peroxisomal matrix proteins carry a peroxisomal targeting signal (PTS; Sparkes and Baker, 2002). Two PTS motifs are known. PTS1, consisting of a three amino acid SKL-motif at the C-terminus of the protein, and PTS2, containing a nonapeptide (R[LI]x5HL) motif at the N-terminus of the protein (Reumann *et al.*, 2004). Cytosolic receptors for PTS1-carrying proteins, PEX5, and for PTS2-carrying proteins, PEX7, target the proteins to the peroxisomal membrane receptor complex PEX13/PEX14 (Sparkes and Baker, 2002). PEX5-PTS1 and PEX7-PTS2 are imported with their cargo, the cargo is released and the receptors are exported for recycling by monoubiquitination for the next round of protein import. The RING finger complex, consisting of PEX2, PEX10 and PEX12, recycles the soluble receptors (Sparkes and Baker, 2002; Hu *et al.*, 2012).

### 1.2.2 Import of peroxisomal membrane proteins

By the current state of knowledge two possible routes for PMP import are discussed. This section focuses mainly on plant PMPs, as the PMP targeting is conserved within all eukaryotic domains (Baerends *et al.*, 2000). The targeting route of PMPs is separated in ER-dependent or independent groups (Hu *et al.*, 2012) and additional in PEX19-dependent or independent classes (Jones *et al.*, 2004; Van Ael and Fransen, 2006).

Group I PMP targeting is mediated by ER-derived vesicles, which fuse to the existing peroxisomes (Hu *et al.*, 2012). In plants, only two PMPs are known to be targeted via ER; ascorbate peroxidase (APX), a carboxy tail-anchored integral membrane protein that plays a major role in detoxifying ROS (section 1.3.3; Lisenbee *et al.*, 2003), and an integral membrane protein PEX16 (Karnik and Trelease, 2007). Group II PMPs are directly targeted to peroxisomes, as it was demonstrated for (i) the Arabidopsis PMP22, a protein with unknown function (Tugal *et al.*, 1999; Murphy *et al.*, 2003), (ii) PEX2, which is involved in peroxisomal matrix protein import (Sparkes *et al.*, 2005), (iii) PEX11, that controls peroxisomal proliferation (Lingard and Trelease, 2006), and (iv) monodehydroascorbate reductase 4 (MDAR4), that is involved in the ascorbate-glutathione cycle (Lisenbee *et al.*, 2005; Eastmond, 2007). Controversial observations have been reported for the PMP targeting receptor PEX3, an integral membrane protein. The Arabidopsis PEX3 protein is directly imported from the cytosol to peroxisomes, whereas its homologue in yeast and mammals enters the peroxisomes via ER (Hunt and Trelease, 2004; Hoepfner *et al.*, 2005; Toro *et al.*, 2009).

Another way to distinguish PMPs is the classification into class I PMPs, which are targeted to peroxisomes via the PMP receptor protein PEX19, and class II PMPs, whose import is independent of PEX19 (Jones *et al.*, 2004; Van Ael and Fransen, 2006). PEX19 was predominantly localized in the cytosol and partly to peroxisomes (Jones *et al.*, 2004). It is known that PEX19 binds to several newly synthesized PMPs in the cytosol. The PEX19-PMP complex is targeted to the peroxisomal membrane, where it interacts with the PEX3 receptor. The PMP is then subsequently incorporated into the peroxisomal bilayer (Hadden *et al.*, 2006; Platta and Erdmann, 2007b). The exact role of PEX19 function is controversial discussed, as PEX19 is required for ER-derived PMP import in yeast (Hoepfner *et al.*, 2005; Lam *et al.*, 2010; Agrawal *et al.*, 2011). Class I PMPs are (i) the Arabidopsis peroxisomal ABC transporter COMATOSE (CTS; Nyathi *et al.*, 2012), (ii) the human PMP22 protein (Sacksteder *et al.*, 2000; Brosius *et al.*, 2002; Jones *et al.*, 2004), (iii) the Arabidopsis and human RING finger peroxin for matrix protein import, PEX10, which is targeted directly from the cytosol to peroxisomes (Sacksteder *et al.*, 2000; Fransen *et al.*, 2001; Sparkes *et al.*, 2005; Hadden *et al.*, 2006), and (iv) the yeast peroxisomal adenosine triphosphate (ATP) transporter Ant1p (Palmieri *et al.*, 2001; van der Zand *et al.*, 2010) and the human coenzyme A (CoA) and flavin adenine dinucleotide (FAD) transporter SLC25A17, which are

targeted to peroxisomes via ER (Sacksteder *et al.*, 2000). Class II PMPs are the human RING finger peroxin PEX2, although the PEX19 yeast two-hybrid assay was difficult to interpret (Sacksteder *et al.*, 2000; Kim *et al.*, 2006), and the yeast protein Inp1p, which is required for peroxisome inheritance (Fagarasanu *et al.*, 2005).

PMPs possess a putative *cis*-acting peroxisomal membrane targeting signal (mPTS) which consists of two functionally distinct domains, a targeting element of hydrophobic and positively charged amino acids, and a membrane-anchoring transmembrane domain (Rottensteiner *et al.*, 2004; Van Ael and Fransen, 2006). However, it is improbable that a conserved mPTS consensus sequence will be responsible for the different import ways (ER or direct from cytosol, PEX19 dependent or independent), implying that PMPs contain more than one import recognition site (Van Ael and Fransen, 2006). The mPTS targeting element of many PMPs is equal to the PEX19 binding site, although other PMPs have distinct mPTS and PEX19 recognition sites (Van Ael and Fransen, 2006).

### 1.3 Peroxisomal metabolism in plants

This section focuses on three nicotinamide adenine dinucleotide ( $\text{NAD}^+$ ) consuming peroxisomal metabolic pathways in plants, fatty acid  $\beta$ -oxidation, photorespiration, and  $\text{H}_2\text{O}_2$  detoxification (Figure 1.1; Reumann and Weber, 2006; Graham, 2008), although over 20  $\text{NAD}^+(\text{H})/\text{NADP}^+(\text{H})$  (nicotinamide adenine dinucleotide phosphate)-dependent dehydrogenases with unknown function are predicted or proven to be peroxisomal localized (Reumann *et al.*, 2004).

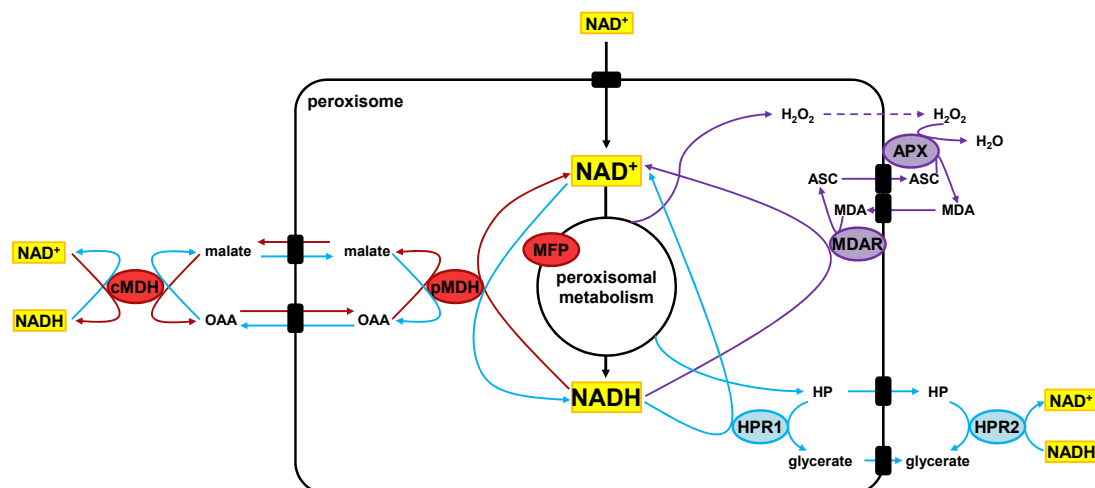


**Figure 1.1 The importance of  $\text{NAD}^+$  in peroxisomal  $\beta$ -oxidation, photorespiration and  $\text{H}_2\text{O}_2$  detoxification**  
 $\text{NAD}^+$  is an important cofactor for different peroxisomal pathways, such as fatty acid  $\beta$ -oxidation (red), photorespiration (blue) and  $\text{H}_2\text{O}_2$  detoxification (purple). Enzymes that directly or indirectly require  $\text{NAD}^+$  are peroxisomal malate dehydrogenase (pMDH), cytosolic malate dehydrogenase (cMDH), multifunctional protein (MFP), hydroxypyruvate reductase (HPR), ascorbate peroxidase (APX), and monodehydroascorbate reductase (MDAR). The corresponding metabolites (ASC, ascorbate, MDA, monodehydroascorbate; OAA, oxaloacetate; HP, hydroxypyruvate) have to cross the peroxisomal membrane by still unknown transport proteins (black boxes). According to Graham (2008) and Hu *et al.* (2012).

### 1.3.1 Fatty acid degradation via peroxisomal $\beta$ -oxidation

In plants, stored fatty acids are broken down to produce energy for germination and seedling establishment. During post-germinative growth fatty acids are released from triacylglycerol (TAG) stored in oil bodies (Theodoulou and Eastmond, 2012). Free or acyl-fatty acid import is mediated by the peroxisomal full-length ABC transporter CTS (COMATOSE, also known as ABCD1, PXA and PED3; Footitt *et al.*, 2002; Footitt *et al.*, 2006; Hayashi and Nishimura, 2006). *cts* knockout mutants revealed a strong  $\beta$ -oxidation phenotype. *cts* seeds are unable to establish without exogenous carbon supply (sucrose dependent phenotype, SDP) and are strongly impaired in TAG breakdown (Footitt *et al.*, 2002). In addition, *cts* seedlings are resistance to the auxin precursors 2,4-dichlorophenoxybutyric acid (2,4-DB) and indole-3-butyric acid (IBA; Zolman *et al.*, 2001; Footitt *et al.*, 2002). The long chain acyl-CoA synthetases LACS6 and LACS7 catalyze the essential activation of fatty acids to acyl-CoAs ( $C_n$ ) by ATP-dependent esterification with CoA (Fulda *et al.*, 2004; Graham, 2008). Acyl-CoAs enter the  $\beta$ -oxidation and are first oxidized to 2-trans-enoyl-CoA by acyl-CoA oxidase (ACX). ACX is a FAD-dependent enzyme and produces  $H_2O_2$ , which is directly detoxified by catalase or the APX/MDAR system (Figure 1.1; section 1.3.3; Eastmond *et al.*, 2000; Graham, 2008). The multifunctional protein (MFP) exhibits 2-trans-enoyl-CoA hydratase activity (MFP/HYD) to convert 2-trans-enoyl-CoA to hydroxyacyl-CoA and L-3-hydroxyacyl-CoA dehydrogenase activity (MFP/DH) for the subsequently production of 3-ketoacyl-CoA (Richmond and Bleecker, 1999; Eastmond and Graham, 2000; Rylott *et al.*, 2006; Arent *et al.*, 2010). Arabidopsis contains two peroxisomal MFPs, abnormal inflorescence meristem 1 (AIM1) and MFP2 (Richmond and Bleecker, 1999; Eastmond and Graham, 2000). MFP2 expression is strongly induced during seedling establishment. The corresponding *mfp2* mutant is impaired in TAG breakdown, contains enlarged peroxisomes, and is unable to grow without exogenous sucrose supply (Rylott *et al.*, 2006). AIM1 is expressed in low levels during post-germinative seedling growth and *aim1* mutants are affected in reproductive development (Richmond and Bleecker, 1999).  $NAD^+$  is reduced to NADH by the MFP dehydrogenase activity and is re-oxidized by the peroxisomal malate dehydrogenase (pMDH)-mediated reduction/oxidation (redox) shuttle (Figure 1.1; Graham, 2008). The last step of  $\beta$ -oxidation is the thiolytic cleavage of 3-ketoacyl-CoA to acyl-CoA ( $C_{n-2}$ ) and acetyl-CoA ( $C_2$ ) facilitated by 3-ketoacyl-CoA thiolase (KAT; Germain *et al.*, 2001). Acyl-CoA ( $C_{n-2}$ ) enters the  $\beta$ -oxidation cycle again to breakdown the complete fatty acid chain (Graham, 2008; Theodoulou and Eastmond, 2012). Acetyl-CoA ( $C_2$ ) enters the glyoxylate cycle for subsequent gluconeogenesis generating sucrose and feeding the tricarboxylic acid (TCA) cycle to gain metabolic energy (Graham, 2008; Theodoulou and Eastmond, 2012).

In plants,  $\beta$ -oxidation has more functions beyond storage oil break down. Degradation of membrane lipids during senescence and steps of the biosynthesis of phytohormones such

as JA, auxin and salicylic acid (SA) are catalyzed by the peroxisomal  $\beta$ -oxidation (Reumann *et al.*, 2004; Delker *et al.*, 2007; Yang and Ohlrogge, 2009).

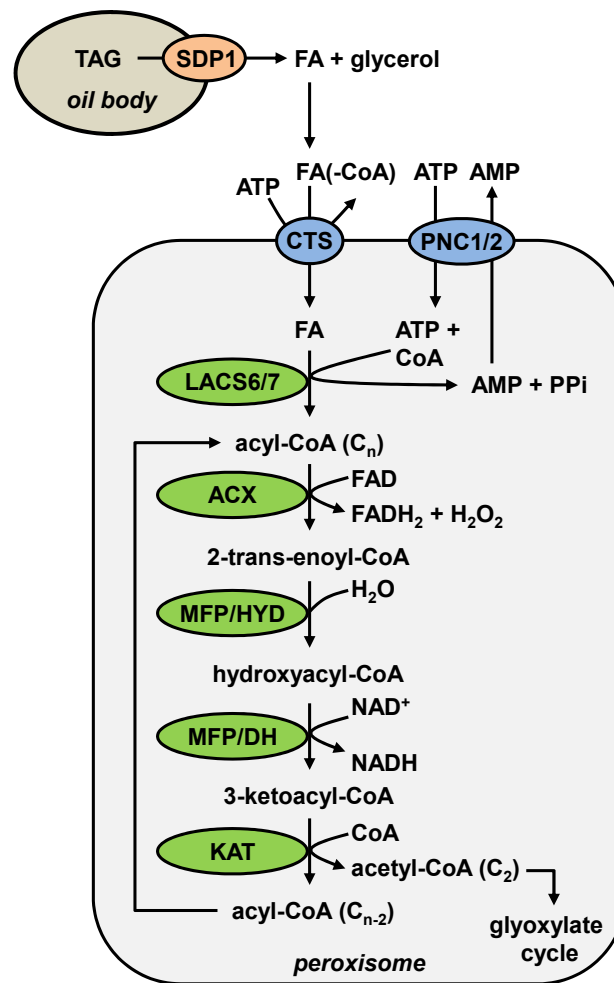


**Figure 1.2 peroxisomal fatty acid  $\beta$ -oxidation pathway**

TAG, stored in oil bodies, is hydrolyzed by SDP1 lipase to free fatty acid (FA) and glycerol. FA or FA-CoA are imported to peroxisomes by CTS and metabolized by the peroxisomal fatty acid  $\beta$ -oxidation to feed the glyoxylate cycle to gain energy. Abbreviations: ACX, acyl-CoA oxidase; CTS, COMATOSE, ABC transporter; KAT, 3-ketoacyl-CoA thiolase; LACS6/7, long chain acyl-CoA synthetase; MFP/HYD, multifunctional protein/ 2-trans-enoyl-CoA hydratase; MFP/DH, multifunctional protein/ L-3-hydroxyacyl-CoA dehydrogenase; PNC1/2, peroxisomal ATP carrier; SDP1, SUGAR DEPENDENT 1 lipase. After Theodoulou and Eastmond (2012).

### 1.3.2 Photorespiration

Plant peroxisomes play a major role in the  $\text{NAD}^+$ -dependent photorespiratory  $\text{C}_2$  cycle, a recycling pathway of the oxygenase reaction of ribulose-1,5-bisphosphate carboxylase/oxygenase (RubisCO), the key enzyme of photosynthesis (Peterhansel and Maurino, 2011). RubisCO fixes  $\text{CO}_2$  for biomass production, but it cannot fully discriminate between  $\text{CO}_2$  and  $\text{O}_2$  (Peterhansel and Maurino, 2011). By the fixation of  $\text{O}_2$  to ribulose-1,5-bisphosphate mediated by the chloroplastic RubisCO, 3-phosphoglycerate and toxic 2-phosphoglycolate are produced. 3-phosphoglycerate can directly enter the Calvin cycle whereas 2-phosphoglycerate is converted to glycolate and transported to peroxisomes.

Inside the peroxisomal matrix glycolate is converted to glyoxylate by the glycolate oxidase (GOX) with the simultaneous production of  $H_2O_2$ . An aminotransferase catalyzes the conversion of glyoxylate to glycine, which enters the mitochondria. There it is metabolized to serine and transported back to peroxisomes. Serine is converted to hydroxypyruvate which is metabolized to glycerate via the hydroxypyruvate reductase HPR1. The conversion of hydroxypyruvate to glycerate can also take place in the cytosol facilitated by cytosolic HPR2 (Timm *et al.*, 2011). After entering the chloroplast, glycerate is converted to 3-phosphoglycerate and enters the Calvin cycle (Peterhansel and Maurino, 2011). During photorespiration peroxisomal HPR1 oxidizes NADH, which is reduced by the pMDH-mediated redox-shuttle (Figure 1.1; Cousins *et al.*, 2008; Cousins *et al.*, 2011).

### 1.3.3 Hydrogen peroxide detoxification

ROS are produced during peroxisomal metabolic pathways, like  $\beta$ -oxidation, photorespiration, or abiotic and biotic stress conditions (e.g. high light, drought, low and high temperature, heavy metals, UV radiation, air pollutants, physical and mechanical wounding, and pathogen infection; Dat *et al.*, 2000; Mittler, 2002; del Rio *et al.*, 2006; Schrader and Fahimi, 2006). The group of ROS contains superoxide radicals ( $O_2^{\cdot-}$ ), hydroxyl radicals ( $\cdot OH$ ), singlet oxygen ( $\cdot O_2$ ), ozone ( $O_3$ ) and hydrogen peroxide ( $H_2O_2$ ; del Rio *et al.*, 2006). Peroxisomes are the main site of  $H_2O_2$  production and breakdown (del Rio *et al.*, 2006). The amount of ROS has to be well-controlled as an over accumulation leads to damage of organelles, oxidation of proteins, damage of RNA and DNA, depletion of antioxidant levels and ultimately trigger cell death (Jambunathan and Mahalingam, 2006). A fine modulation of ROS concentrations is necessary, as ROS species function as signalling molecule to control processes like programmed cell death, abiotic stress response, pathogen defence and systemic signalling (Mittler, 2002). Plants contain several antioxidative defence systems to control and detoxify ROS. One example is the superoxide dismutase (SOD) which detoxifies  $O_2^{\cdot-}$  radicals to  $H_2O_2$  (del Rio *et al.*, 1992).  $H_2O_2$  is degraded by catalase or the APX/MDAR system (Graham, 2008; Mhamdi *et al.*, 2012). Ascorbate acts as an antioxidant within the APX/MDAR system (Figure 1.1) that is involved in scavenging  $H_2O_2$  which was not detoxified by catalase and diffused through the peroxisomal membrane (Graham, 2008). APX degrades  $H_2O_2$  by oxidation of ascorbate to monodehydroascorbate, which is transported into the peroxisomal matrix. The peroxisomal MDAR4 requires NADH as cofactor for the reduction of monodehydroascorbate to ascorbate. Ascorbate is again exported serving the next round of  $H_2O_2$  detoxification. The transport process of ascorbate and monodehydroascorbate over the peroxisomal membrane is still unknown.



## 1.4 NAD<sup>+</sup> biosynthesis and degradation

NAD<sup>+</sup> biosynthesis exclusively takes place in the cytosol. Nicotinate mononucleotide (NaMN) is the common precursor of NAD<sup>+</sup> *de novo* synthesis, which starts with a two-step conversion of aspartate to NaMN, and the NAD<sup>+</sup> recycling pathway (Figure 1.3; Noctor *et al.*, 2006; Hashida *et al.*, 2009; Gossmann *et al.*, 2012). NaMN is metabolized to nicotinate adenine dinucleotide (NaAD) by nicotinate/nicotinamide mononucleotide adenylyltransferase (NMNAT) and further to NAD<sup>+</sup> via NAD<sup>+</sup> synthetase (NADS). Five steps are required to convert NAD<sup>+</sup> to nicotinamide (Nam), which is a product of NAD<sup>+</sup> recycling and is released during NAD<sup>+</sup>-dependent signalling processes (Gossmann *et al.*, 2012). Nam is subsequently metabolized to NaMN via nicotinate (Na) in order to replenish the cellular NAD<sup>+</sup> pools before the recycling pathway starts over (Noctor *et al.*, 2006; Hashida *et al.*, 2009; Gossmann *et al.*, 2012).

NAD<sup>+</sup> biosynthesis and recycling occur in the cytoplasm, but some NAD<sup>+</sup>-modifying enzymes are localized in plant peroxisomes. It was recently shown that a NADH kinase 3 (NADK3) is localized in peroxisomes and mediates the phosphorylation of NADH to NADPH (Chai *et al.*, 2006; Waller *et al.*, 2010). NADK3 expression is induced during abiotic stress and the corresponding *nadk3* knock-out line is sensitive to oxidative and osmotic stress, and abscisic acid (ABA; Chai *et al.*, 2006). This indicates that the conversion of NADH to NADPH is necessary for stress tolerance. NADK3 maintains the important NADH/NADPH ratio and provides NADPH for NADPH-dependent anti-oxidant systems (Chai *et al.*, 2006).

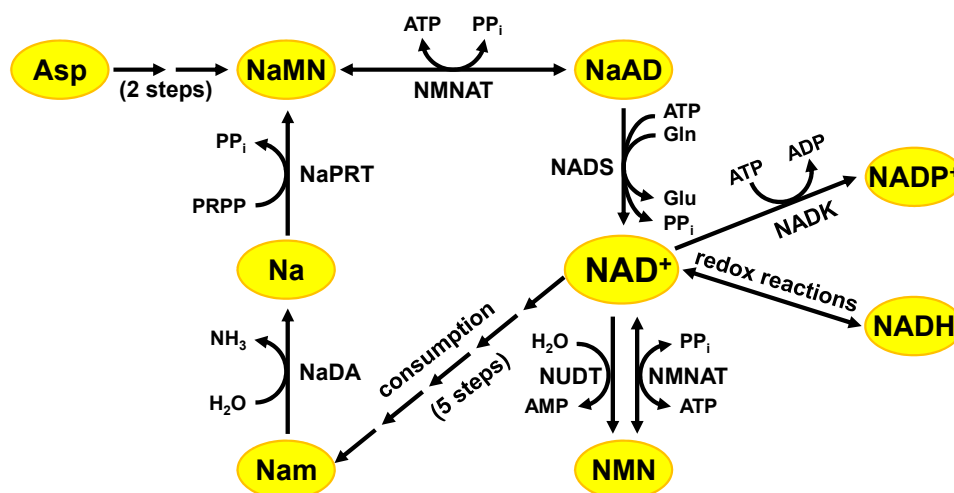


**Figure 1.3 Model of cytosolic NAD<sup>+</sup> biosynthesis, consumption, and recycling pathways**

Schematic model of NAD<sup>+</sup> *de novo* biosynthesis and recycling pathways operated in the cytosol. Abbreviations: Asp, aspartate; Gln, glutamine; Glu, glutamate; Na, nicotinate; NaAD, nicotinate adenine dinucleotide; NAD<sup>+</sup>, nicotinamide adenine dinucleotide; NaDA, nicotinamide deamidase; NADK, NAD<sup>+</sup> kinase, NADP<sup>+</sup>, nicotinamide adenine dinucleotide phosphate; NADS, NAD synthetase; Nam, nicotinamide; NaMN, nicotinate mononucleotide; NaPRT, nicotinate phosphoribosyltransferase; NMN, nicotinamide mononucleotide; NMNAT, nicotinate/nicotinamide mononucleotide adenylyltransferase; NUDT, Nudix hydrolases; PP<sub>i</sub>, pyrophosphate; PRPP, 5'-phosphoribosyl-1'-pyrophosphate. After Noctor *et al.* (2006), Hashida *et al.* (2009), and Gossmann *et al.* (2012)

Other NAD<sup>+</sup> consuming proteins are nudix hydrolases (nucleoside diphosphate linked to some moiety X; NUDT) that hydrolyze nucleoside diphosphate derivatives to control the cellular concentration of their substrates (Bessman *et al.*, 1996; Ogawa *et al.*, 2005; Kraszewska, 2008). Arabidopsis contains 29 NUDT localized in cytosol, chloroplasts, mitochondria, and peroxisomes (Kraszewska, 2008). By proteomic studies, NUDT7 and NUDT19 were predicted to localize to peroxisomes due to their PTS1 signal (Reumann *et al.*, 2004). Lingner and co-workers could verify the peroxisomal localization of NUDT19 in onion epidermis cells via transient transformation of a N-terminal yellow fluorescent protein (YFP) fusion (Lingner *et al.*, 2011), although previous studies localized NUDT19 to chloroplasts via C-terminal fusion to green fluorescent protein (GFP; Ogawa *et al.*, 2008). NUDT19 hydrolyzes NADH and NADPH to reduced NMN (NMNH) and adenosine monophosphate (AMP) or 2',5'-adenosine diphosphate (2',5'-ADP; Ogawa *et al.*, 2008). *nudt19* mutant plants showed no obvious phenotype (Ogawa *et al.*, 2008).

The cytosolic localization of NUDT7 was recently proven by transient expression of a GFP-NUDT7 fusion protein in Arabidopsis protoplasts (Olejnik *et al.*, 2011). NUDT7 is well characterized as an important factor to maintain the cellular redox homeostasis, as it hydrolyzes NADH and ADP-ribose to NMNH and AMP and to ribose 5-P and AMP *in vitro* and therefore regulates the NADH:NAD<sup>+</sup> balance (Ogawa *et al.*, 2005; Jambunathan and Mahalingam, 2006; Olejnik *et al.*, 2011). *nudt7* mutant plants have a pleiotropic phenotype with smaller size, curled leaves, increased levels of ROS and NADH under controlled and oxidative stress conditions (Jambunathan and Mahalingam, 2006; Kraszewska, 2008; Ishikawa *et al.*, 2009).

## **1.5 Supplying peroxisomes with cofactors**

As peroxisomal metabolism is essential in all eukaryotic organisms, the exchange of metabolites and cofactors is important for optimal function. Although our understanding about the function of plant peroxisomes has greatly increased in recent years, the detailed knowledge about membrane proteins mediating the exchange of metabolites and cofactors is little (Linka and Esser, 2012).

### **1.5.1 Permeability of the peroxisomal membrane for cofactors**

Specialized membrane transport proteins enable the import and export of metabolites and cofactors, due to the impermeability of the peroxisomal membrane for solutes and bigger molecules (Donaldson, 1981; Antonenkov and Hiltunen, 2006; Linka and Esser, 2012). The impermeability of the peroxisomal membrane for “bulky” solutes like cofactors (NAD<sup>+</sup>/H, ATP, CoA) and the existence of peroxisomal transport proteins could be shown with different approaches in *Ricinus communis* (castor bean), rat, and yeast (Donaldson, 1981; Van

Veldhoven *et al.*, 1983; Van Veldhoven *et al.*, 1987; Antonenkov *et al.*, 2004). For example, external NAD<sup>+</sup> and CoA provided to isolated and intact peroxisomes from rat and castor bean did not affect the activity of peroxisomal NAD<sup>+</sup> and CoA-dependent enzymes, indicating the impermeability of the peroxisomal membrane for these substrates (Donaldson, 1981; Antonenkov *et al.*, 2004). Uptake assays performed with reconstituted peroxisomal membrane fractions of isolated rat peroxisomes indicated the existence of specialized transport proteins mediating the diffusion of NAD<sup>+</sup>, CoA, and ATP (Van Veldhoven *et al.*, 1983; Van Veldhoven *et al.*, 1987). In addition, it was shown that a yeast  $\Delta mdh3p$  mutant, lacking the peroxisomal malate dehydrogenase gene, is impaired in fatty acid  $\beta$ -oxidation, because NAD<sup>+</sup> is not regenerated (van Roermund *et al.*, 1995). If the peroxisomal membrane would be permeable for NAD<sup>+</sup>, the  $\beta$ -oxidation could be fed with cytosolic NAD<sup>+</sup> and the  $\Delta mdh3p$  mutant would not exhibit a  $\beta$ -oxidation phenotype.

Permeability of the peroxisomal membrane for small solutes was identified by electrophysiological studies of isolated peroxisomes from spinach leaves (Reumann *et al.*, 1995). The studies revealed a peroxisomal porin-like channel with a strong anion selectivity, that might be involved in the transport of photorespiratory metabolites like glycolate and glycerate (Reumann *et al.*, 1995).

### **1.5.2 Peroxisomal members of the mitochondrial carrier family**

The genome of Arabidopsis encodes for 58 members of the mitochondrial carrier family (MCF), which are located in mitochondrion, chloroplast, ER, plasma membrane and peroxisome (Todisco *et al.*, 2006; Leroch *et al.*, 2008; Linka *et al.*, 2008b; Palmieri *et al.*, 2011; Rieder and Neuhaus, 2011). In Arabidopsis, proven peroxisomal localized MCF members are the peroxisomal ATP transporter PNC1 and PNC2, and At2g39920, a gene of unknown function (Linka *et al.*, 2008b). Characteristic for all MCF members are six transmembrane-spanning domains, three tandem repeated homologous domains of about 100 amino acids, and homodimerization (Picault *et al.*, 2004; Palmieri *et al.*, 2011; Haferkamp and Schmitz-Esser, 2012). MCF members demonstrated different substrate specificities (Palmieri *et al.*, 2011) and act as antiporter like the PNCs (Linka *et al.*, 2008b), or as uniporter like the chloroplastic AMP transporter Brittle1 (Leroch *et al.*, 2005; Kirchberger *et al.*, 2008).

Two Arabidopsis peroxisomal adenine nucleotide carriers, called PNC1 and PNC2, mediate the import of ATP in exchange with ADP or AMP (Arai *et al.*, 2008; Linka *et al.*, 2008b). Peroxisomal ATP supply via PNC1 and PNC2 is essential for the activation of free fatty acids for  $\beta$ -oxidation (section 1.3.1; Arai *et al.*, 2008; Linka *et al.*, 2008b). Plants repressing both pnc genes showed a sugar dependent phenotype, resistance to 2,4-DB and IBA, and are impaired in fatty acid degradation (Arai *et al.*, 2008; Linka *et al.*, 2008b).

### 1.5.3 Peroxisomal NAD<sup>+</sup> and CoA carrier

The cofactors NAD<sup>+</sup> and CoA are required for peroxisomal metabolism (section 1.3; Graham, 2008; Bauwe *et al.*, 2012). NAD<sup>+</sup> biosynthesis exclusively takes place in the cytosol (section 1.4; Noctor *et al.*, 2006; Hashida *et al.*, 2009) and CoA biosynthesis is separated in cytosol, mitochondrion, and chloroplast (Leonardi *et al.*, 2005). CoA is required for the essential activation of fatty acids inside peroxisomes (section 1.3.1; Graham, 2008). The generation of a peroxisomal CoA pool is controversially discussed. The yeast and human ABC transporter imports activated fatty acids as acyl-CoA esters. Upon import, CoA is cleaved off and released to the peroxisomal CoA pool (Kemp *et al.*, 2011; Antonenkov and Hiltunen, 2012). Another possibility could be the existence of a peroxisomal CoA transport protein. Recently, the human peroxisomal MCF member SLC25A17 was characterized as CoA, FAD, and NAD<sup>+</sup> transporter, but the *in vivo* role was not further investigated (Agrimi *et al.*, 2012a).

NAD<sup>+</sup> is involved in redox reactions and thus required for  $\beta$ -oxidation, photorespiration and H<sub>2</sub>O<sub>2</sub> detoxification (section 1.4; Cousins *et al.*, 2008; Graham, 2008). The peroxisomal metabolism generates either NAD<sup>+</sup> (e.g. photorespiration and H<sub>2</sub>O<sub>2</sub> degradation) or NADH (e.g.  $\beta$ -oxidation). A role in the exchange of NAD<sup>+</sup>/NADH for regeneration plays the malate/oxaloacetate (malate/OAA) shuttle mediated by the peroxisomal (pMDH) and cytosolic malate dehydrogenases (cMDH; Figure 1.1; section 1.3.1; Pracharoenwattana *et al.*, 2007; Graham, 2008). To build up or to maintain the NAD<sup>+</sup> pool inside peroxisomes, either specialized transport proteins supply the peroxisomes with NAD<sup>+</sup> or peroxisomes are pre-filled with NAD<sup>+</sup> when ER-derive vesicles fused to pre-existing peroxisomes.

It was recently shown that At2g39970, the closest homologue of Arabidopsis PNC proteins and the human SLC25A17, was localized to peroxisomes in yeast and pumpkin cotyledons (Fukao *et al.*, 2001; Linka *et al.*, 2008b). In addition, the peroxisomal localization of At2g39970 in Arabidopsis was predicted by proteomic studies (Eubel *et al.*, 2008; Reumann *et al.*, 2009). Peroxisomal co-localization of At2g39970-YFP fusion protein with a peroxisomal marker (cyan fluorescent protein (CFP)-PTS1) was verified in tobacco protoplasts expressing the corresponding expression constructs (Wilkinson, 2009).

At2g39970 encodes a protein of 331 amino acids with a calculated molecular mass of 36.2 kDa and is annotated as peroxisomal membrane protein 38 kDa (PMP38; Fukao *et al.*, 2001). At2g39970 was predicted to mediate the transport of ATP because of its high sequence similarity to Arabidopsis and yeast ATP transporters and to human SLC25A17 and *Candida boindinii* PMP47, which are homologues of mitochondrial ATP carriers and were supposed as ATP transporter, even though SLC25A17 was recently characterized as CoA, FAD and NAD<sup>+</sup> transporter (Nakagawa *et al.*, 2000; Fukao *et al.*, 2001; Visser *et al.*, 2002; Linka *et al.*, 2008b; Agrimi *et al.*, 2012a). Linka and co-workers could show that At2g39970

could not rescue the phenotype of a yeast mutant lacking Ant1p (Linka *et al.*, 2008b), suggesting a different substrate specificity for At2g39970. In addition, it was shown that the At2g39970 mutant plants contain enlarged peroxisomes as it was demonstrated for some  $\beta$ -oxidation mutants (Hayashi *et al.*, 1998; Germain *et al.*, 2001; Pinfield-Wells *et al.*, 2005; Rylott *et al.*, 2006; Mano *et al.*, 2011). In this thesis, it is postulated that At2g39970 is a potential candidate for mediating  $\text{NAD}^+$  import into plant peroxisomes, because  $\text{NAD}^+$  is a structurally similar compound to ATP.

## **1.6 Goals of this thesis**

The aim of this thesis was the characterization of a peroxisomal  $\text{NAD}^+$  carrier in plants, whose existence was controversially discussed for decades. The supply of  $\text{NAD}^+$  for peroxisomal metabolism mediated by a transport protein was hypothesized, because  $\text{NAD}^+$  biosynthesis exclusively takes place in the cytosol (Noctor *et al.*, 2006; Hashida *et al.*, 2009) and the peroxisomal membrane being impermeable for  $\text{NAD}^+$  (Antonovkov and Hiltunen, 2006). This thesis focused on the impact of peroxisomal  $\text{NAD}^+$  supply, mediated by the peroxisomal  $\text{NAD}^+$  carrier and its role in fatty acid  $\beta$ -oxidation during germination, seedling establishment, and on  $\text{H}_2\text{O}_2$  detoxification.

In this thesis, the MCF member At2g39970 was characterized as candidate for the peroxisomal  $\text{NAD}^+$  carrier. (i) The *in vitro* function of At2g39970 was analyzed by expression recombinant protein, reconstitution into artificial lipid bodies and performing uptake studies to identify the transport substrate. Substrate specificity was measured to detect the exchange substrate. In addition, the influence on the transport mode of the extended loop region and phosphorylation site within At2g39970 was studied by generating mutated At2g39970 proteins and performing uptake studies with recombinant mutated PXN proteins. (ii) Homozygous At2g39970 T-DNA lines were established and examined if seedlings are impaired in fatty acid  $\beta$ -oxidation. In addition the impact of At2g39970 during oxidative stress was analyzed *in vivo* by physiological experiments and *in silico* by expression data analysis. (iii) The impact of the malate/OAA shuttle mediated by MDHs and the possibly redundancy to the  $\text{NAD}^+$  carrier was examined by creating mutants lacking both systems.

A second project was the analysis of peroxisomal targeting of At2g39970 and if its extended loop region and the phosphorylation site exhibits an impact on the peroxisomal import. To investigate whether the cytosolic receptor PEX19 is involved in the import of the peroxisomal  $\text{NAD}^+$  carrier and other PMPs, two studies were performed. (i) A pull-down assays with recombinant PEX19 protein and PMPs were performed to study the *in vitro* interaction. (ii) A mis-localization experiment was assayed to analyze the *in vivo* interaction of PEX19 and PMPs by transient expression of YFP-PMP and nuclear localization signal NLS-PEX19 fusion proteins in tobacco leaves.

## 2 Material and Methods

### 2.1 Consumables and chemicals

Consumables were purchased from Sarstedt AG & Co (Nümbrecht, Germany) and Carl Roth (Karlsruhe, Germany) and chemicals from Sigma-Aldrich (Steinheim, Germany) unless stated otherwise. Radioactivity was obtained from Perkin Elmer (Rodgau, Germany) and Hartmann Analytic (Braunschweig, Germany).

### 2.2 General methods

#### 2.2.1 Cloning

Standard molecular techniques for cloning were performed as described in Sambrook *et al.* (1989). DNA sequences were verified by DNA sequencing (GATC Biotech, Konstanz, Germany). Oligonucleotides were synthesized by Sigma-Aldrich. GeneRuler 1kb DNA Ladder (Fermentas, St. Leon-Rot, Germany) was used for agarose gel electrophoresis. Constructs generated in this thesis are shown in section 7.6.

**Table 2.1 *Escherichia coli* strains used for cloning**

*E. coli* strains DH5 $\alpha$  and XL1-Blue were used for standard cloning. *E. coli* strain DB3.1 was used for Gateway Technology based cloning (Invitrogen, Darmstadt, Germany). DB3.1 strain carries the *gyrA462* allele for providing resistance to the toxic effects of the *ccdB* gene which is coded on Gateway plasmids.

Strain	Genotype	References
DH5 $\alpha$	F <sup>-</sup> , endA1, hsdR17 (rk <sup>-</sup> , mk <sup>-</sup> ), supE44, thi-1, recA1, gyrA96, relA1, $\Phi$ 80d, lacZ[ $\Delta$ ]M15	Hanahan (1983)
XL1-Blue	endA1 gyrA96(nal <sup>R</sup> ) thi-1 recA1 relA1 lac glnV44 F' [::Tn10 proAB <sup>+</sup> lacI <sup>q</sup> $\Delta$ (lacZ)M15] hsdR17(rk <sup>-</sup> mk <sup>+</sup> )	Stratagene (La Jolla, USA)
DB3.1	F- <i>gyrA462</i> endA1 glnV44 $\Delta$ (sr1-recA) mcrB mrr hsdS20(r <sub>B</sub> <sup>-</sup> , m <sub>B</sub> <sup>-</sup> ) ara14 galK2 lacY1 proA2 rpsL20(Sm <sup>I</sup> ) xyl5 $\Delta$ leu mtl1	Invitrogen

**Table 2.2 Plasmids used for cloning**

Plasmids were used for sub-cloning and empty plasmids for plant, WGE, yeast, and *E.coli* expression. \*<sup>1</sup> Prof. Dr. Karin Schumacher, Heidelberg University, Germany. \*<sup>2</sup> Dr. Nicole Linka, Heinrich-Heine University (HHU) Düsseldorf, Germany. Vector maps: section 7.6.1.

Name	Organism	Function	Resistance	Reference
pJET 1.2	/	sub-cloning	Amp <sup>R</sup>	Fermentas
pDONR207	/	sub-cloning	Gent <sup>R</sup>	Invitrogen

Name	Organism	Function	Resistance	Reference
pBi121	plant	GUS reporter gene	Kan <sup>R</sup>	Chen <i>et al.</i> (2003)
pUT Kan	plant	UBQ10 promoter	Spec <sup>R</sup>	K. Schumacher* <sup>1</sup>
pMDC7	plant	Estradiol inducible Promoter	Spec <sup>R</sup>	Curtis and Grossniklaus (2003)
pMDC32	plant	35S promoter	Kan <sup>R</sup>	Curtis and Grossniklaus (2003)
pCAMBIA3301	plant	35S promoter	Kan <sup>R</sup>	Cambia (Brisbane, Australia)
pUBN-YFP	plant	N-terminal YFP fusion	Spec <sup>R</sup>	Grefen <i>et al.</i> (2010)
pKB65 (pMDC32)	plant	replacement of 35S with UBQ10 promoter	Kan <sup>R</sup>	this thesis
pRS300	plant	artificial microRNA	Amp <sup>R</sup>	<a href="http://wmd3.weigelworld.org">http://wmd3.weigelworld.org</a>
pEU3a	WGE, CF Science	SP6 promoter	Amp <sup>R</sup>	CellFree Science (Yokohama, Japan)
pNL22 (pEU3a)	WGE, CF Science	SP6 promoter, C-terminal His-tag	Amp <sup>R</sup>	Bernhardt <i>et al.</i> (2012a)
pIVEX1.3	WGE, 5Prime	T7 promoter, C-terminal His-tag	Amp <sup>R</sup>	5PRIME (Hamburg, Germany)
pNL14 (pYES2)	yeast	GAL promoter, C-terminal His-tag	Amp <sup>R</sup>	N. Linka* <sup>2</sup>
pET-16b	<i>E. coli</i>	Lac/ T7 promoter N-terminal His-tag	Amp <sup>R</sup>	Merck Biosciences (Darmstadt, Germany)

## 2.2.2 Protein biochemistry

SDS-PAGE and immunoblot analysis were performed according to Sambrook *et al.* (1989). Protein concentrations were determined using a bichinonic acid protein assay (ThermoFisher Scientific, Bonn, Germany). PageRuler Prestained Protein Ladder (Fermentas) was used for SDS-PAGE analysis.

**Table 2.3 Antibodies used for immunoblot analysis**

First and second antibodies were used for immunodetection of plant and recombinant protein. AP, alkaline phosphatase; HRP, horseradish peroxidase. \* Prof. Dr. Johannes M. Herrmann, University of Kaiserslautern, Germany.

Type	Name	Organism	Company
1 <sup>st</sup>	penta-His antibody	Mouse	Qiagen (Hilden, Germany)
1 <sup>st</sup>	Phosphoserine Q5 antibody	Mouse	Qiagen
1 <sup>st</sup>	anti-PXN-specific serum	Rabbit	this thesis
1 <sup>st</sup>	anti-ScCOX2	Rabbit	J.M. Herrmann*
2 <sup>nd</sup>	AP-conjugated anti-mouse IgG	Goat	Promega (Mannheim, Germany)
2 <sup>nd</sup>	AP-conjugated anti-rabbit IgG	Donkey	Promega

Type	Name	Organism	Company
2 <sup>nd</sup>	HRP-conjugated anti-mouse IgG	Goat	Santa Cruz Biotechnology (Heidelberg, Germany)
2 <sup>nd</sup>	HRP-conjugated anti-rabbit IgG	Donkey	GE Healthcare (Munich, Germany)

### 2.2.3 *In silico* expression and co-expression analysis

*In silico* co-expression analysis was performed using web-based ATTEDII, GeneMANIA, Genevestigator, and Arabidopsis Co-response databases (Table 7.5). PXN expression data were received from Arabidopsis eFP Browser (Table 7.5).

## 2.3 Plant work

### 2.3.1 Plant lines

Wild type *Arabidopsis thaliana* (ecotype Columbia; Col-0) was obtained from the Arabidopsis sequencing project, LEHLE SEEDS, Round Rock, USA. Arabidopsis mutants were obtained from the ABRC at the Ohio State University. *pmdh1 pmdh2* and *pmdh1 pmdh2 hpr1* mutants were kindly provided by Prof. Dr. Steven Smith (The University of Western Australia, Australia).

**Table 2.4 Arabidopsis mutant lines**

Arabidopsis T-DNA and point mutation lines were used for physiological experiments.

Name	Locus	Eco-type	Line	Mutation	Resistance	References
<i>pxn-1</i>	At2g39970	Col-0	GABI_046_D01	T-DNA	Sul <sup>R</sup>	Bernhardt <i>et al.</i> (2012a)
<i>pxn-2</i>	At2g39970	Col-0	GABI_830_A06	T-DNA	Sul <sup>R</sup>	Bernhardt <i>et al.</i> (2012a)
<i>pxn-3</i>	At2g39970	Col-0	SAIL_636_F12	T-DNA	Gluf <sup>R</sup>	Bernhardt <i>et al.</i> (2012a)
<i>pmdh1</i>	At2g22780	Col-0	GABI_363_B11	T-DNA	Sul <sup>R</sup>	Prachoenwattana <i>et al.</i> (2007)
<i>pmdh2</i>	At5g09660	Col-0	GABI_326_G02	T-DNA	Sul <sup>R</sup>	Prachoenwattana <i>et al.</i> (2007)
<i>hpr1</i>	At1g68010	Col-0	SALK_143584	T-DNA	Kan <sup>R</sup>	Prachoenwattana <i>et al.</i> (2010)
<i>pxa1</i>	At4g39850	Col-0	CS3950	EMS point mutation	/	Zolman <i>et al.</i> (2001)
<i>abi4</i>	At2g40220	Col-0	/	irradiation point mutation	/	Finkelstein (1994)



### 2.3.2 Plant growth conditions

Chlorine gas surface sterilization of *Arabidopsis* seeds was performed according to Bernhardt *et al.* (2012b). Seeds were stratified for four days at 4°C and germinated on 0.8% (w/v) agar-solidified half-strength Musharige & Skoog (MS) medium (Duchefa, Haarlem, Netherlands) supplemented with 1% (w/v) sucrose. Plants for seed production were incubated at long-day conditions (16 h light/ 8 h dark cycle; 22/18°C) in growth chambers (100  $\mu\text{mol m}^{-2} \text{s}^{-1}$  light intensity). Plants for seed germination, seedling growth, 2,4-DB and 2,4-D experiments, fatty acid analysis, lipid staining, and plant membrane isolation were grown as described by Bernhardt *et al.* (2012a). Seedlings were photographed and roots or hypocotyls were measured using IMAGEJ (Table 7.5). For transmission electron microscope (TEM) analysis seedlings were grown on half-strength MS agar in constant darkness. Response to oxidative stress was analyzed by growing seedlings on half-strength MS agar containing either 10  $\mu\text{M}$   $\text{H}_2\text{O}_2$ , 2  $\mu\text{M}$  3-aminotriazole, 75 mM sodium chloride (Philipp, 2010; Trippelsdorf, 2012).

### 2.3.3 Arabidopsis transformation

Floral-dip *Arabidopsis* transformation using agrobacteria (Koncz and Schell, 1986), selection of positive transformants, and segregation analysis was performed according to Bernhardt *et al.* (2012b).

**Table 2.5 *Agrobacterium tumefaciens* strains**

Agrobacteria were used for stable transformation of *Arabidopsis* and for transient transformation of tobacco leaves.

Strain	Genotype	Reference
GV3101::pMP90	C58 Rif <sup>R</sup> , pMP90 (pTic58 $\Delta$ T-DNA, Gent <sup>R</sup> )	Koncz and Schell (1986)
p19	Rif <sup>R</sup> , Amp <sup>R</sup> , Kan <sup>R</sup>	Voinnet <i>et al.</i> (2003)

**Table 2.6 Produced *Arabidopsis* mutant lines by agrobacteria-mediated transformation**

Plant lines were generated by agrobacteria-mediated *Arabidopsis* transformation.

Name	Initial line	Plasmid	Resistance	Generation
pPXN::GUS	Col-0	pKB49	Kan <sup>R</sup>	T <sub>3</sub>
pUBQ10::PXN	Col-0	pKB52	Kan <sup>R</sup>	T <sub>3</sub>
pUBQ10::PXN <i>pxn-1</i>	<i>pxn-1</i>	pKB52	Kan <sup>R</sup>	T <sub>3</sub>
pUBQ10::PXN <i>pxn-2</i>	<i>pxn-2</i>	pKB52	Kan <sup>R</sup>	T <sub>3</sub>
pUBQ10::PXN <i>pxn-3</i>	<i>pxn-3</i>	pKB52	Kan <sup>R</sup>	T <sub>3</sub>

Name	Initial line	Plasmid	Resistance	Generation
pUBQ10::amiR- <i>PXN</i>	Col-0	pKB67	Hyg <sup>R</sup>	T <sub>1</sub>
pUBQ10::amiR- <i>PXN</i> <i>pmdh1 pm dh2</i>	<i>pmdh1 pm dh2</i>	pKB67	Hyg <sup>R</sup>	T <sub>1</sub>
pUBQ10::amiR- <i>PXN</i> <i>pmdh1 pm dh2 hpr1</i>	<i>pmdh1 pm dh2 hpr1</i>	pKB67	Hyg <sup>R</sup>	T <sub>1</sub>
pLexA::amiR- <i>PXN</i>	Col-0	pKB68	Hyg <sup>R</sup>	T <sub>1</sub>
pLexA::amiR- <i>PXN</i> <i>pmdh1 pm dh2</i>	<i>pmdh1 pm dh2</i>	pKB68	Hyg <sup>R</sup>	/
pLexA::amiR- <i>PXN</i> <i>pmdh1 pm dh2 hpr1</i>	<i>pmdh1 pm dh2 hpr1</i>	pKB68	Hyg <sup>R</sup>	T <sub>1</sub>
p35S::siR- <i>PNC1/2 PXN</i>	<i>pxn-1</i>	pMSU98	Kan <sup>R</sup>	T <sub>2</sub>
pAlcA::siR- <i>PNC1/2 PXN</i>	<i>pxn-1</i>	pMSU253	Kan <sup>R</sup>	T <sub>2</sub>

### 2.3.4 Arabidopsis mutant lines generating by crossing

Crossing of Arabidopsis T-DNA lines was performed as published on the NASC website (Table 7.4).

**Table 2.7 Produced Arabidopsis mutant lines by crossing**

T-DNA lines were used for generating triple and quadruple mutants by crossing.

Name	Lines for crossing	Resistance	Generation
<i>pmdh1 pm dh2 pxn</i>	<i>pmdh1 pm dh2 hpr1</i> and <i>pxn-1</i>	Sul <sup>R</sup>	T <sub>1</sub>
<i>pmdh1 pm dh2 hpr1 pxn</i>	<i>pmdh1 pm dh2 hpr1</i> and <i>pxn-1</i>	Sul <sup>R</sup>	T <sub>1</sub>

### 2.3.5 Verifying of T-DNA insertion lines

Genomic DNA of Arabidopsis plants was isolated after Berendzen *et al.* (2005). PCR-based screening was used to identify homozygous T-DNA insertion lines for *PXN* using gene-specific primers (NL29/NL30 for *pxn-1*, 899 bp; NL319/NL320 for *pxn-2*, 1015 bp; NL291/NL292 for *pxn-3*, 1216 bp) and primers for T-DNA/gene junction (NL29/P52 for *pxn-1*, 605 bp; NL320/P52 for *pxn-2*, 623 bp; NL292/P49 for *pxn-3*, 492 bp). To verify T-DNA insertions for *pmdh1 pm dh2* and *pmdh1 pm dh2 hpr1* lines, PCR-based screening was performed using gene-specific primers (KB27/KB28 for *pmdh1*, 1560 bp; KB29/KB30 for *pmdh2*, 1340 bp; KB31/KB32 for *hpr1*, 2310 bp) and primers for T-DNA/gene junction (KB27/P52 for *pmdh1*, 760 bp; KB29/P52 for *pmdh2*, 1550 bp; KB31/P47 for *hpr1*). Vector specific primers was used to verify positive Arabidopsis lines transformed with pUBQ10::*PXN* (KB6/KB10; 1016 bp; pKB52), pUBQ10::amiR-*PXN* (P98/KB34, 692 bp; pKB67), pLexA::amiR-*PXN* (P77/KB34, 797 bp; pKB68), p35S::siR-*PNC1/2* (P26/P70, 756 bp; pMSU98), and pAlcA::siR-*PNC1/2* (P26/P35, 860 bp; pMSU253). As positive control, amplification of ACTIN2 (*ACT2*) was performed using primers P33/P34 (977 bp).

**Table 2.8 Oligonucleotides used for gDNA screening of transgenic plants**

Primers used for verifying T-DNA insertion lines.

Name	5'-3' sequence	Binding site
KB6	CACACCTGCAGCATGGCGGACGCTTTGAT	PXN
KB10	GTGTGCTGCAGTTAGCTAGAGGTAGCGTTTGAGAGC	PXN
KB27	CAGATTGCTGACGGGTCAGG	<i>pmdh1</i>
KB28	GCCGTACACTTCATCGATCC	<i>pmdh1</i>
KB29	CTCAGATGGAGGCCAAGAAC	<i>pmdh2</i>
KB30	GCTGATACACTTCCTCTGC	<i>pmdh2</i>
KB31	CTCTACCATGGCGAAACCGG	<i>hpr1</i>
KB32	TCATAGCTTCGAAACAGGC	<i>hpr1</i>
KB34	GACTGGGACCTTTAATACGATTATCAAAGAGAATCAATGA	amiR-PXN
NL29	CCACAGGTAAGTAATCCGTCAATG	<i>pxn-1</i>
NL30	TGCTGGGCTTAATGTAGTCAAGTC	<i>pxn-1</i>
NL291	CAGGAAATGAACAACAATCCC	<i>pxn-3</i>
NL292	TACATTTTCTTTGGTCCGTGG	<i>pxn-3</i>
NL319	AAGAAAATGAGGAAAATATTTTCAGTC	<i>pxn-2</i>
NL320	CAAATCAGAGCAAATCAAGGC	<i>pxn-2</i>
P26	CTTCGTCTTACACATCACTTGTC	siRNA- <i>pnc12</i>
P33	GTTGGGATGAACCAGAAGGA	ACT2
P34	GAACCACCGATCCAGACACT	ACT2
P35	AGCAGAGACGGAGCACTTTC	AlcA promoter
P47	GCGTGGACCGCTTGCTGCAACT	SALK LB
P49	TAGCATCTGAATTTTCATAACCAATCTCGATACAC	SAIL LB
P52	CCCATTTGGACGTGAATGTAGACAC	GABI LB
P70	CTTCGCAAGACCCTTCCTC	35S promoter
P77	ATCATCCCCTCGACGTA CTG	LexA promoter
P98	CGATTTTCTGGGTTTGATCG	UBQ10 promoter

### 2.3.6 Plant membrane isolation of etiolated seedlings

Total membranes from six-day-old etiolated seedlings were extracted as described in Bernhardt *et al.* (2012a). The membrane pellets were analyzed by SDS-PAGE and immunoblot using PXN-specific and ScCOX2-specific antibodies (Table 2.3).

### 2.3.7 PXN-specific polyclonal antibody generation

The hydrophobic loop between the third and fourth transmembrane domain of the PXN protein (Figure 3.1) was used as an antigen for the generation of a polyclonal antiserum in rabbits (Pineda Antikörper Service, Berlin, Germany). Antibody generation was performed by Sabrina Wilkinson (Wilkinson, 2009) and described in Bernhardt *et al.* (2012a). In this thesis, the PXN-antibody was purified against the antigen according to Sauer and Stadler (1993).

### 2.3.8 Silencing of gene expression using artificial microRNA and small interfering RNA

The artificial microRNA for PXN silencing (5'-ATGGGACCTTTAATACGATTC-3') was designed using WMD3-Web MicroRNA Designer (Table 7.5). Cloning was performed with the primers KB33, KB34, KB35, KB36, P64, and P65 using the vector pRS300 as template according to the WMD3-Web MicroRNA Designer website (Table 7.5; Schwab *et al.*, 2006). PXN microRNA was inserted into pDONR207 by BP reaction using the primers gSV1 and miFB14. The destination vectors pKB65 for constitutive expression (UBQ10 promoter, pKB67) and pMDC7 for estradiol inducible expression (LexA promoter, pKB68) were used for the LR reaction (Gateway Technology, Invitrogen) to gain the expression vectors. Constructs encoding for the small interfering RNA for simultaneous silencing of PNC1 and PNC2 were provided by Dr. Nicole Linka, HHU Düsseldorf, Germany (Linka *et al.*, 2008b). pMSU98 expressed the siR-*PNC1/2* under the control of the constitutive 35S promoter and pMSU253 of the ethanol inducible pAlcA promoter.

**Table 2.9 Oligonucleotides used for generating PXN microRNA expressing vectors**

Primers were designed using WMD3-Web MicroRNA Designer (Table 7.5) for generating artificial microRNA for PXN silencing.

Name	5'-3' sequence	Purpose
KB33	GATAATCGTATTAAAGGTCCCAGTCTCTCTTTTGT ATTCC	I amiRNA PXN
KB34	GACTGGGACCTTTAATACGATTATCAAAGAGAATC AATGA	II amiRNA PXN
KB35	GACTAGGACCTTTAAAACGATTTTCACAGGTCGTG ATATG	III amiRNA PXN
KB36	GAAAATCGTTTTAAAGGTCCTAGTCTACATATATAT TCCT	IV amiRNA PXN
gSV1	GGGGACAAGTTTGTACAAAAAGCAGGCTCCACC CTGCAAGGCGATTAAGTTGG	amiRNA PXN Gateway
miFB14	GGACCACTTTGTACAAGAAAGCTGGGTCGCGGAT ACAATTTACACAGG	amiRNA PXN Gateway
P64	CTGCAAGGCGATTAAGTTGGGTAAC	A amiRNA PXN
P65	GCGGATAACAATTTACACAGGAAACAG	B amiRNA PXN

**Table 2.10 Plasmids used for gene silencing**

Plasmids were used for agrobacteria-mediated Arabidopsis transformation for silencing PXN and PNC expression. Vector maps: section 7.6.2.

Name	Initial vector	Insert	Reference
pKB67	pKB65	pUBQ10::amiR- <i>PXN</i>	this thesis
pKB68	pMDC7	pLexA::amiR- <i>PXN</i>	this thesis
pMSU98	pART27	p35S::siR- <i>PNC1/2</i>	Linka <i>et al.</i> (2008b)

Name	Initial vector	Insert	Reference
pMSU253	pBIN-19	pAlcA::siR- <i>PNC1/2</i>	Linka <i>et al.</i> (2008b)

### 2.3.9 Generation of PXN over-expression lines

PXN coding sequence was amplified using primers KB6/10 (1016 bp) and inserted into pUT Kan vector via PstI for PXN over-expression under the control of the UBQ10 promoter (pUBQ10::PXN; pKB52; Vector map: section 7.6.3). This construct was used for Arabidopsis WT, *pxn-1*, *pxn-2*, and *pxn-3* transformation and homozygous lines were selected (section 2.3.3).

**Table 2.11 Oligonucleotides used for creating PXN over-expression construct**

Primer used for amplifying PXN coding sequence. Restriction sites are underlined.

Name	Enzyme	5'-3' sequence	Purpose
KB6	PstI	CACAC <u>CTGCAGCAT</u> GGCGGACGCTTTGAT	PXN
KB10	PstI	GTGTG <u>CTGCAGT</u> TAGCTAGAGGTAGCGTT TGAGAGC	PXN

### 2.3.10 PXN promoter GUS analysis

The PXN promoter region was amplified using primers KB1/KB3 (3050 bp) and cloned via Gateway BP-reaction into pDONR207 vector using BP-clonase (Gateway Technology, Invitrogen). LR-reaction using LR-clonase (Gateway Technology, Invitrogen) was performed with pBI121 to fuse the PXN promoter region to the  $\beta$ -glucuronidase (GUS) reporter gene (pKB49; Vector map: section 7.6.4). Agrobacteria-mediated transformation of Arabidopsis WT plants with pPXN::GUS (pKB49) was done and homozygous lines were selected according to section 2.3.3. GUS-staining was performed as previously described (Rosar *et al.*, 2012).

**Table 2.12 Oligonucleotides used for creating a PXN promoter GUS construct**

Primer used for amplifying the PXN promoter region.

Name	5'-3' sequence	Purpose
KB1	GGGGACAAGTTTGTACAAAAAAGCAGGCTCGCTGTGG AATTCATTAA	PXN Promoter
KB3	GGGGACCACTTTGTACAAGAAAGCTGGGTGATTTCTA TATTCCAACACCAAC	PXN Promoter

### 2.3.11 Transient expression of YFP fusions in tobacco

For the expression of mutated PXN protein (section 2.4.4), tagged at the N-terminus with YFP, were the PXN coding sequences amplified using primers KB104/KB106 (PXN and PXN S155: 1055 bp; PXN  $\Delta$ loop: 974 bp). The PCR products were introduced via BP reaction into pDONR207 and subsequent fused N-terminal to YFP by LR reaction with pUBN-YFP vector

(Gateway technology, Invitrogen). *Nicotiana benthamiana* or *N. tabaccum* leaves (Table 2.13) were infiltrated with corresponding constructs (Table 2.15) using agrobacteria (Romeis *et al.*, 2001). The infiltrated leaves were analyzed with a Zeiss Laser scanning microscope 780 (Zeiss, Oberkochen, Germany) one to five days after co-infiltration. Excitation line 514 nm (YFP) and 405 nm (CFP) and a band-pass filter of 516-621 nm were used for imaging. Digital images were processed using the LSM Image Browser 4.2 (Zeiss).

**Table 2.13 Tobacco plants used for transient transformation**

Tobacco plants used for transient expression of plant expression vectors, mediated by infiltration of agrobacteria.

Line	Stable transformed	Reference
<i>Nicotiana benthamiana</i>	/	/
<i>Nicotiana tabacum</i>	CFP-SKL	Zhang <i>et al.</i> (2011)

**Table 2.14 Oligonucleotides used for cloning YFP-PXN fusion protein**

Primer used for amplification of PXN for N-terminal YFP fusion.

Name	5'-3' sequence	Purpose
KB104	GGGGACAAGTTTGTACAAAAAAGCAGGCTTCATGGCGGA CGCTTTGATCAAT	PXN YFP-fusion
KB106	GGACCACTTTGTACAAGAAAGCTGGGTCTTAGCTAGAGG TAGCGTTTGAGAGCAAC	PXN YFP-fusion

**Table 2.15 Plasmids used for co-localization**

Plant expression vectors for transient expression in tobacco leaves mediated by agrobacteria infiltration.

\* Jan Wiese, HHU Düsseldorf, Germany. Vector maps: section 7.6.5.

Name	Initial vector	Insert	Reference
pMSU205	pCAMBIA3301	p35S::PNC1-YFP	Linka <i>et al.</i> (2008b)
pMSU206	pCAMBIA3301	p35S::PNC2-YFP	Linka <i>et al.</i> (2008b)
pMSU266	pCAMBIA3301	p35S::YFP-PXN	Linka <i>et al.</i> (2008b)
pKB109	pUBN-YFP	pUBQ10::YFP-PXN S155A	this thesis
pKB110	pUBN-YFP	pUBQ10::YFP-PXN S155C	this thesis
pKB111	pUBN-YFP	pUBQ10::YFP-PXN S155D	this thesis
pKB112	pUBN-YFP	pUBQ10::YFP-PXN $\Delta$ loop	this thesis
pJW20	pUBC-YFP	pUBQ10::PMP22-YFP	J. Wiese*
pJW22	pUBC-YFP	pUBQ10::PMP22 like-YFP	J. Wiese*
ALDP-YFP	pCAMBIA1300	p35S::ALDP-YFP	Zhang <i>et al.</i> (2011)

Name	Initial vector	Insert	Reference
ALDR-YFP	pCAMBIA1300	p35S::ALDR-YFP	Zhang <i>et al.</i> (2011)
pCAMBIA 1300-H2B-AtPex19-1	pCAMBIA1300	p35S::NLS-PEX19.1	Zhang <i>et al.</i> (2011)
CFP-PTS1	pPZP211	p35S::CFP-PTS1	Linka <i>et al.</i> (2008b)

### 2.3.12 Fatty acid analysis

Fatty acids content of Arabidopsis seedlings were analyzed by fatty acid methyl ester (FAME) analysis according to Browse *et al.* (1986) and Bernhardt *et al.* (2012a). The fatty acid 17:0 was used as an internal standard to enable quantification.

### 2.3.13 Staining of lipid bodies

Lipid bodies of four-day-old etiolated seedlings were stained with Nile red (Invitrogen). A 5 mg/mL stock solution of Nile red dissolved in acetone was diluted in water to a final concentration of 1 µg/mL. Seedlings were incubated for 5 min in the solution and washed twice with water (Bernhardt *et al.*, 2012a). Images were recorded with a Zeiss laser scanning microscope 510 Meta (Zeiss; excitation, 488 nm; emission, 530–600 nm). Digital images were processed using the LSM Image Browser 4.2 (Zeiss).

### 2.3.14 Transmission electron microscope pictures

Cotyledons of five-day-old seedlings grown in continuous darkness were used for TEM analysis. After fixation in 0.1 M phosphate buffer (pH 7.4) and 2.5% glutaraldehyde for 2 h, the samples were incubated in 2% osmium tetroxide for 1 h and in 2% uranyl acetate for 30 min. Following treatment was performed as described in Richard *et al.* (2009).

### 2.3.15 NAD<sup>+</sup> level measurement of Arabidopsis seedlings

Total NAD<sup>+</sup> concentration of four-day-old WT and *pxn-1* seedlings grown under short-day condition (8 h light/ 16 h dark cycle; 22/18°C) were measured with an endpoint assay using phenazine ethosulfate (PES) and 3-(4,5-dimethylthiazolyl-2)-2,5-diphenyltetrazolium bromide (MTT) according to Gibon and Larher (1997) and Trippelsdorf (2012).

## 2.4 Biochemistry of recombinant protein

### 2.4.1 Two-step protein expression using wheat germ extract

*In vitro* cell-free expression using wheat germ extract (WGE) was performed using a two-step protein expression system with independently transcription and translation reaction (CellFree Science). Recombinant proteins, such as PXN-His and the mutated versions (S155A,

S155C, S155D, and  $\Delta$ loop; section 2.4.4), NDT1-His, NDT2-His, PNC1-His, and PNC2 were expressed according to Bernhardt *et al.* (2012a). For C-terminal His-tag fusion of the target proteins, the vector pNL22, a derivative of the pEU3a vector, was used (CellFree Sciences, (Bernhardt *et al.*, 2012a). Coding sequences were amplified by PCR using the following primer pairs: KB37/KB38 (NDT1, 960 bp, pKB73) and KB40/KB41 (NDT2, 1113 bp, pKB75). PCR products were inserted via NcoI/BamHI into pNL22. PNC1 and PXN in pNL22 was used as described in Bernhardt *et al.* (2012a). PNC2 in pEU3a vector were provided by Sarah Vigelius (Vigelius, 2009). Cloning strategy of modified PXN versions, see section 2.4.4.

**Table 2.16 Oligonucleotides used for cloning vectors for two-step protein WGE expression**

Primers used for amplification of NDT1 and NDT2 coding sequences and for *in vitro* transcription. Restriction sites are underlined.

Name	Enzyme	5'-3' sequence	Purpose
KB37	NcoI	CACAC <u>CC</u> CATGGGAATGTCCGCTAATTCTC ATCCTCCTAATTC	NDT1 WGE
KB38	BamHI	GTGTGGGATCC <u>A</u> AGTATAGAGCTTTGCTC AGAAGGTATATGAGTG	NDT1 WGE, yeast
KB40	NcoI	CACAC <u>CC</u> CATGGGAATGATTGAACATGGGA ACTCTACCTTTG	NDT2 WGE
KB41	BamHI	GTGTGGGATCC <u>T</u> TTGCTTCCAAGAGGGAT ATGGG	NDT2 WGE, yeast
P73	/	CACATACGATTTAGGTGACACTATAGAA	WGE
P74	/	GATAATCTCATGACCAAATCCCTTA	WGE

**Table 2.17 Plasmids used for *in vitro* two-step WGE expression**

Plasmids used for recombinant protein expression using two-step WGE expression system. \* Dr. Nicole Linka, HHU Düsseldorf, Germany. Vector maps: section 7.6.6.

Name	Initial vector	Insert	Reference
pMSU356	pNL22	pSP6::PNC1-His	Bernhardt <i>et al.</i> (2012a)
pMSU358	pEU3a	pSP6::PNC2	Vigelius (2009)
pMSU361	pEU3a	pSP6::PXN	N. Linka*
pMSU362	pNL22	pSP6::PXN-His	Bernhardt <i>et al.</i> (2012a)
pKB73	pNL22	pSP6::NDT1-His	Bernhardt <i>et al.</i> (2012a)
pKB75	pNL22	pSP6::NDT2-His	Bernhardt <i>et al.</i> (2012a)
pKB81	pMSU362	pSP6::PXN-His S155A	this thesis
pKB82	pMSU362	pSP6::PXN-His S155C	this thesis
pKB83	pMSU362	pSP6::PXN-His S155D	this thesis



Name	Initial vector	Insert	Reference
pKB86	pMSU362	pSP6::PXN-His $\Delta$ loop	this thesis

## 2.4.2 One-step protein expression using wheat germ extract

One-step cell-free protein expression using a transcription/translation coupled WGE system (5PRIME) was performed to synthesize recombinant protein of PXN-His and the mutated PXN versions (S155A, S155C, S155D, and  $\Delta$ loop), PNC1-His, PNC2-His, PMP22-His, mitoPMP22-His, CTS-FL-His, CTS-N-His, CTS-C-His, and MEP1-His for PEX19 pull-down assay (section 2.5). Gene specific primers for PXN, PXN S155A, PXN S155C, PXN S155D (KB58/KB111, 1017 bp), PXN  $\Delta$ loop (KB58/KB111, 936 bp), PNC1 (KB112/113, 984 bp), and PNC2 (KB114/KB115, 984 bp) were used for PCR based amplification and the coding sequence was introduced via NcoI/XhoI into pIVEX1.3 vector (5PRIME) for C-terminal His-tag fusion. pIVEX1.3 vectors carrying coding sequences of PMP22-His, mitoPMP22-His, CTS-FL-His, CTS-N-His, CTS-C-His, and MEP1-His were provided by Jan Wiese (HHU Düsseldorf, Germany), Thea Pick (HHU Düsseldorf, Germany), and Dr. Frederica L. Theodoulou (Rothamsted Research, UK; Nyathi *et al.* (2012)). Recombinant protein expression was performed according to the RTS 100 Wheat Germ CECF Kit manual (5PRIME).

**Table 2.18 Oligonucleotides used for cloning of one-step WGE expression vectors**

Primers used for amplification of PXN, PNC1 and PNC2 coding sequences. Restriction sites are underlined.

Name	Enzyme	5'-3' sequence	Purpose
KB58	NcoI	CACAC <u>CC</u> ATGGGAATGGCGGACGCTTTGATCAAT	PXN WGE
KB111	XhoI	GTGTG <u>CTCG</u> AGGCTAGAGGTAGCGTTTGAGAGCAACA	PXN WGE
KB112	NcoI	CACAC <u>CC</u> ATGGGTGTCGATTTGGAATC	PNC1 WGE
KB113	XhoI	GTGTG <u>CTCG</u> AGAGGACTTCTTAACTTACCCTTTGTGTTTGT	PNC1 WGE
KB114	NcoI	CACAC <u>CC</u> ATGGGTGTTGATTTGGATTTG	PNC2 WGE
KB115	XhoI	GTGTG <u>CTCG</u> AGGTCTGGACTTTTCAATCTAGCCTTTGTG	PNC2 WGE

**Table 2.19 Plasmids used for *in vitro* one-step WGE expression**

Plasmids used for expression of recombinant protein using one-step WGE expression system. \*<sup>1</sup> Dr. Frederica L. Theodoulou, Rothamsted Research, UK. \*<sup>2</sup> Jan Wiese, HHU Düsseldorf, Germany. \*<sup>3</sup> Thea Pick, HHU Düsseldorf, Germany. Vector maps: section 7.6.7.

Name	Initial vector	Insert	Reference
pKB120	pIVEX1.3	pT7::PNC1-His	this thesis
pKB121	pIVEX1.3	pT7::PNC2-His	this thesis

Name	Initial vector	Insert	Reference
pKB122	pIVEX1.3	pT7::PXN-His	this thesis
pKB123	pIVEX1.3	pT7::PXN-His S155A	this thesis
pKB124	pIVEX1.3	pT7::PXN-His S155C	this thesis
pKB125	pIVEX1.3	pT7::PXN-His S155D	this thesis
pKB126	pIVEX1.3	pT7::PXN-His $\Delta$ loop	this thesis
pIVEX_CTS-FL	pIVEX1.3	pT7::CTS-FL-His	F. Theodoulou <sup>*1</sup>
pIVEX_CTS-N	pIVEX1.3	pT7::CTS-N-His	Nyathi <i>et al.</i> (2012)
pIVEX_CTS-C	pIVEX1.3	pT7::CTS-C-His	Nyathi <i>et al.</i> (2012)
pHHU120	pIVEX1.3	pT7::PMP22-His	J. Wiese <sup>*2</sup>
pJW110	pIVEX1.3	pT7::mitoPMP22-His	J. Wiese
pIVEX_MEP	pIVEX1.3	pT7::MEP1-His	T. Pick <sup>*3</sup>

### 2.4.3 Protein expression in yeast

PXN-His and Ant1p-His were expressed in *Saccharomyces cerevisiae* strain INVSc1 (genotype: *MATa his3D1 leu2 trp1-289 ura3-52*; Invitrogen). PXN-His (pMSU219) and Ant1p-His (pMSU222) expression constructs were provided by Dr. Nicole Linka (HHU Düsseldorf, Germany). Galactose induced protein expression and isolation of total yeast membranes was performed according to Linka *et al.* (2008a).

**Table 2.20 Plasmids used for protein expression in yeast**

Plasmids used for galactose induced protein expression of PXN-His and Ant1p-His in yeast. \* Dr. Nicole Linka, HHU Düsseldorf, Germany.

Name	Initial vector	Insert	Reference
pMSU219	pNL14	pGAL::PXN-His	N. Linka*
pMSU222	pNL14	pGAL::Ant1p-His	N. Linka*

### 2.4.4 Site-directed mutagenesis of PXN S155 and PXN loop deletion

Mutated versions of the PXN protein were generated using the *in vitro* QuickChange II Site-Directed Mutagenesis (SDM) system according to the manufacture manual (Agilent Technologies). Primers were designed using the QuickChange Primer Design Program (Table 7.5; Agilent Technologies). The two-step cell-free WGE expression system was performed to produce recombinant PXN-His protein. Therefore, the expression vector pMSU362 was used as template and PXN-His Serine155 was exchanged to alanine (S155A;

KB49/KB50, 4843 bp; pKB81), cysteine (S155C; KB51/KB52, 4843 bp; pKB82), and aspartate (S155D; KB53/KB54, 4843 bp; pKB83). For PXN loop deletion was the PXN coding sequence amplified using PXN specific primers (KB6/KB10, 1016 bp) and sub-cloned into pJET1.2. This construct was linearized via NdeI (cutting site in the loop region) and the whole vector was amplified without the loop region using primers KB56 and KB57 (3912 bp). After ligation of the PCR product using T4 ligase (Fermentas) the vector was sequenced (GATC Biotech). At the ligation site, two nucleotides were missing that were introduced using *in vitro* QuickChange II Site-Directed Mutagenesis Kit (Agilent Technologies) and the primers KB60 and KB61 (3912 bp). The coding region of PXN  $\Delta$ loop was amplified using primers KB58 and KB59 (936 bp). The PCR product was inserted via NcoI/BamHI into pNL22 for two-step WGE expression (pKB86).

**Table 2.21 Oligonucleotides used for generating of mutated PXN proteins**

Primers used for cloning and site-directed mutagenesis of mutated PXN proteins for two-way WGE expression. Restriction sites are underlined

Name	Enzyme	5'-3' sequence	Purpose
KB6	PstI	CACAC <u>CTGCAG</u> CATGGCGGACGCTTTGAT	PXN
KB10	PstI	GTGTGCTGCAGTTAGCTAGAGGTAGCGTT TGAGAGC	PXN
KB49	/	CAGCGGCCCGAGGCTCCTTCTTCTAAT GCA	S155A SDM
KB50	/	TGCATTAGAAGAAGGAGCCTCGGGGGCC GCTG	S155A SDM
KB51	/	AACAGCGGCCCGAGTGCCCTTCTTCTA ATGC	S155C SDM
KB52	/	GCATTAGAAGAAGGGCACTCGGGGGCCG CTGTT	S155C SDM
KB53	/	CAAACAGCGGCCCGAGGATCCTTCTTC TAATGCAGAAG	S155D SDM
KB54	/	CTTCTGCATTAGAAGAAGGATCCTCGGGG GCCGCTGTTTG	S155D SDM
KB56	/	TATGGGACCTTTAATACGATTCGAGAGG	PXN $\Delta$ loop
KB57	/	TCTGTGGGTCTGCATACGCGTAAC	PXN $\Delta$ loop
KB58	NcoI	CACAC <u>CCATGGG</u> AATGGCGGACGCTTTGA TCAAT	PXN $\Delta$ loop WGE
KB59	BamHI	GTGTG <u>GGATCC</u> GCTAGAGGTAGCGTTTGA GAGCAACA	PXN $\Delta$ loop WGE
KB60	/	CGTATGCAGACCCACAGATATGGGACCTT TAATACGA	PXN $\Delta$ loop SDM
KB61	/	TCGTATTAAAGGTCCCATATCTGTGGGTCT GCATACG	PXN $\Delta$ loop SDM

#### 2.4.5 Reconstitution of recombinant protein into liposomes and transport activity measurements using radioactive labelled substrates

The *in vitro* expressed recombinant proteins (section 2.4.1) were reconstituted into liposomes by the freeze-thaw procedure (Kasahara and Hinkle, 1976). The liposomes were made of 3% (w/v) phospholipids. In case of the reconstitution of the mitochondrial NDT2 carrier, liposomes consist of 2.85% (w/v) phospholipids and 0.15% (w/v) cardiolipin. [ $\alpha$ - $^{32}$ P]-NAD<sup>+</sup> (Perkin Elmer) uptake assays and determination of kinetic constants were performed as described in Bernhardt *et al.* (2012a). Modified uptake assays with radioactive labelled [ $\alpha$ - $^{32}$ P]-ATP (Hartmann Analytic) were performed according to Linka *et al.* (2008b). 150 mM sodium acetate (pH 7.6) was used for equilibration of the Dowex AG1-X8 columns (acetate form, 100–200 mesh; Bio-Rad) and for elution of the flow-through containing the proteoliposomes. Analyses of the obtained data were performed using GraphPad PRISM 5.0d and as described in Bernhardt *et al.* (2012a).

#### 2.5 PEX19 interaction studies

*In vitro* PEX19 pull-down assay was performed as described in Nyathi *et al.* (2012) using recombinant transport proteins, expressed in one-step cell-free WGE expression system (section 2.4.2) and recombinant PEX19 protein, expressed in *E. coli* strain BL21 (DE3) (genotype: F<sup>-</sup> ompT gal dcm lon hsdS<sub>B</sub>(r<sub>B</sub><sup>-</sup> m<sub>B</sub><sup>-</sup>)  $\lambda$ (DE3 [lacI lacUV5-T7 gene 1 ind1 sam7 nin5]; Novagen, Darmstadt, Germany). *In vivo* PEX19 mis-localization assay was done according to Zhang *et al.* (2011). PEX19 binding site prediction was performed using PEX19 binding site predictor (Table 7.5).

#### 2.6 Accession numbers

DNA and protein sequences were received from the Aramemnon database, *Saccharomyces* Genome Database (SGD) and human gene database (Table 7.5) with the accession numbers At2g39970 (PXN), At3g05290 (PNC1), At5g27520 (PNC2), At4g04470 (PMP22), At4g14305 (PMP22 like), At3g24570 (mitoPMP22), At2g47490 (NDT1), At1g25380 (NDT2), At4g39850 (PXA/CTS), At2g22780 (pMDH1), At5g09660 (pMDH2), At1g68010 (HPR1), At1g79870 (HPR2), At1g12550 (HPR3), At3g06860 (MFP2), At4g29010 (AIM1), At1g32080 (MEP1), At3g18780 (ACTIN2), YPR128C (Ant1p), YIL006W (Ndt1p), YEL006W (Ndt2p), HsABCD1 (ADLP), and HsABCD2 (ALDR). Amino acid sequences were aligned using CLUSTALW and the alignment layout was performed with GENEDOC (Table 7.5).

### 3 Results

Peroxisomes play an essential role in different metabolic processes and share many reactions with other cell compartments. To connect the peroxisomal metabolism of the other organelles, all metabolites, cofactors and other molecules have to exchange across the peroxisomal membrane (Linka and Esser, 2012). The peroxisomal membrane is impermeable for “bulky” solutes larger than 300 Da (section 1.5.1; Antonenkov and Hiltunen, 2006). As nicotinamide adenine dinucleotide ( $\text{NAD}^+$ ; 663 Da) is exclusively synthesized in the cytosol and as the peroxisomal membrane is impermeable for  $\text{NAD}^+$ , the cofactor has to be imported into peroxisomes to maintain the function of  $\text{NAD}^+$ -dependent enzymes (Antonenkov and Hiltunen, 2006; Noctor *et al.*, 2006; Hashida *et al.*, 2009). The aims of this thesis were to identify the peroxisomal  $\text{NAD}^+$  carrier in Arabidopsis using a candidate gene approach and characterize its biochemical and physiological function.

#### 3.1 Homology among At2g39970 and other members of the mitochondrial carrier family

A candidate for the peroxisomal  $\text{NAD}^+$  carrier (PXN) is At2g39970 (section 1.5.3). PXN is a member of the mitochondrial carrier family (MCF) and encodes a protein of 331 amino acids with a calculated molecular mass of 36.2 kDa. PXN consists of six transmembrane-spanning domains and three mitochondrial energy transfer signature domains (Figure 3.1), which are conserved in the MCF (Picault *et al.*, 2004; Palmieri *et al.*, 2011). PXN contains a unique expanded hydrophilic loop region between transmembrane domain three and four (Figure 3.1). The peroxisomal localization of PXN was confirmed by different approaches (Figure 3.30; section 1.5.3; Fukao *et al.*, 2001; Eubel *et al.*, 2008; Linka *et al.*, 2008b; Reumann *et al.*, 2009; Wilkinson, 2009).

A phylogenetic tree (Figure 3.2), based on amino acid sequences from members of the MCF from Arabidopsis, yeast, and human was generated. The peroxisomal adenine nucleotide transporter PNC1, PNC2 (section 1.5.2; Arai *et al.*, 2008; Linka *et al.*, 2008b), and Ant1p (Palmieri *et al.*, 2001) clustered in one group. A second cluster consists of PXN and chloroplastic, mitochondrial, and peroxisomal  $\text{NAD}^+$  carrier NDT1, NDT2 (Palmieri *et al.*, 2009), Ndt1p, Ndt2p (Todisco *et al.*, 2006), and SLC25A17 (Agrimi *et al.*, 2012a). PXN exhibits strong amino acid homology to  $\text{NAD}^+$  carrier like NDT1 (27% identity), NDT2 (23% identity), Ndt1p (21% identity), Ndt2p (22% identity), and SLC25A17 (29% identity; Figure 3.2, Figure 3.1). Even if PXN is a close homologue to the adenosine triphosphate (ATP) transporter PNC1 (25% identity), PNC2 (23% identity), and Ant1p (23% identity; Figure 3.2; Figure 3.1), it was shown that PXN exhibited another unknown substrate specificity (section 1.5.3; Linka *et al.*, 2008b; Wilkinson, 2009).

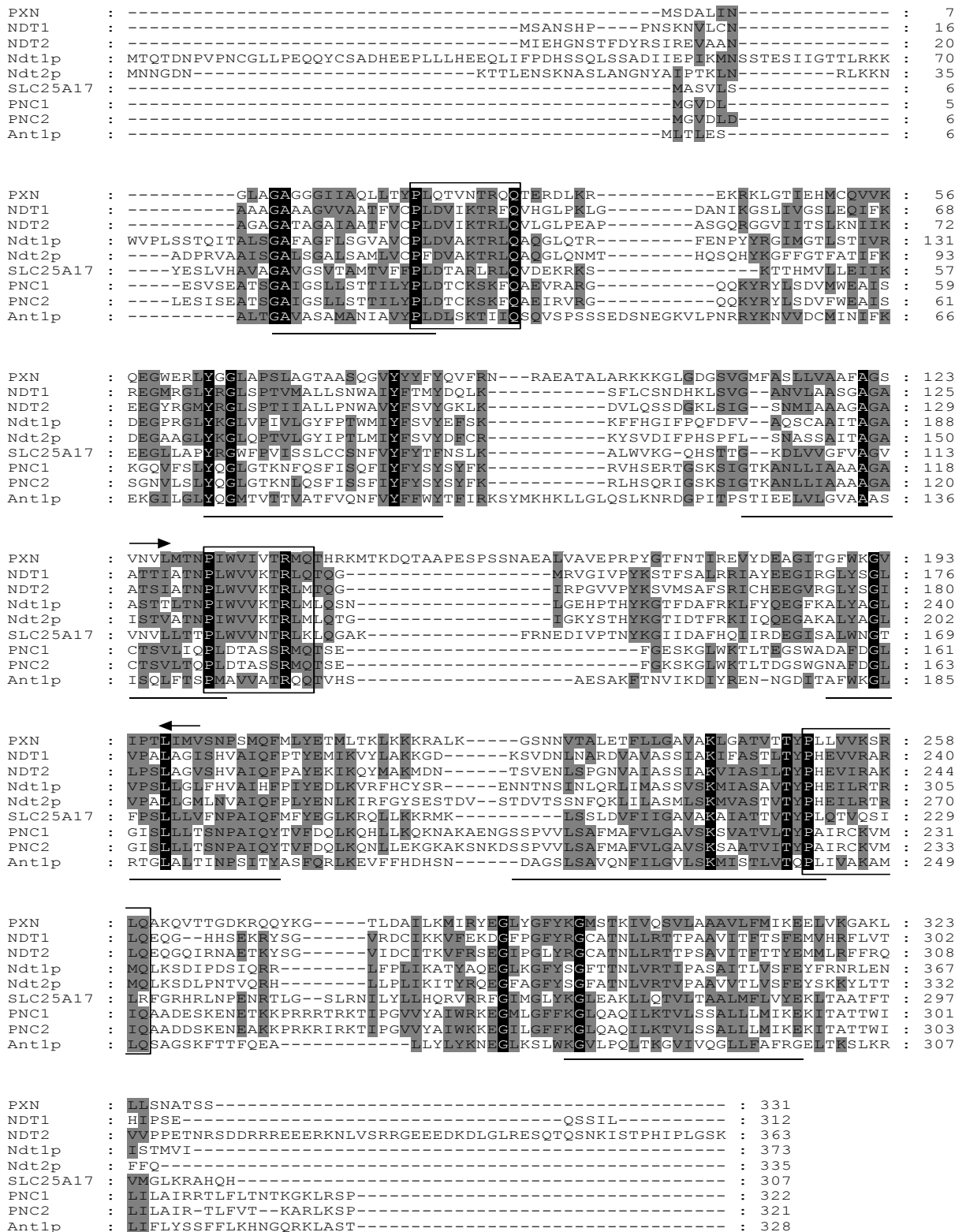


**Figure 3.1** Amino acid sequence homology of PXN to NAD<sup>+</sup> and ATP carrier of the MCF

An amino acid alignment of PXN and known chloroplastic, mitochondrial, and peroxisomal NAD<sup>+</sup> carriers and peroxisomal ATP carriers from Arabidopsis, yeast and human is displayed. Black shading indicates identical amino acid residues in all nine sequences, whereas grey shading indicates similar amino acid residues in at least five sequences. The mitochondrial energy transfer signature domains are boxed and the six predicted transmembrane-spanning domains are underlined. Arrows mark the region of the hydrophilic loop between the third and fourth transmembrane domain that was used for a PXN-specific antibody.

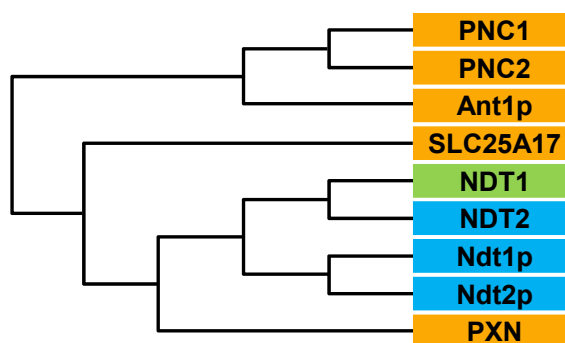


**Figure 3.2 Phylogenetic tree of the NAD<sup>+</sup> and ATP carriers of the MCF of Arabidopsis, yeast and human**

Phylogenetic tree based on amino acid sequences of ATP transporter (Arabidopsis PNC1 and PNC2, and yeast Ant1p), NAD<sup>+</sup> carrier (human SLC25A17, Arabidopsis NDT1 and NDT2, and yeast Ndt1p and Ndt2p), and the putative Arabidopsis peroxisomal NAD<sup>+</sup> carrier, PXN. Localization: orange, peroxisome; green, chloroplast; blue, mitochondrion. The phylogenetic tree was created using [www.phylogeny.fr](http://www.phylogeny.fr) (Dereeper *et al.*, 2008).

### 3.2 Biochemistry of recombinant PXN protein

To examine the transport function of PXN, recombinant protein was expressed using a cell-free wheat germ expression (WGE) system and uptake studies were performed using radioactively labelled substrates.

#### 3.2.1 NAD<sup>+</sup> transport activity of recombinant PXN protein

As PXN exhibits close sequence homology to known peroxisomal, chloroplastic, and mitochondrial NAD<sup>+</sup> carrier from Arabidopsis, yeast and human (section 3.1), the uptake of radioactively labelled [ $\alpha$ -<sup>32</sup>P]-NAD<sup>+</sup> was tested using an *in vitro* transport system (section 0). Cell-free expressed PXN protein (section 2.4.1), fused at the C-terminus to a His-tag, was detected with the expected calculated mass of 37.3 kDa by immunoblot analysis using an anti-His antibody, whereas recombinant PXN protein without a His-tag was not detectable (Figure 3.3 B).

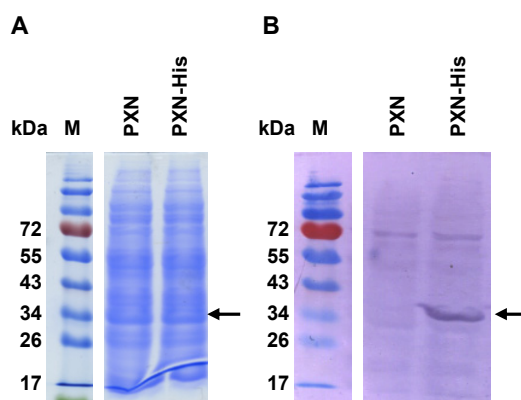


**Figure 3.3 Recombinant PXN protein expressed in the cell-free WGE system**

(A) Coomassie-stained SDS-PAGE and (B) immunoblot analysis of recombinant expressed PXN protein. In contrast to PXN without His-tag, PXN-His protein could be detected using an anti-His antibody. The arrow indicates the expressed PXN-His protein with the calculated mass of 37.3 kDa. M, marker proteins.

Artificial lipid bodies, called liposomes, were reconstituted with recombinant PXN and PXN-His protein and preloaded with 30 mM NAD<sup>+</sup>, or without internal substrate (section 0). 125 μM radioactively labelled [ $\alpha$ -<sup>32</sup>P]-NAD<sup>+</sup> was offered outside and the time-dependent uptake rate of [ $\alpha$ -<sup>32</sup>P]-NAD<sup>+</sup> into the proteoliposomes was measured (Figure 3.4 A-D; section 0). The reconstituted PXN protein mediated high NAD<sup>+</sup> uptake activities in exchange with NAD<sup>+</sup> (Figure 3.4 A and B). In the absence of a counter-exchange substrate no uptake activity was measured (Figure 3.4 A and B). Uptake activities of C-terminally His-tagged protein were 1.6-fold increased in comparison to recombinant PXN protein without His-tag (Figure 3.4; A and B). The subsequent uptake assays were performed with recombinant PXN-His protein, if not otherwise stated. Reconstituted WGE without recombinant protein and heat-inactivated PXN-His protein was used as control for the uptake measurements. The controls did not mediate NAD<sup>+</sup> uptake in the absence or presence of NAD<sup>+</sup> (Figure 3.4 C and D). *In vitro* expressed PXN-His protein showed NAD<sup>+</sup> uptake in an antiport mechanism, which followed first-order rate kinetics with an equilibrium plateau ( $V_{max}$ ) of  $1.3 \pm 0.3 \mu\text{mol NAD}^+ \text{mg protein}^{-1}$  and an initial rate of  $0.03 \pm 0.002 \mu\text{mol NAD}^+ \text{mg protein}^{-1}$  (Figure 3.4 A).

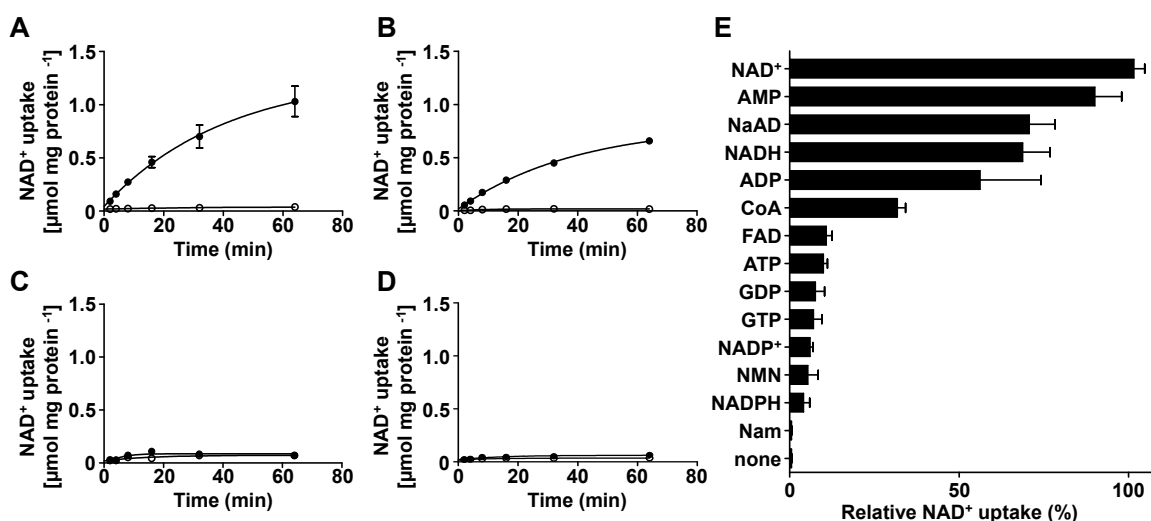


**Figure 3.4** [ $\alpha$ -<sup>32</sup>P]-NAD<sup>+</sup> uptake activity and substrate specificity of recombinant PXN protein

(A-D) [ $\alpha$ -<sup>32</sup>P]-NAD<sup>+</sup> exchange with NAD<sup>+</sup> (filled symbols) or without counter-exchange substrate (open symbols). Recombinant PXN protein (A) with C-His tag and (B) without His-tag mediated NAD<sup>+</sup> uptake activity in exchange with NAD<sup>+</sup> and not without internal substrates. (C) Reconstituted WGE without expressed recombinant protein and (D) inactivated PXN-His protein showed no NAD<sup>+</sup> uptake activity. The data from (A) and (C) represents the arithmetic means  $\pm$  SEs of three independent experiments. Experiment (B) and (D) was performed once. (E) Substrate specificity of recombinant PXN-His protein was measured by [ $\alpha$ -<sup>32</sup>P]-NAD<sup>+</sup> uptake of proteoliposomes preloaded with different substrates (20 mM). The relative NAD<sup>+</sup> uptake rates in relation to NAD<sup>+</sup>/NAD<sup>+</sup> homo-exchange were calculated. The data represent the arithmetic means  $\pm$  SEs of three independent experiments.

To identify the *in vitro* exchange substrate, the substrate specificity (s. spec.) of PXN was investigated using proteoliposomes preloaded with 14 different putative substrates (20 mM). The initial velocity was measured after starting the uptake experiment with 125 μM radioactively labelled [ $\alpha$ -<sup>32</sup>P]-NAD<sup>+</sup> (Figure 3.4 E; section 0). The NAD<sup>+</sup> uptake rate of



NAD<sup>+</sup>/NAD<sup>+</sup> homo-exchange was set to 100% and was compared with relative NAD<sup>+</sup> uptake values of the other hetero-exchange uptake rates. The Michaelis constant ( $K_M$ ) of PXN-His was determined by measuring time-dependent uptake of different external NAD<sup>+</sup> concentrations (10  $\mu$ M – 2 mM) and an internal concentration of 30 mM NAD<sup>+</sup> (section 0). For the determination of the competitive inhibitor constant ( $K_i$ ), the NAD<sup>+</sup>/NAD<sup>+</sup> homo-exchange was measured with increasing substrate concentrations (16  $\mu$ M – 8 mM), offered outside of proteoliposomes preloaded with 30 mM NAD<sup>+</sup> (section 0).

**Table 3.1  $K_M$  (NAD<sup>+</sup>) and  $K_i$  values of recombinant PXN-His protein for various metabolites**

[ $\alpha$ -<sup>32</sup>P]-NAD<sup>+</sup> uptake activity of reconstituted PXN-His protein was measured. The Michaelis constant ( $K_M$ ) for NAD<sup>+</sup> was measured using different external NAD<sup>+</sup> concentrations (10  $\mu$ M – 2 mM) and an equal internal NAD<sup>+</sup> concentration (30 mM). The competitive inhibition constant ( $K_i$ ) of [ $\alpha$ -<sup>32</sup>P]NAD<sup>+</sup> uptake (125  $\mu$ M) was analyzed with increasing inhibitor concentrations (16  $\mu$ M – 8 mM). The data represent the arithmetic means  $\pm$  SEs of three independent experiments.

	substrate	$\mu$ M
$K_M$	NAD <sup>+</sup>	246 $\pm$ 64
$K_i$	NAD <sup>+</sup>	352 $\pm$ 1
$K_i$	NADH	150 $\pm$ 1
$K_i$	NaAD	536 $\pm$ 1
$K_i$	ADP	251 $\pm$ 1
$K_i$	AMP	356 $\pm$ 1
$K_i$	CoA	137 $\pm$ 1

The NAD<sup>+</sup>/NAD<sup>+</sup> homo-exchange mediated by PXN-His exhibited the highest uptake activity (s. spec.: 100  $\pm$  3%;  $K_i$ : 352  $\pm$  1  $\mu$ M NAD<sup>+</sup>). The  $K_M$  constant measured for NAD<sup>+</sup> was 246  $\pm$  64  $\mu$ M. The second highest NAD<sup>+</sup> uptake activity was measured with proteoliposomes preloaded with adenosine monophosphate (AMP; s. spec.: 90  $\pm$  8%;  $K_i$ : 356  $\pm$  1  $\mu$ M NAD<sup>+</sup>). High exchange rates were also observed with the reduced form of NAD<sup>+</sup>, NADH (s. spec.: 69  $\pm$  8%;  $K_i$ : 150  $\pm$  1  $\mu$ M NAD<sup>+</sup>) and adenosine diphosphate (ADP; s. spec.: 56  $\pm$  18%;  $K_i$ : 251  $\pm$  1  $\mu$ M NAD<sup>+</sup>). Nicotinate adenine dinucleotide (NaAD), the precursor of NAD<sup>+</sup> biosynthesis (section 1.4; Noctor *et al.*, 2006; Hashida *et al.*, 2009), mediated high NAD<sup>+</sup> exchange (s. spec.: 71  $\pm$  8%), but had a low inhibitory affect ( $K_i$ : 537  $\pm$  1  $\mu$ M NAD<sup>+</sup>). Recombinant PXN-His mediated the transport of coenzyme A (CoA; s. spec.: 32  $\pm$  3%) with a specific  $K_i$  value of 137  $\pm$  1  $\mu$ M NAD<sup>+</sup>. The  $K_i$  values for flavin adenine dinucleotide (FAD), ATP, guanosine diphosphate (GDP), guanosine triphosphate (GTP), nicotinamide adenosine dinucleotide phosphate (NADP<sup>+</sup>), NADPH, nicotinamide mononucleotide (NMN), and nicotinamide (Nam) were not determined due to the low relative NAD<sup>+</sup> uptake rates (s. spec.: around or less than 10%; Figure 3.4 E).

PXN-His was expressed in *Saccharomyces cerevisiae* (section 2.4.3) to confirm the uptake

results that were mediated by cell-free expressed PXN-His protein. Additionally, it was tested if the yeast peroxisomal ATP transporter Ant1p mediates  $\text{NAD}^+$  transport, as no other peroxisomal MCF-type transporter exists in yeast. PXN-His protein, with a calculated mass of 37.2 kDa and Ant1p (37.4 kDa) protein were detected by immunoblot analysis using anti-His antibody (Figure 3.5).

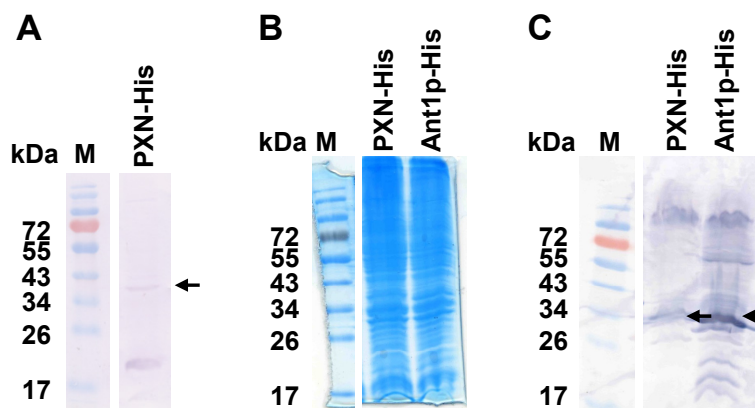


**Figure 3.5 Expression of PXN-His and Ant1p-His in yeast**

(A) PXN-His protein expressed in yeast and detected with anti-His antibody. (B and C) PXN-His and Ant1p-His protein were expressed in yeast. (B) Coomassie-stained SDS-PAGE. (D) Detection of recombinant protein using anti-His antibody. Arrows indicated the expressed proteins with the calculated molecular mass of 37.2 kDa (PXN-His) and 37.4 kDa (Ant1p-His). M, marker proteins.

Heterologously expressed PXN-His protein mediated a time-dependent  $[\alpha\text{-}^{32}\text{P}]\text{-NAD}^+$  uptake in exchange with  $\text{NAD}^+$ , AMP and NADH (Figure 3.6 A and B; Table 3.2).  $\text{NAD}^+/\text{NAD}^+$  homo-exchange was measured with  $50\ \mu\text{M}$   $[\alpha\text{-}^{32}\text{P}]\text{-NAD}^+$  and a different protein batch (Figure 3.5 A and Figure 3.6 A; Table 3.2) as the  $\text{NAD}^+/\text{AMP}$  and  $\text{NAD}^+/\text{NADH}$  hetero-exchange, which were measured with  $150\ \mu\text{M}$   $[\alpha\text{-}^{32}\text{P}]\text{-NAD}^+$  (Figure 3.5 B and C, and Figure 3.6 B; Table 3.2).

**Table 3.2 Kinetic values of  $[\alpha\text{-}^{32}\text{P}]\text{-NAD}^+$  and  $[\alpha\text{-}^{32}\text{P}]\text{-ATP}$  uptake of recombinant PXN-His and Ant1p-His protein expressed in yeast**

The equilibrium plateau ( $V_{\text{max}}$ ) and initial rate was calculated of time-dependent  $[\alpha\text{-}^{32}\text{P}]\text{-ATP}$  ( $150\ \mu\text{M}$ ) and  $[\alpha\text{-}^{32}\text{P}]\text{-NAD}^+$  uptake.  $50\ \mu\text{M}$   $\text{NAD}^+$  was offered for  $\text{NAD}^+/\text{NAD}^+$  homo-exchange and  $150\ \mu\text{M}$   $\text{NAD}^+$  for NADH and AMP hetero-exchange and uniport (w/o, without preloading). Recombinant PXN-His and Ant1p-His protein were expressed in yeast. Proteoliposomes were preloaded with AMP, NADH or without internal substrate. n.d. not determined.

preloading	PXN-His		Ant1p-His			
	nmol $\text{NAD}^+$ mg protein $^{-1}$				nmol ATP mg protein $^{-1}$	
	$V_{\text{max}}$	Initial rate	$V_{\text{max}}$	Initial rate	$V_{\text{max}}$	Initial rate
w/o	6.45	0.094	8.39	0.843	0.90	0.161
AMP	23.74	3.824	9.07	12.759	24.82	4.523
$\text{NAD}^+$	90.30	5.292	n.d.	n.d.	n.d.	n.d.
NADH	25.88	1.289	12.16	5.313	n.d.	n.d.

Yeast expressed Ant1p-His proteins did not catalyze [ $\alpha$ - $^{32}$ P]-NAD $^{+}$  (150  $\mu$ M) hetero-exchange with AMP and NADH, as the transport rates were comparable to the activity values measured with proteoliposomes preloaded without internal substrate (Figure 3.6 C; Table 3.2). [ $\alpha$ - $^{32}$ P]-ATP (150  $\mu$ M) transport activity of heterologously expressed Ant1p-His was measured to test the protein functionality (Figure 3.6 D; Table 3.2). Ant1p-His protein showed high ATP uptake activity in exchange with AMP (Figure 3.6 D; Table 3.2).

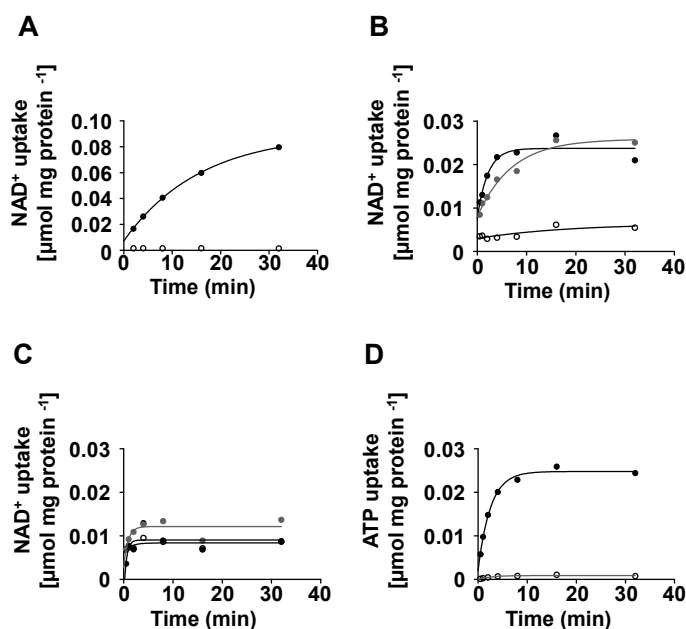


**Figure 3.6 Time-dependent [ $\alpha$ - $^{32}$ P]-NAD $^{+}$  and [ $\alpha$ - $^{32}$ P]-ATP uptake of recombinant PXN-His and Ant1p-His protein expressed in yeast**

(A) Time-dependent [ $\alpha$ - $^{32}$ P]-NAD $^{+}$  (50  $\mu$ M) uptake in exchange with NAD $^{+}$  (filled symbols) was measured of recombinant PXN-His protein. Open symbols: without preloading. (B and C) [ $\alpha$ - $^{32}$ P]-NAD $^{+}$  (150  $\mu$ M) uptake in exchange with AMP (black, filled symbols), NADH (grey, filled symbols), or without counter-substrate (black, open symbols) was measured of proteoliposomes reconstituted with (B) PXN-His, (C) Ant1p-His protein. (D) [ $\alpha$ - $^{32}$ P]-ATP (150  $\mu$ M) uptake was measured of reconstituted Ant1p-His protein in exchange with AMP (filled symbols) or without counter-substrate (open symbols).

### 3.2.2 Comparison of peroxisomal, chloroplastic, and mitochondrial NAD $^{+}$ carrier

The kinetic data and substrate specificity of NAD $^{+}$ /AMP hetero-exchange mediated by PXN-His (s. spec.:  $90 \pm 8\%$ ;  $K_i$ :  $356 \pm 1 \mu$ M NAD $^{+}$ ) were comparable to the chloroplastic (NDT1: s. spec.:  $71\%$ ,  $K_i$ :  $120 \pm 20 \mu$ M NAD $^{+}$ ) and mitochondrial (NDT2: s. spec.:  $73\%$ ,  $K_i$ :  $380 \pm 40 \mu$ M NAD $^{+}$ ; Ndt1p: s. spec.:  $74\%$ ,  $K_i$ :  $980 \pm 90 \mu$ M NAD $^{+}$ ) NAD $^{+}$  carrier from Arabidopsis and yeast (Todisco *et al.*, 2006; Palmieri *et al.*, 2009). In addition, PXN mediated NAD $^{+}$ /NADH (s. spec.:  $69 \pm 8\%$ ;  $K_i$ :  $150 \pm 1.2 \mu$ M NAD $^{+}$ ) and NAD $^{+}$ /CoA (s. spec.:  $32 \pm 3\%$ ;  $K_i$ :  $137 \pm 1.2 \mu$ M NAD $^{+}$ ) hetero-exchange, which is unique for PXN in comparison to the other NAD $^{+}$  carrier (NADH: s. spec.:  $<17\%$ ; CoA: s. spec.:  $<10\%$ ;  $K_i$  values were not determined). The  $K_M$  constant of PXN ( $246 \pm 64 \mu$ M NAD $^{+}$ ) was similar to chloroplastic NDT1 ( $240 \pm 40 \mu$ M NAD $^{+}$ ), mitochondrial NDT2 ( $150 \pm 10 \mu$ M NAD $^{+}$ ) and Ndt1p ( $380 \pm 40 \mu$ M NAD $^{+}$ ; Table 3.3;

Todisco *et al.*, 2006; Palmieri *et al.*, 2009). A comparison of substrate specificity, Michaelis constants ( $K_M$ ) and the inhibitory constants ( $K_i$ ) of plant peroxisomal, chloroplastic, and mitochondrial  $NAD^+$  carrier as well of the yeast mitochondrial  $NAD^+$  carrier are shown in Table 3.3.

**Table 3.3 Comparison of substrate specificity,  $K_M$  and  $K_i$  levels of plant and yeast  $NAD^+$  carrier**

Substrate specificity, Michaelis constants ( $K_M$ ) and the inhibitory constants ( $K_i$ ) of plant peroxisomal (PXN), chloroplastic (NDT1) and mitochondrial (NDT2) as well as yeast mitochondrial (Ndt1p)  $NAD^+$  carrier in comparison. The substrate specificity of  $NAD^+/NAD^+$  homo-exchange was set to 100%. Grey shadowed are the relevant counter substrates. N.d., not determined. Data were obtained from Todisco *et al.* (2006) and Palmieri *et al.* (2009).

	PXN (peroxisomal)	NDT1 (chloroplastic)	NDT2 (mitochondrial)	Ndt1p (mitochondrial)
<b>Substrate specificity [%]</b>				
$NAD^+$	100	100	100	100
NADH	69	14	16	17
NADP	< 10	< 10	< 10	< 10
NADPH	< 10	< 10	< 10	< 10
NaAD	71	44	63	61
NMN	< 10	66	58	22
Nam	< 10	< 10	< 10	< 10
AMP	90	71	73	74
ADP	56	72	77	34
ATP	10	38	29	<10
GDP	< 10	35	47	37
GTP	< 10	19	15	19
FAD	11	21	24	16
CoA	32	< 10	< 10	< 10
none	< 10	< 10	< 10	< 10
<b><math>K_M</math> and <math>K_i</math> values [<math>\mu M NAD^+</math>]</b>				
$K_M (NAD^+)$	246 ( $\pm 64$ )	240 ( $\pm 40$ )	150 ( $\pm 10$ )	380 ( $\pm 40$ )
$K_i (AMP)$	357 ( $\pm 1.3$ )	120 ( $\pm 20$ )	380 ( $\pm 40$ )	980 ( $\pm 90$ )
$K_i (ADP)$	251 ( $\pm 1.6$ )	360 ( $\pm 50$ )	1500 ( $\pm 100$ )	1950 ( $\pm 240$ )
$K_i (NAD^+)$	352 ( $\pm 1.2$ )	n.d.	n.d.	330 ( $\pm 30$ )
$K_i (NADH)$	150 ( $\pm 1.2$ )	n.d.	n.d.	n.d.
$K_i (NaAD)$	537 ( $\pm 1.4$ )	500 ( $\pm 100$ )	1800 ( $\pm 300$ )	1290 ( $\pm 170$ )
$K_i (CoA)$	137 ( $\pm 1.2$ )	n.d.	n.d.	n.d.

In previous studies, NDT1, NDT2, and Ndt1p were expressed in an *Escherichia coli* expression system (Todisco *et al.*, 2006; Palmieri *et al.*, 2009). In this study, the influence of the WGE expression system on the unique  $NAD^+/NADH$  and  $NAD^+/CoA$  hetero-exchange of PXN was analyzed. It was shown before that the *E. coli* expression system is not suitable for PXN expression (Wilkinson, 2009) and therefore the NDT proteins were expressed in the WGE- or yeast expression system.

To test if the plant NDT proteins mediate the exchange of  $NAD^+$  with NADH or CoA, NDT1 and NDT2 were expressed using the WGE expression system (section 2.4.1), reconstituted into liposomes and the uptake of radioactively labelled [ $\alpha$ - $^{32}P$ ]- $NAD^+$  was measured (section 0). *In vitro* expressed C-terminal His-tagged NDT1 protein (35.0 kDa), carrying the chloroplast transit peptide, and NDT2 protein (40.6 kDa) were detected with the

calculated masses by immunoblot analysis using an anti-His antibody (Figure 3.7. A and B). Time-dependent [ $\alpha$ - $^{32}$ P]-NAD<sup>+</sup> (125  $\mu$ M) uptake in the presence or absence of internal NAD<sup>+</sup> (30 mM) was measured (Figure 3.7 C-E).

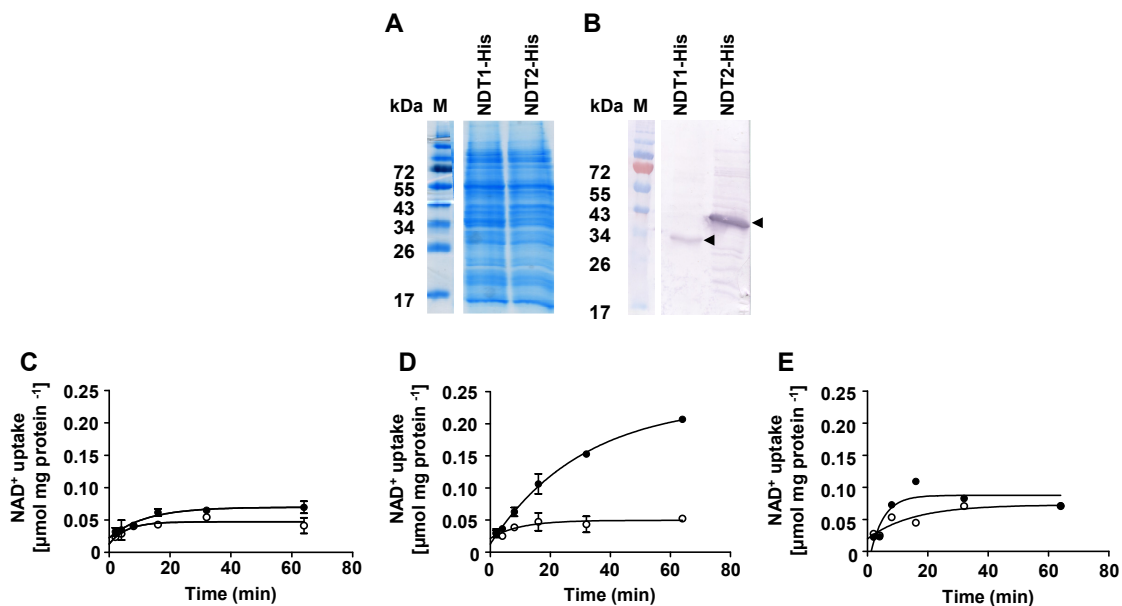


**Figure 3.7** [ $\alpha$ - $^{32}$ P]-NAD<sup>+</sup> uptake activity of recombinant NDT1-His and NDT2-His protein expressed in WGE (A) and (B) C-terminal His-tagged recombinant NDT1 and NDT2 protein were expressed in the WGE system. (A) Coomassie-stained SDS-PAGE. (B) Immunoblot analysis using anti-His antibody detected recombinant NDT1-His (35.0 kDa) and NDT2-His (40.6 kDa) protein with the expected calculated masses, indicated by the arrowheads. (C-E) Time-dependent [ $\alpha$ - $^{32}$ P]-NAD<sup>+</sup> (125  $\mu$ M) uptake was performed with or without 30 mM NAD<sup>+</sup> preloading. NAD<sup>+</sup>/NAD<sup>+</sup> exchange (filled circles) and NAD<sup>+</sup> uniport (without preloading, open circles) was measured of reconstituted (C) NDT1-His, (D) NDT2-His, and (E) WGE. The data represent the arithmetic means  $\pm$  SEs of two independent experiments.

Although NDT1-His protein was expressed using the WGE expression system (Figure 3.7. A and B), no NAD<sup>+</sup> uptake activity was detectable and its uptake rate was comparable with NAD<sup>+</sup> uptake of reconstituted WGE extract (Figure 3.7. C and E). Recombinant NDT2-His protein mediated NAD<sup>+</sup> uptake (Figure 3.7. D), but its transport activity was 10-fold decreased in comparison to recombinant PXN-His protein (Figure 3.4 A). In comparison to WGE, NDT2-His protein mediated NAD<sup>+</sup> homo-exchange and followed first-order rate kinetics with a  $V_{\max}$  of  $0.23 \pm 0.02$   $\mu$ mol NAD<sup>+</sup> mg protein<sup>-1</sup> and an initial rate of  $0.0072 \pm 0.0001$   $\mu$ mol NAD<sup>+</sup> mg protein<sup>-1</sup>. The kinetic rates of NDT2-His were six-fold lower for  $V_{\max}$  and four-fold lower for the initial rate in comparison to PXN-His (section 3.2.1).

### 3.2.3 NAD<sup>+</sup> uptake activity of recombinant PNC1-His and PNC2 protein

Because of the similar structure of NAD<sup>+</sup> and ATP, it was tested if the peroxisomal ATP transporters PNC1 and PNC2 (Linka *et al.*, 2008b) could also mediate NAD<sup>+</sup> transport. Recombinant C-terminal His-tagged PNC1-His protein and PNC2 protein without a His-tag were expressed using the cell-free WGE system (section 2.4.1). Recombinant PNC1-His

protein, with a calculated mass of 36.6 kDa was detected by immunoblot analysis using an anti-His antibody (Figure 3.8 A and B). Cell-free expressed PNC2 protein, with a calculated mass of 35.2 kDa, could not be visualized due to the missing His-tag (Figure 3.8 A and B).

To analyze the functional expression of recombinant PNC proteins, the uptake of radioactively labelled  $[\alpha\text{-}^{32}\text{P}]\text{-ATP}$  was performed (Figure 3.8 C and D). The uptake reaction was started with 50  $\mu\text{M}$   $[\alpha\text{-}^{32}\text{P}]\text{-ATP}$  and the proteoliposomes were preloaded with or without 30 mM AMP. Both PNC proteins were functional expressed, exhibiting a ATP/AMP uptake activity with a  $V_{\text{max}}$  of 701.5 nmol ATP mg protein<sup>-1</sup> and an initial rate of 31.0 nmol ATP mg protein<sup>-1</sup> for PNC1-His (Figure 3.8 C) and a  $V_{\text{max}}$  of 292.2 nmol ATP mg protein<sup>-1</sup> and an initial rate of 9.4 nmol ATP mg protein<sup>-1</sup> for PNC2 (Figure 3.8 D). PNC1-His showed a three-fold increased activity compared to PNC2.  $\text{NAD}^+/\text{NAD}^+$  homo-exchange was performed with 125  $\mu\text{M}$   $[\alpha\text{-}^{32}\text{P}]\text{-NAD}^+$  offered outside and 30 mM  $\text{NAD}^+$  inside of the proteoliposomes (Figure 3.8 E - G). PNC1-His (Figure 3.8 E) and PNC2 (Figure 3.8 F) exhibited  $\text{NAD}^+/\text{NAD}^+$  transport activity similar to the background activity mediated by reconstituted WGE (Figure 3.8 G).

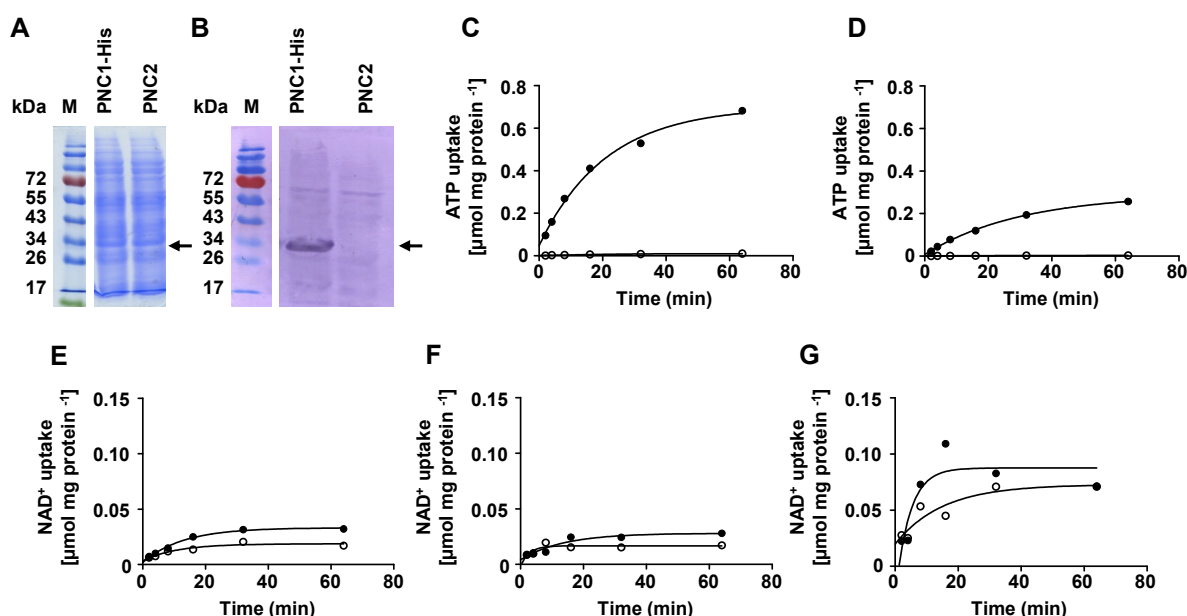


**Figure 3.8  $[\alpha\text{-}^{32}\text{P}]\text{-ATP}$  and  $[\alpha\text{-}^{32}\text{P}]\text{-NAD}^+$  uptake activity of recombinant PNC1-His and PNC2 protein**

*In vitro* expressed PNC1-His (36.6 kDa; indicated with an arrow) and PNC2 (35.2 kDa) proteins were reconstituted into proteoliposomes. (A) Coomassie-stained SDS-PAGE and (B) detection of recombinant protein using anti-His antibody. M, marker proteins. (C and D)  $[\alpha\text{-}^{32}\text{P}]\text{-ATP}$  uptake in exchange with AMP (closed symbols) and (E - G)  $[\alpha\text{-}^{32}\text{P}]\text{-NAD}^+$  uptake in exchange with  $\text{NAD}^+$  (closed symbols) were measured. Open symbols: without preloading. (C and E) PNC1 fused to C-terminal His-tag (D and F) PNC2 without His-tag. (G) Reconstituted WGE. Data represent one experiment.

### 3.3 PXN antibody generation

A specific antibody was raised against the unique hydrophilic loop extension of the PXN protein (indicated with arrows in Figure 3.1). The loop region between the third and fourth transmembrane domain is unique for members of the MCF (Figure 3.1). Ni-NTA purified *E. coli* expressed PXN loop protein was used as antigen for generating an antibody in rabbits (section 2.3.7; Wilkinson, 2009).

In this thesis, the specificity of the anti-PXN antibody was tested. Therefore recombinant proteins of PXN-His, NDT1-His, NDT2-His, PNC1-His, and PNC2 were expressed using the *in vitro* WGE system and were analyzed by immunoblot analysis (Figure 3.9; section 2.4.1). Recombinant PXN-His protein, with a calculated mass of 37.3 kDa, NDT1-His (35.0 kDa), NDT2-His (40.6 kDa), and PNC1-His (36.6 kDa) proteins were detected by immunoblot analysis using an anti-His antibody (Figure 3.9, B). The functional expression of PNC2 protein (35.2 kDa) was verified by transport activity (Figure 3.8). The anti-PXN antibody detects only recombinant PXN-His protein with the expected calculated molecular mass of 37.3 kDa (Figure 3.9, C). An additional protein of ~60 kDa was detected in all samples by the anti-PXN antibody (Figure 3.9, C). Anti-PXN specific serum was not purified for immunoblot analysis of cell-free expressed proteins.

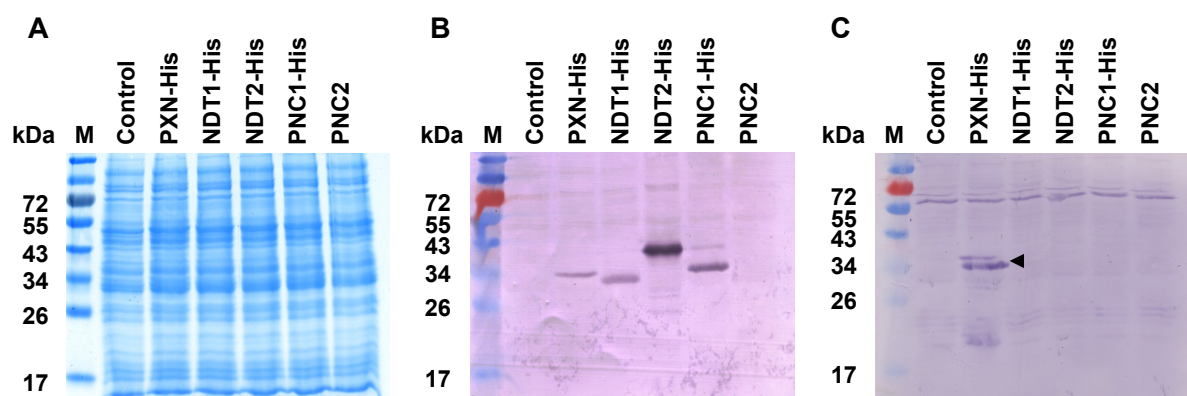


**Figure 3.9 Anti-PXN antibody specificity on recombinant protein**

Recombinant proteins expressed using the *in vitro* WGE system were analyzed by SDS-PAGE and immunoblot analysis. PXN-His (37.3 kDa), NDT1-His (35.0 kDa), NDT2-His (40.6 kDa), and PNC1-His (36.6 kDa), except PNC2 (35.2 kDa), are fused C-terminal to a His-tag. (A) Coomassie staining. (B) Immunoblot detection using an anti-His antibody. (C) Immunoblot detection using an anti-PXN antibody. Anti-PXN antibody detects only recombinant PXN protein with the expected molecular mass of 37.3 kDa (indicated with an arrowhead). M, marker proteins.

### **3.4 PXN expression and co-expression analysis**

*In silico* expression and co-expression analysis were performed to identify the physiological role of PXN in plant metabolism. Computer based expression analysis was conducted to examine the tissue and developmental specific expression of PXN. Co-expression analysis was used for gene function prediction as it is assumed that genes with a similar expression pattern are involved in the same biological process and are often expressed in the same tissue (Usadel *et al.*, 2009). In addition, a histochemical localization of  $\beta$ -glucuronidase (GUS) activity through the PXN promoter was performed to examine the tissue specific PXN expression.

#### **3.4.1 *In silico* PXN expression analysis**

Online available databases like the Arabidopsis eFP Browser and several publications were screened for altered PXN expression during plant development. It is known that the activity of several enzymes is mainly controlled at the level of transcription during lipid mobilization (Rylott *et al.*, 2001).

Expression data, obtained from the eFP Browser database, exhibited increased PXN expression levels during germination and senescence (Figure 3.10; Nakabayashi *et al.*, 2005; Schmid *et al.*, 2005; Winter *et al.*, 2007; Bassel *et al.*, 2008). The expression levels during germination of dry seeds and of seeds imbibed in water for 1 h, 3 h, 6 h, 12 h, and 24 h were analyzed (Nakabayashi *et al.*, 2005; Winter *et al.*, 2007; Bassel *et al.*, 2008). The PXN expression level increased eight-fold from dry seeds to 24 h imbibed seeds (Figure 3.10 A; Nakabayashi *et al.*, 2005; Winter *et al.*, 2007; Bassel *et al.*, 2008). Immunodetection of Arabidopsis PXN protein confirmed the expression during seedling establishment in pumpkin cotyledons (Fukao *et al.*, 2001).

The expression data obtained from the eFP Browser revealed a 2.6-fold increased PXN expression level in senescence leaves in comparison to rosette leaves (Figure 3.10 A; Schmid *et al.*, 2005; Winter *et al.*, 2007; Bassel *et al.*, 2008). In addition, the increased PXN expression level was confirmed by a transcription analysis during developmental and induced senescence (Figure 3.10 B; van der Graaff *et al.*, 2006). During developmental leaf senescence (NS), the PXN expression value was 6.1-fold increased in comparison to not senescent leaves. In addition, the increased PXN expression level correlated with the increased percentage of yellow leaf surface, exhibiting chlorophyll degradation (Figure 3.10 B). Beside natural senescence, induced senescence stimulated the expression of PXN. Induced senescence was achieved by covering a still attached rosette leaf with aluminium foil for up to nine days (2.9-fold increased PXN expression level; Figure 3.10 B, DIS) or by incubation of a detached leaf in darkness for up to six days (3.5-fold increased PXN expression level; Figure 3.10 B, DET).



The expression pattern of PXN during germination and senescence is similar to essential key enzymes of the fatty acid  $\beta$ -oxidation (section 1.3.1). The expression level of COMATOSE (CTS), long chain acyl-CoA synthetases 6 (LACS6), LACS7, acyl-CoA oxidase (ACX), multifunctional protein 2 (MFP2), 3-ketoacyl-CoA thiolase (KAT2), PCN1 and PNC2 were increased during germination and senescence (Germain *et al.*, 2001; Rylott *et al.*, 2001; Winter *et al.*, 2007; Bassel *et al.*, 2008). The expression of peroxisomal malate dehydrogenase 2 (pMDH2) was increased during germination (Nakabayashi *et al.*, 2005; Winter *et al.*, 2007; Bassel *et al.*, 2008).

Besides germination and senescence, the PXN expression was altered during oxidative stress conditions (section 3.7).

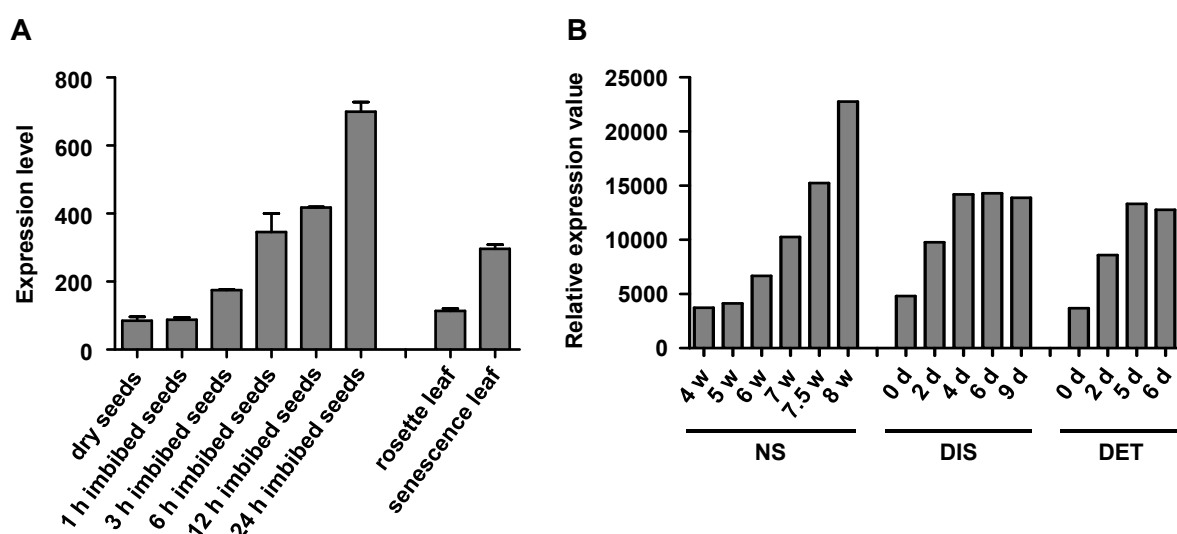


**Figure 3.10 PXN expression level during germination and senescence**

PXN expression levels were increased during germination and senescence. (A) Microarray analysis data of Arabidopsis Col-0 seeds and leaves were obtained from the Arabidopsis eFP Browser database (Nakabayashi *et al.*, 2005; Schmid *et al.*, 2005; Winter *et al.*, 2007; Bassel *et al.*, 2008). (B) Relative expression values of PXN during developmental leaf senescence (NS), from individually shaded leaves, which were still attached to the plant (DIS) and detached dark-induced leaves (DET). NS leaves from seven-week-old plants exhibited ~25%, 7.5-week-old ~50% and eight-week-old ~75% yellow surface. Data were obtained from van der Graaff *et al.* (2006).

### 3.4.2 *In silico* co-expression analysis

Highly co-expressed genes may be involved in the same metabolic pathway. To examine the physiological function of PXN, different co-expression databases were screened for co-expressed genes. Publicly available microarray data of Arabidopsis were received from ATTED-II, Genemania, Genevestigator, and the Arabidopsis Co-Response Databases (Table 7.5; section 2.2.3).

PXN is strongly co-expressed with genes coding for key enzymes of the fatty acid  $\beta$ -oxidation (e.g. ACX3, CTS, LACS6, LACS7, MFP2, pMDH1, and PNC2; Table 3.4 yellow), the tricarboxylic acid (TCA) cycle (e.g. cytosolic malate dehydrogenase (cMDH), isocitrate

dehydrogenase 2 (IDH2), IDH5, and succinate dehydrogenase 2 (SDH-2); Table 3.4 blue), and with genes required for senescence like the  $\beta$ -oxidation enzymes and B12D, a senescence associated enzyme of unknown enzymatic function (Table 3.4 yellow and white).

Ascorbate peroxidase 1 (APX1), APX3, monodehydroascorbate reductase 1 (MDAR1), and MDAR2 are enzymes necessary for the detoxification of hydrogen peroxide ( $H_2O_2$ ) and are co-expressed with PXN (Table 3.4 purple). Peroxisomal membrane protein (PMP) import specific peroxin 19-1 (PEX19-1), PEX19-2, and PEX3-1 proteins exhibited the same expression profile as PXN (Table 3.4 green).

### Table 3.4 Co-expression analysis for PXN

PXN co-expression analyzes were performed with different co-expression databases: Genemania, ATTED-II, Genevestigator, and the Arabidopsis Co-Response Database (AthCoR DB;

Table 7.5). Yellow,  $\beta$ -oxidation; blue, TCA-cycle; purple, oxidative stress; green, PMP import.

AGI	Name	Description	Genemania	ATTED-II	Genevestigator	AthCoR DB
At1g06290	ACX3	acyl-CoA oxidase			X	
At4g39850	CTS	Comatose, peroxisomal ABC transporter	X			
At3g05970	LACS6	long-chain acyl-CoA synthetase 6	X	X	X	
At5g27600	LACS7	long-chain acyl-CoA synthetase 7		X	X	X
At5g43330	cMDH	cytosolic malate dehydrogenase				X
At2g22780	pMDH1	peroxisomal malate dehydrogenase				X
At3g06860	MFP2	multifunctional protein 2	X	X	X	
At5g27520	PNC2	peroxisomal adenine nucleotide carrier 2	X			
At2g17130	IDH2	subunit 2 of NAD-dependent isocitrate dehydrogenase				X
At5g03290	IDH5	isocitrate dehydrogenase V				X
At5g40650	SDH-2	succinate dehydrogenase 2		X		
At1g07890	APX1	ascorbate peroxidase 1		X		
At4g35000	APX3	ascorbate peroxidase 3		X		
At3g52880	MDAR1	monodehydroascorbate reductase 1		X		
At5g03630	MDAR2	monodehydroascorbate reductase 2		X		
At3g03490	PEX19-1	peroxin 19-1	X			X
At5g17550	PEX19-2	peroxin 19-2	X			
At3g18160	PEX3-1	peroxin 3-1	X			
At3g48140	B12D	senescence associated		X		
At1g25380	NDT2	mitochondrial NAD <sup>+</sup> transporter 2	X			

### 3.4.3 PXN promoter-GUS analysis

Promoter-GUS analysis was performed to examine the expression pattern of PXN in six-day-old seedlings and six-week-old rosette leaves (section 2.3.10; Trippelsdorf, 2012).

Representative six-day-old seedling exhibited the PXN promoter activity in the whole leaf area and in the vascular tissue of cotyledons (Figure 3.11 A and B). In addition, GUS activities were detectable in the shoot and root apical meristem, at the transition zone from hypocotyl to root, in the root vascular tissue, and in the root tip (Figure 3.11 A). A representative six-week-old rosette leaf showed the same PXN promoter activity pattern as

cotyledons with a light blue stained leaf area and the dark blue stained vascular tissue (Figure 3.11 C).

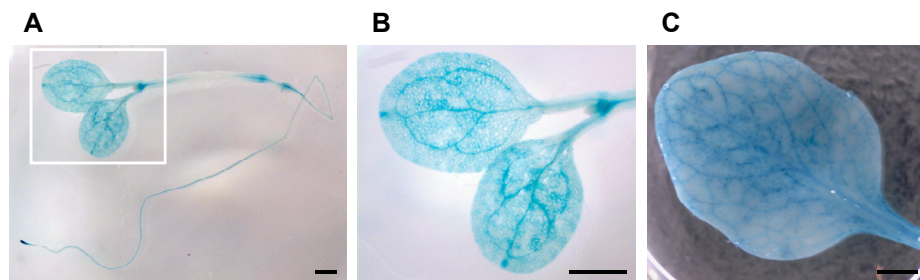


**Figure 3.11 PXN promoter-GUS activity in seedlings and rosette leaves**

(A and B) Six-day-old cotyledons and (C) six-week-old rosette leaf of wild type (WT) plants expressing GUS reporter gene under the control of the PXN promoter (Trippelsdorf, 2012). (B) Close-up of framed section in (A). Scale bars: 1 mm.

### 3.5 *pxn* T-DNA insertion lines

Arabidopsis mutant lines, generated by T-DNA insertion in the *pxn* gene, were obtained to examine the physiological function of PXN *in planta*. Three independent T-DNA lines were analyzed on genomic DNA (gDNA) level and regarding the protein level. Additionally, PXN complementation lines were generated.

#### 3.5.1 Genotype of Arabidopsis *pxn* mutant lines

Three independent *pxn* T-DNA insertion lines were generated to investigate the plant physiological function of PXN (Figure 3.12; Wilkinson, 2009). T-DNA insertion sites were located in the first (*pxn-2*), seventh (*pxn-3*) and ninth exon (*pxn-1*; Figure 3.12 A). Homozygous *pxn* T-DNA insertion lines were verified using gene and T-DNA specific primers on genomic DNA isolated from leaves (Figure 3.12 B; section 2.3.5). Primers specific for ACTIN2 (ACT2) were used as positive control (Figure 3.12, B; section 2.3.5).

Sabrina Wilkinson analyzed the transcript level of *PXN* expression using reverse transcription (RT)-PCR and primers specific for full-length and truncated mRNA (Wilkinson, 2009). All three *pxn* T-DNA insertion lines exhibited no full-length *PXN* transcript but truncated mRNA (Wilkinson, 2009).

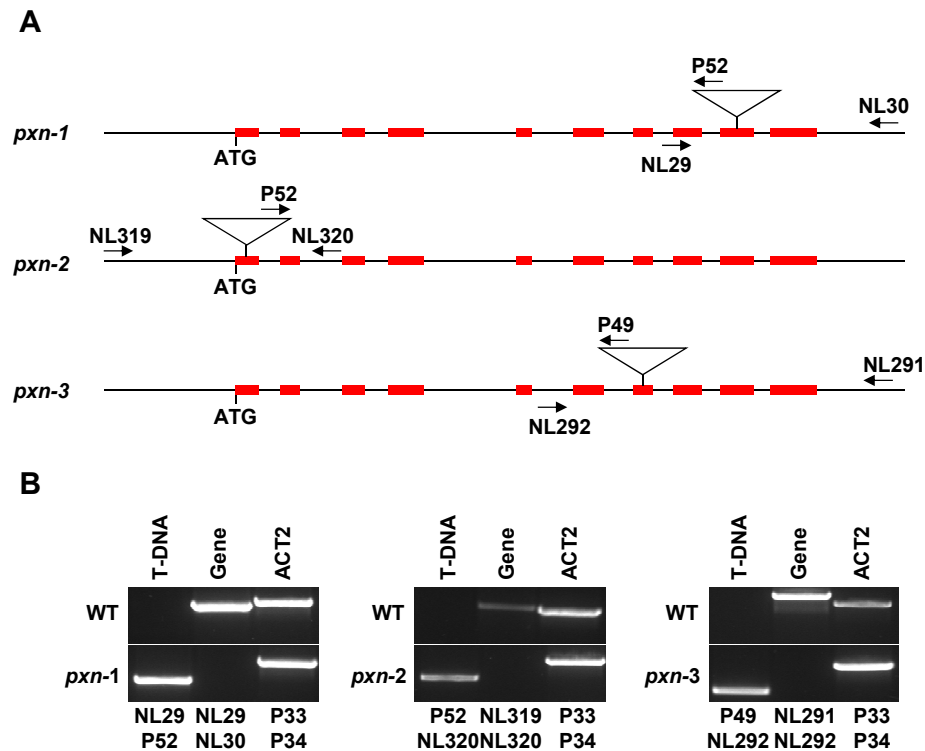


**Figure 3.12 Genotype of three independent T-DNA insertion lines for PXN**

(A) Model of *pxn-1*, *pxn-2*, and *pxn-3* T-DNA insertion lines. The red boxes indicate exons and untranslated regions, the black line indicates introns, the white triangles the location of the T-DNA in the *pxn* gene, and the arrows the primer binding sites. *pxn-1*: T-DNA in the ninth exon; *pxn-2*: T-DNA in the first exon; *pxn-3*: T-DNA in the seventh exon. (B) PCR-based verification of homozygous *pxn* T-DNA insertion lines on gDNA level with gene and T-DNA specific primer pairs. ACT2 specific primers were used as positive control for gDNA isolation. Expected PCR products: see section 2.3.5.

### 3.5.2 PXN protein level of *pxn* mutant lines

PXN protein levels of the *pxn* mutant lines were verified to investigate if the expressed truncated PXN transcripts (Wilkinson, 2009) are translated to proteins.

To detect PXN protein level in *pxn* mutant lines, membrane proteins of WT and *pxn* mutants were isolated from etiolated six-day-old seedlings because PXN is highly abundant during seedling establishment (section 2.3.6; Fukao *et al.*, 2001; Winter *et al.*, 2007). The membrane protein samples were examined by immunoblot analysis using different antibodies. Equal amounts of membrane fractions were analyzed of WT and *pxn* lines, verified by immunodetection using an antibody raised against the mitochondrial cytochrom C oxidase subunit 2 (ScCOX2) from *S. cerevisiae* (22 kDa expected molecular mass of ScCOX2 in Arabidopsis, Figure 3.13 C; Herrmann *et al.*, 1995) that detected similar amounts of Arabidopsis COX protein in each membrane fraction. A fragment of the expected size of PXN (~36 kDa) was detected in WT and *pxn-2* membrane fraction by immunoblot analysis using purified anti-PXN antibody (Figure 3.13 B; section 2.3.7). However, the PXN protein amount of *pxn-2* seedlings was reduced in comparison to WT. In *pxn-1* and *pxn-3* mutant

lines no PXN protein could be detected although the T-DNA lines transcribe truncated mRNA (Figure 3.13 B; Wilkinson, 2009). Due to the PXN protein amount detected in membrane fractions of *pxn-1* and *pxn-3* lines, both are indicated as loss-of-function mutants and *pxn-2* as a knock-down mutant.

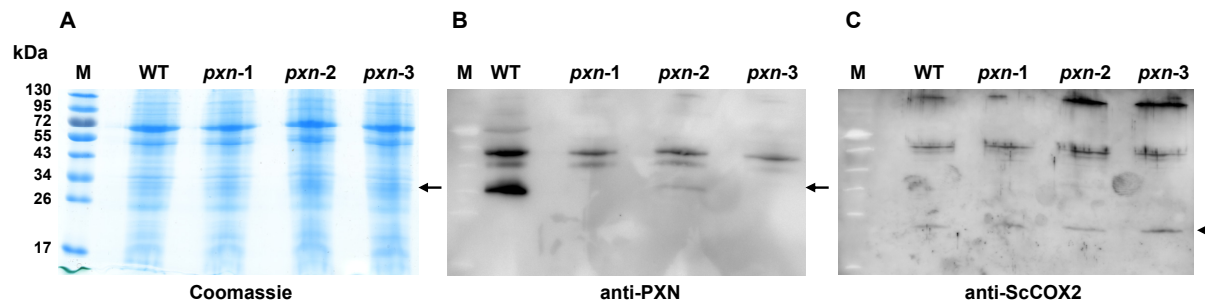


**Figure 3.13 PXN protein detection of isolated membranes from etiolated *pxn* seedlings**

Plant membranes of six-day-old etiolated seedlings were isolated and analyzed by SDS-PAGE and immunoblot analysis. (A) Coomassie-stained SDS-PAGE. (B) Immunoblot analysis using purified anti-PXN antibody. (C) Immunoblot analysis using anti-ScCOX2 antibody. Arrows indicate the expected molecular mass of PXN (36 kDa) and the arrowhead the expected molecular mass of ScCOX2 (22 kDa) in *Arabidopsis* (Herrmann *et al.*, 1995). M, marker proteins.

### 3.5.3 PXN complementation lines

A PXN over-expression construct (pUBQ10::PXN) was generated for PXN over-expression and for complementation of different mutant lines (section 2.3.9). WT and *pxn* plants were transformed with the pUBQ10::PXN construct and homozygous lines were established (section 2.3.9). The growth phenotype was similar to that of WT.

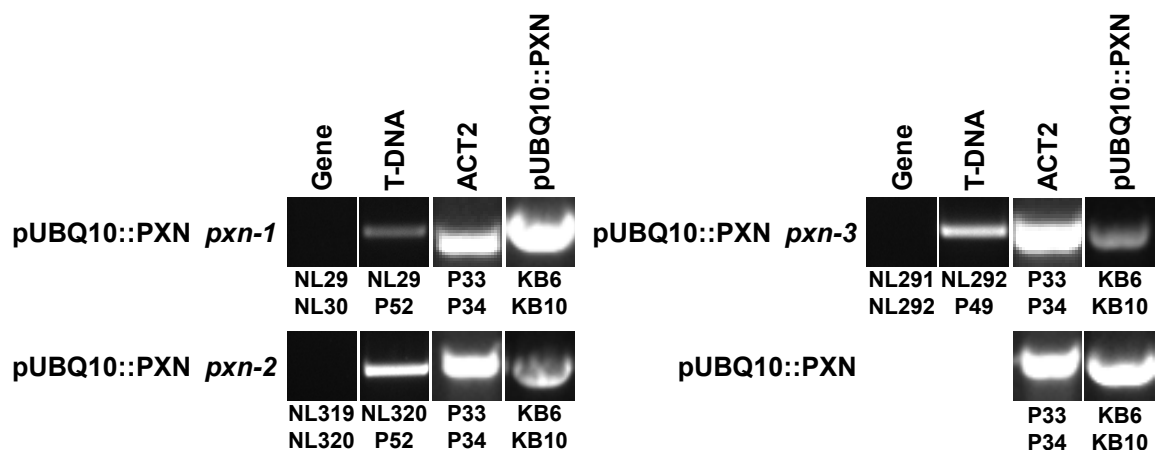


**Figure 3.14 Genotype of PXN over-expression lines**

PCR-based screening on gDNA of WT (pUB10::PXN) and *pxn* lines (pUBQ10::PXN *pxn-1*, pUBQ10::PXN *pxn-2*, and pUBQ10::PXN *pxn-3*) transformed with a PXN over-expression construct (pUBQ10::PXN). Gene and T-DNA primers were used. ACT2 was used as control for gDNA isolation. Expected PCR product: see section 2.3.5. All plants were homozygous for the T-DNAs.

### 3.6 The impact of PXN on $\beta$ -oxidation

Expression (section 3.4.1) and co-expression analysis (section 3.4.2), and immunodetection of PXN protein in establishing pumpkin seedlings (Fukao *et al.*, 2001) possess a link between PXN function and  $\beta$ -oxidation during germination and seedling establishment. Different approaches were performed using *pxn* T-DNA insertion lines (section 3.5.1) to investigate the impact of PXN on NAD<sup>+</sup>-dependent  $\beta$ -oxidation.

#### 3.6.1 Seedling establishment of *pxn* mutants

Plant lines lacking functional  $\beta$ -oxidation need exogenous supply of carbon sources for seedling establishment since they are not able to convert the storage fatty acids to sugar via  $\beta$ -oxidation and gluconeogenesis (Graham, 2008; Quettier *et al.*, 2008; Quettier and Eastmond, 2009). Mutants of peroxisomal NAD<sup>+</sup>-dependent enzymes, like MFP2, pMDH1, pMDH2, and MDAR4, showed a sucrose dependent phenotype (Rylott *et al.*, 2006; Eastmond, 2007; Pracharoenwattana *et al.*, 2007). To test if the *pxn* mutants exhibited a sucrose dependent phenotype, seeds were incubated with or without sucrose as exogenous carbon source under short day and continuous darkness conditions for six days (Figure 3.15, Figure 7.1; section 0).

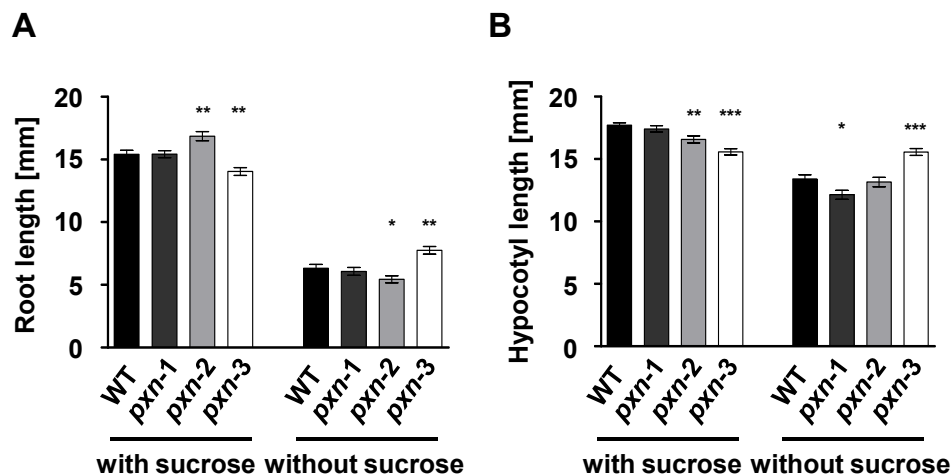


**Figure 3.15 Sucrose-dependent establishment of *pxn* seedlings**

WT and *pxn* seedlings were grown vertically on agar plates with or without sucrose addition for six days. (A) Seedlings were grown under short-day conditions and the root length was measured. (B) Hypocotyl length of seedlings grown under continuous darkness condition was measured. *pxn* seedlings exhibited no sucrose dependent phenotype. Error bars indicate  $\pm$  SE values of three independent replicates ( $n = 35$  seedlings). An unpaired t-test was performed. Asterisks indicate significance levels; \* $P < 0.05$  (significant); \*\* $P < 0.01$  (very significant); \*\*\* $P < 0.001$  (extremely significant).

Under short day conditions, the root growth was reduced in WT (59% reduced root length), *pxn-1* (60%), *pxn-2* (68%), and *pxn-3* (44%) seedlings, grown in the absence of exogenous carbon source in comparison to seedlings grown with sucrose addition (Figure 3.15 A). The hypocotyl length of WT (24% reduced hypocotyl length), *pxn-1* (30%), and *pxn-2* (20%)

seedlings grown under continuous darkness condition, was reduced without sucrose feeding (Figure 3.15 B). The *pxn-3* mutant exhibited the same hypocotyl length grown in the presence ( $15.6 \pm 0.253$  mm) or absence ( $15.6 \pm 0.278$  mm) of exogenous sucrose addition (Figure 3.15 B). However, the inconsistent growth of the *pxn* seedlings can be explained by the biological variance of the independent mutant alleles. It can be concluded that *pxn* seedlings showed no sucrose dependent phenotype like WT.

### 3.6.2 Sensitivity to the root growth inhibitor 2,4-DB of *pxn* seedlings

A sensitive approach to reveal a  $\beta$ -oxidation phenotype was performed by the treatment of seedlings with 2,4-dichlorophenoxybutyric acid (2,4-DB). 2,4-DB is metabolized via peroxisomal  $\beta$ -oxidation to the root growth inhibitor 2,4-dichlorophenoxyacetic acid (2,4-D; Hayashi *et al.*, 1998). Mutants lacking functional  $\beta$ -oxidation show increased root growth on media containing 2,4-DB, as they are unable to convert 2,4-DB to 2,4-D (Hayashi *et al.*, 1998).

The root length of six-day-old WT and *pxn* seedlings, grown on agar plates containing either 2,4-DB or 2,4-D, was determined (section 0). *pxn-1* (19% reduced root length in comparison to control conditions), *pxn-2* (32%), and *pxn-3* (36%) seedlings were less sensitive to 2,4-DB than WT (48%) seedlings, indicated by significant longer roots in the presence of 2,4-DB (Figure 3.16). Nevertheless, all *pxn* and WT seedlings exhibited around 70% reduced root growth in presence of 2,4-D in comparison to control conditions (Figure 3.16). *pxn* seedlings showed partial resistance against the root growth inhibitor 2,4-DB, indicating an impact of PXN on the conversion of 2,4-DB to 2,4-D via peroxisomal  $\beta$ -oxidation.

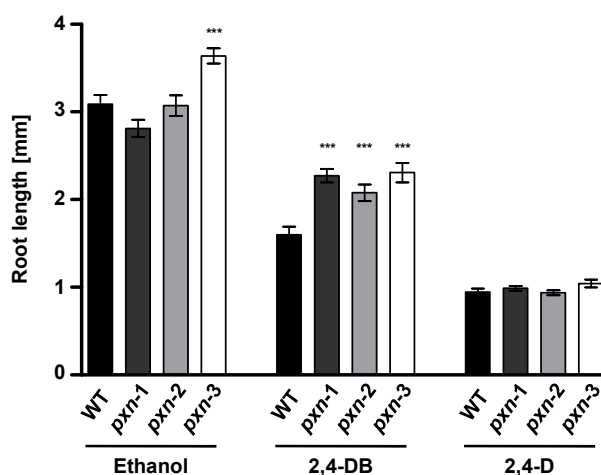


**Figure 3.16 2,4-DB and 2,4-D assay of *pxn* seedlings**

Seedlings were grown vertically on agar plates containing  $0.8 \mu\text{M}$  2,4-DB or  $0.23 \mu\text{M}$  2,4-D, dissolved in ethanol which was used as control. The root length of six-day-old *pxn* seedlings was measured. Seedlings were less sensitive to the root growth inhibitor 2,4-DB than WT. Error bars indicate  $\pm$  SE values of three independent replicates ( $n = 35$  seedlings). An unpaired t-test was performed. Asterisks indicate significance levels; \*\*\*  $P < 0.001$  (extremely significant).

### 3.6.3 Impact of PXN on fatty acid degradation during seedling establishment

The degradation of storage oil in *pxn* seedlings was examined, as the  $\beta$ -oxidation efficiency is impaired in mutants lacking PXN expression (section 3.6.2).

To analyze the breakdown of storage oil during germination and seedling establishment, the fatty acid contents of WT and *pxn* seeds and seedlings grown under short-day and continuous darkness condition were examined using fatty acid methyl ester (FAME) analysis (section 2.3.12). Eicosenoic acid C20:1 was used as marker for triacylglycerol (TAG) breakdown (Lemieux *et al.*, 1990). Relative to seeds, the C20:1 levels of seedlings were calculated. Eicosenoic acid content of two-day-old WT and *pxn* seedlings grown in short-day conditions was slightly reduced (2 - 4%; Figure 3.17 A). WT seedlings broke TAG rapidly down (four-day-old, 81% degradation; six-day-old, complete breakdown; Figure 3.17 A). C20:1 levels were not changed of four-day-old *pxn* seedlings (6% degradation) but was decreased abruptly in six-day-old seedlings (87% degradation; Figure 3.17, A). Seedlings grown in continuous darkness broke TAG continuously down (Figure 3.17 B). But in comparison to WT, the C20:1 content was around 22% enhanced in two-, four-, and six-day-old *pxn* seedlings (Figure 3.17, B).

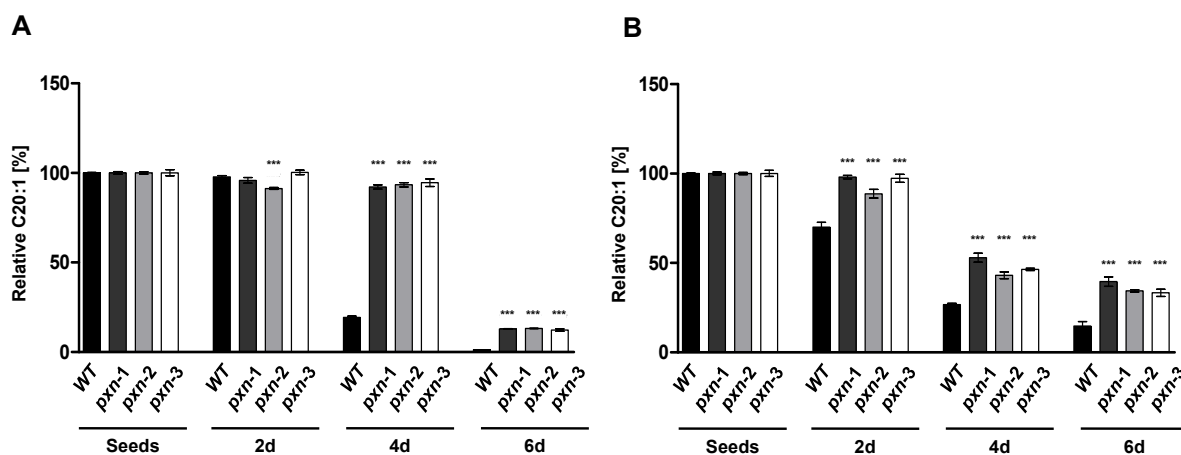


**Figure 3.17 Fatty acid analysis of *pxn* seedlings**

Fatty acid analyzes of seedlings, germinated under (A) short-day and (B) continuous darkness conditions were performed using FAME analysis. Eicosenoic acid C20:1 was used as marker for TAG breakdown. The C20:1 levels of seedlings were calculated relative to seed C20:1 content. Data plotted are means  $\pm$  SEs of measurements on three batches of 10 mg seeds or 20 mg seedlings. An unpaired t-test was performed. Asterisks indicate significance levels; \*\*\*  $P < 0.001$  (extremely significant).

It was investigated if the delayed fatty acid degradation of the *pxn* seedlings is visible in retained oil bodies, the storage compartments of storage oil. The lipophilic dye Nile red was used to stain lipid bodies (Siloto *et al.*, 2006). The *pxa1* mutant allele was used as positive control, because the  $\beta$ -oxidation is completely blocked in this mutant line (Zolman *et al.*, 2001). Hypocotyl tissues of four-day-old etiolated seedlings were stained with Nile red and analyzed using laser scanning confocal microscopy (section 2.3.13). WT hypocotyl cells did



not reveal stained lipid bodies in comparison to all three *pxn* lines and *pxa1* mutant, which accumulated oil bodies (Figure 3.18).

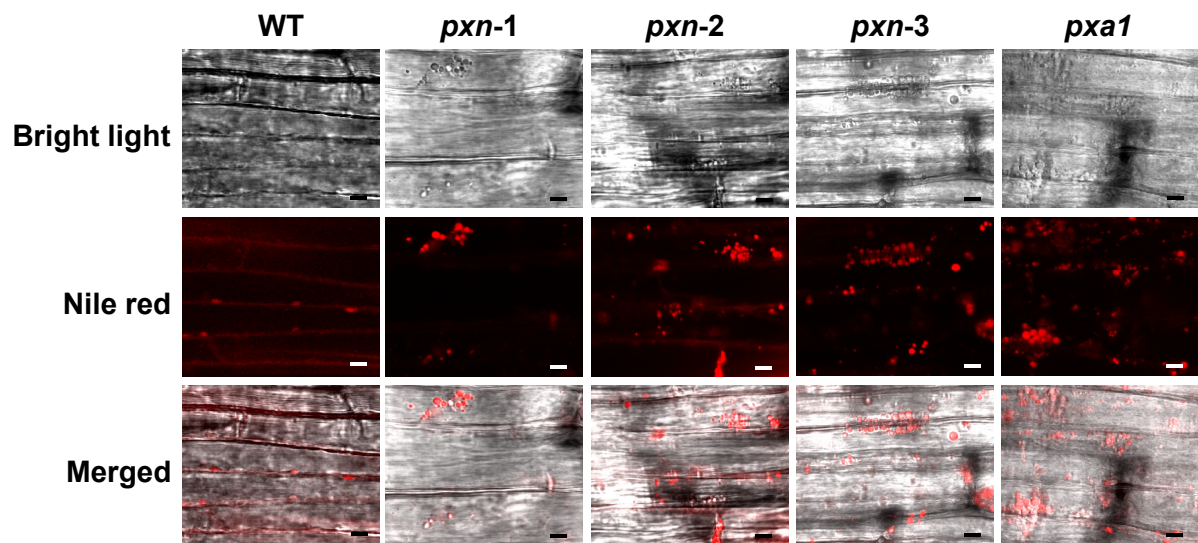


**Figure 3.18 Nile red staining of oil bodies in WT, *pxn* and *pxa1* seedlings**

Nile red stained lipid bodies in hypocotyl cells of four-day-old etiolated WT, *pxn*, and *pxa1* seedlings. *pxn* and *pxa1* seedlings exhibited retained lipid bodies in comparison to WT seedlings. Scale bar: 5  $\mu$ m.

To confirm the retention of lipid bodies, cotyledons of five-day-old etiolated WT and *pxn-1* seedlings were analyzed using transmission electron microscopy (TEM; section 2.3.14). The *pxn-1* cotyledon cells (Figure 3.19 B) showed homogenous grey stained lipid bodies, which were absent in WT (Figure 3.19 A).

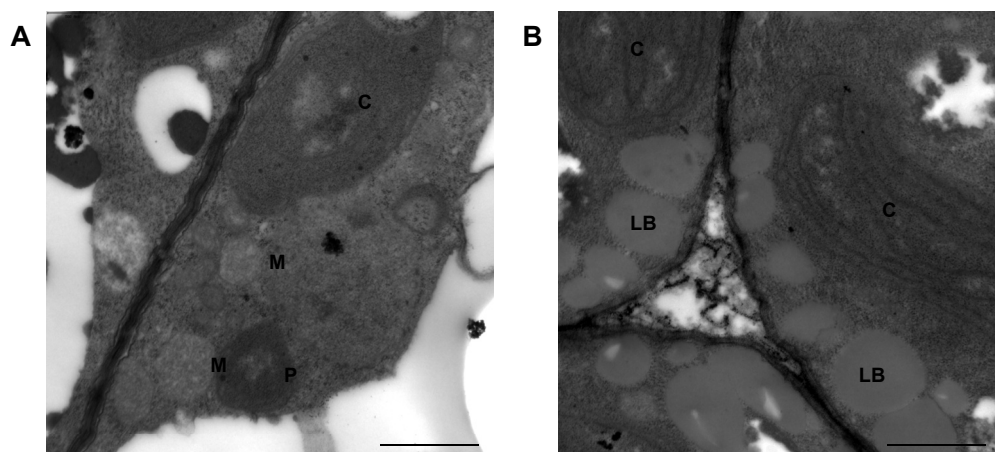


**Figure 3.19 TEM images of five-day-old etiolated cotyledon cells**

TEM pictures of five-day-old (A) WT and (B) *pxn-1* cotyledon cells. *pxn-1* seedlings accumulated fatty acids in lipid bodies. Abbreviations: C, chloroplast; LB, lipid body; M, mitochondrion; P, peroxisome. Scale bars: 1  $\mu$ m.

### 3.6.4 Germination efficiency of *pxn* seeds

The germination efficiency of *pxn* seeds was analyzed in order to test if the delayed fatty acid degradation of *pxn* seedlings was present due to a reduced  $\beta$ -oxidation rate or because of a delayed germination process. To test the hypothesis that the *pxn* mutants were impaired prior or during germination, a time-dependent germination assay was performed on agar

plates with and without sucrose addition. After 24 h, 48 h, and 72 h, these seeds were counted where the roots emerged from the seed coat (section 0). The abscisic acid (ABA) insensitive 4 (*abi4*) and *pmdh1 pm dh2* double mutant was used as positive control as they exhibited a germination phenotype (Finkelstein, 1994; Pracharoenwattana *et al.*, 2007; Pracharoenwattana *et al.*, 2010).

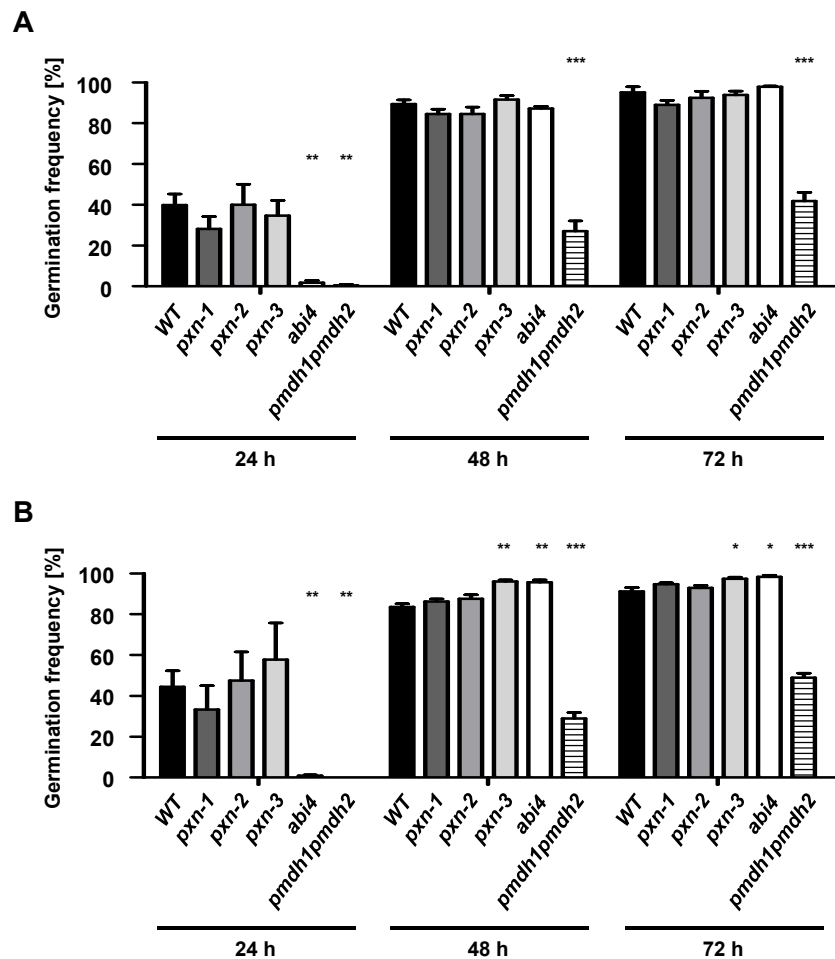


**Figure 3.20 Germination assay of WT, *pxn*, *abi4*, and *pmdh1 pm dh2* seeds**

Seeds were spotted on agar plates (A) with and (B) without exogenous sucrose addition, stratified for four days and germinated under long-day conditions. The percentage of seeds was calculated from those whose roots emerged from the seed coat. Values are mean  $\pm$  SE of three replicates ( $n = 75$  seeds). An unpaired t-test was performed. Asterisks indicate significance levels; \* $P < 0.05$  (significant); \*\* $P < 0.01$  (very significant); \*\*\* $P < 0.001$  (extremely significant).

The germination frequency (GF) was calculated in the presence (GF<sup>+</sup>) or absence (GF<sup>-</sup>) of sucrose. Independent of sucrose supply, *abi4* seeds were delayed in germination in the first 24 h (2% GF<sup>+</sup> and 1% GF<sup>-</sup>), but the number of germinated seeds was similar to WT after 48 h (*abi4*: 87% GF<sup>+</sup> and 96% GF<sup>-</sup>; WT: 89% GF<sup>+</sup> and 84% GF<sup>-</sup>) and 72 h (*abi4*: 98% GF<sup>+</sup> and 98% GF<sup>-</sup>; WT: 95% GF<sup>+</sup> and 91% GF<sup>-</sup>; Figure 3.20). After the first 24 h, the *pmdh1 pm dh2* double mutant did not germinate and was significantly delayed in germination during the next 48 h. After 72 h, 42% (GF<sup>+</sup>) and 49% (GF<sup>-</sup>) of the *pmdh1 pm dh2* seeds germinated. *pxn*

seeds germinated like the WT, independent of exogenous sugar supply, except for *pxn-3* seeds grown on MS media without sucrose supply. They showed a slight but significant increase in germination frequency after 48 h (96% GF<sup>-</sup>) and 72 h (97% GF<sup>-</sup>; Figure 3.20).

### **3.7 Role of PXN during oxidative stress**

The cofactor NAD<sup>+</sup> is not just required for peroxisomal metabolism like fatty acid  $\beta$ -oxidation or photorespiration. NADH is also essential for the scavenging of toxic H<sub>2</sub>O<sub>2</sub> (Figure 1.1; section 1.3.3). During oxidative stress and other peroxisomal metabolic pathways, H<sub>2</sub>O<sub>2</sub> accumulates and is then detoxified by catalase and the APX/MDAR system by simultaneous oxidation of NADH to NAD<sup>+</sup> (section 1.3.3; Graham, 2008).

In this section, it was investigated if the NAD<sup>+</sup> import mediated by PXN plays a role during H<sub>2</sub>O<sub>2</sub> detoxification by supplementing the APX/MDAR system with its cofactor. In addition, PXN is co-expressed with MDAR and APX (Table 3.4) and therefore the role of PXN in abiotic and biotic stress conditions was analyzed by plant physiological experiments using *pxn* mutant lines (section 3.5). Furthermore, *in silico* analysis of PXN expression data during stress conditions were obtained from the eFP Browser (section 2.2.3).

#### **3.7.1 Response to H<sub>2</sub>O<sub>2</sub>, 3-aminotriazole, and methylviologen**

Oxidative stress is directly connected with reactive oxygen species (ROS) production and therefore with the most stable species, H<sub>2</sub>O<sub>2</sub>. The direct influence of H<sub>2</sub>O<sub>2</sub> and 3-aminotriazole (3-AT) to *pxn* seedling root growth was analyzed. 3-AT is an irreversible inhibitor of the catalase and consequently, the NAD<sup>+</sup>-dependent APX/MDAR system has to detoxify the escaping H<sub>2</sub>O<sub>2</sub> (Walton and Pizzitelli, 2012).

WT and *pxn* seedlings were grown on agar plates containing 10  $\mu$ M H<sub>2</sub>O<sub>2</sub>, 2  $\mu$ M 3-AT, or both substrates, expecting a decreased root and hypocotyl growth. The root length of around 40 seedlings was examined (Figure 3.21; Trippelsdorf, 2012). The root growth of ten-day-old *pxn* seedlings was similar to WT seedlings grown under all three conditions (H<sub>2</sub>O<sub>2</sub>, 3-AT, or H<sub>2</sub>O<sub>2</sub> and 3-AT), except *pxn-2* and *pxn-3* seedlings, which exhibited significant longer root length when grown on media containing 3-AT (WT: 4.1  $\pm$  0.4 mm; *pxn-2*: 5.7  $\pm$  0.4 mm; *pxn-3*: 6.4  $\pm$  0.4 mm) and *pxn-3* grown on H<sub>2</sub>O<sub>2</sub> and 3-AT containing media (WT: 2.6  $\pm$  0.2 mm; *pxn-3*: 3.2  $\pm$  0.1 mm; Figure 3.21). Additionally, seedlings were incubated in continuous darkness condition with H<sub>2</sub>O<sub>2</sub> and/or 3-AT. The hypocotyl length was measured and no different phenotype of *pxn* to WT was observed (Trippelsdorf, 2012). In addition, Friederike Philipp analyzed the response of *pxn* and WT seedlings to H<sub>2</sub>O<sub>2</sub> and could not detect any obvious differences of the root growth (Philipp, 2010).

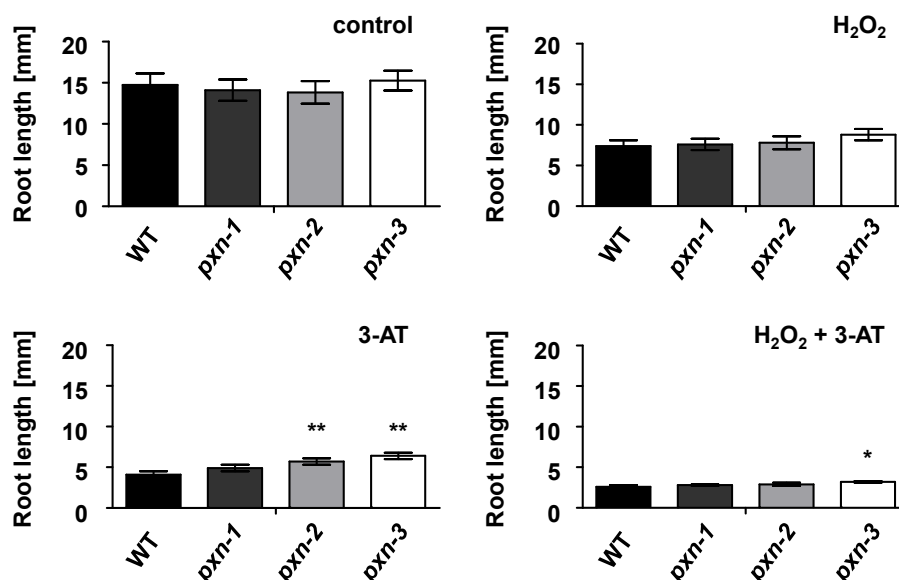


**Figure 3.21 Root growth of seedlings in response to H<sub>2</sub>O<sub>2</sub> and 3-AT**

The root length of ten-day-old seedlings grown on agar plates containing either 10  $\mu$ M H<sub>2</sub>O<sub>2</sub>, 2  $\mu$ M 3-AT, or 10  $\mu$ M H<sub>2</sub>O<sub>2</sub> and 2  $\mu$ M 3-AT were analyzed (Trippelsdorf, 2012). WT and *pxn* seedlings were similarly sensitive to the additives with the exception that *pxn-2* and *pxn-3* showed an increased root growth on media containing 3-AT. Values are mean  $\pm$  SD of one experiment (n= 40 seedlings). An unpaired t-test was performed. Asterisks indicate significance levels. \*P < 0.05 (significant); \*\*P < 0.01 (very significant).

*In silico* PXN expression data of 18-day-old Arabidopsis Col-0 plants, incubated with 10  $\mu$ M methylviologen (paraquat), were received from the eFP Browser. Methylviologen induced oxidative stress and therefore ROS production (Kilian *et al.*, 2007; Winter *et al.*, 2007). Figure 3.22 illustrated the similar PXN expression pattern in shoot and root tissue under control and oxidative stress conditions. The PXN expression levels did not change during 24 h of analysis.

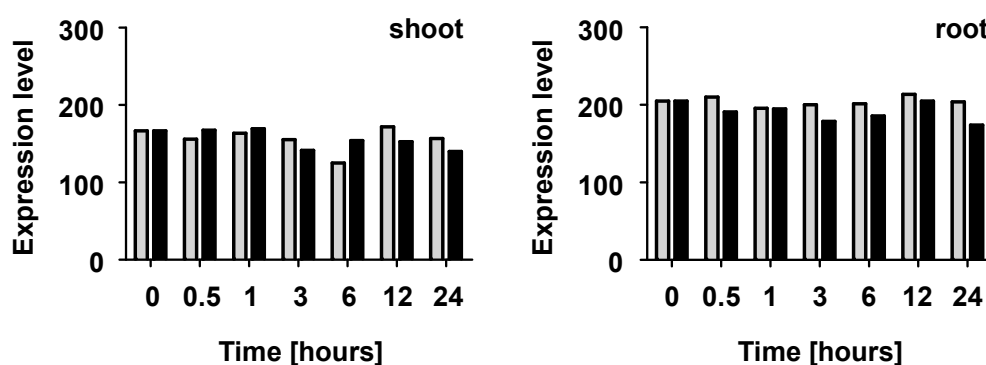


**Figure 3.22 *In silico* analysis of PXN expression level using eFP Browser – oxidative stress**

The PXN expression level of 18-day-old WT plants was analyzed during oxidative stress that was induced by 10  $\mu$ M methylviologen (black bars). Expression levels under controlled conditions are labelled in grey. The PXN expression level in shoot and root tissues were similar under controlled and oxidative stress conditions. Data were obtained from eFP Browser (Kilian *et al.*, 2007; Winter *et al.*, 2007).

### 3.7.2 PXN Expression level in response to low pH

It could be shown before that plants, incubated at low pH, revealed decreased root growth and increased ROS production (Koyama *et al.*, 2001; Babourina *et al.*, 2006). Expression data from Arabidopsis Col-0 plants that were transferred from standard pH 5.7 to low pH 4.6 were obtained from eFP Browser (Winter *et al.*, 2007; Iyer-Pascuzzi *et al.*, 2011).

PXN was highly expressed under low pH condition (pH 4.6; Figure 3.23). On average, the PXN expression level was six-fold increased at low pH (pH 4.6) in comparison to standard pH (pH 5.7).

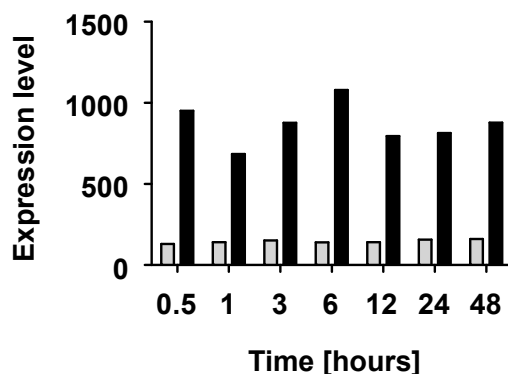


**Figure 3.23** *In silico* analysis of PXN expression level using eFP Browser – low pH

PXN expression values of root tissue determined under low pH 4.6 (black bars) and standard pH 5.7 (grey bars). PXN is stronger expressed at low pH. Data were obtained from eFP Browser (Winter *et al.*, 2007; Iyer-Pascuzzi *et al.*, 2011).

### 3.7.3 Response to *Pseudomonas syringae*

Besides abiotic stress, plants have to deal with biotic stress like infection of bacteria or viruses. Plants, infected with virulent and avirulent *Pseudomonas syringae* strains accumulate ascorbate and glutathione as antioxidants and reduction/oxidation (redox) signalling molecules, as well as H<sub>2</sub>O<sub>2</sub> (Grosskinsky *et al.*, 2012). *In silico* expression analysis from WT leaves that were infiltrated with different *P. syringae* strains were obtained from the eFP Browser (Winter *et al.*, 2007). Leaves of five-week-old Arabidopsis Col-0 plants were infiltrated with either a virulent (*pv. tomato DC3000*), avirulent (*pv. tomato avrRpm1*), type III-secretion system deficient (*pv. tomato DC3000 hrcC-*), or a nonhost (*pv. phaseolicola*) *P. syringae* strain, and with 10 mM MgCl<sub>2</sub> as control.

The PXN expression level of *P. syringae* treated leaves was the same compared with control treatment after 2 h (Figure 3.24). The PXN expression levels were not altered by the infiltration of the virulent and avirulent strains after 6 h, whereas it was increased by infiltration of the deficient (1.3-fold increased) and nonhost (1.4-fold increased) strains. After 24 h the PXN expression levels were slightly increased after infiltration of the deficient (1.4-fold increased) and nonhost (1.5-fold increased) strains and were strongly increased after

infiltration of the virulent (3-fold increased) and the avirulent (2.3-fold increased) *P. syringae* strains in comparison to the expression under control treatment (Figure 3.24).

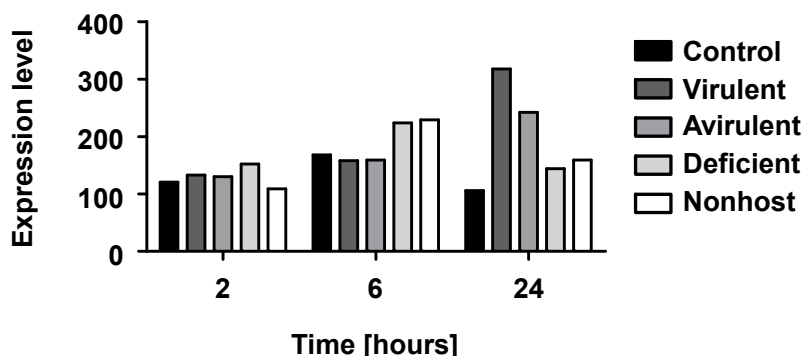


**Figure 3.24** *In silico* analysis of PXN expression level using eFP Browser – *Pseudomonas syringae*

Gene expression values of WT leaf tissue infected with different *P. syringae* strains. PXN expression increased after infiltration of a virulent and avirulent *P. syringae* strain after 24 h. Data were obtained from eFP Browser (Winter *et al.*, 2007).

### 3.8 Redundant systems for supplementing peroxisomes with NAD<sup>+</sup>

A redundant system for the PXN function has to exist, as a severe  $\beta$ -oxidation phenotype of Arabidopsis plants lacking functional PXN expression was expected but not confirmed (section 3.6). Candidates for NAD<sup>+</sup>/AMP exchange are the peroxisomal PNC proteins because ATP and NAD<sup>+</sup> are similar in structure (section 3.2.3). Another possible redundant system is the malate/OAA shuttle system mediating the NAD<sup>+</sup>/NADH redox shuttle over the peroxisomal membrane by pMDH and cMDH (section 1.3.1 and 1.3.3; Pracharoenwattana *et al.*, 2007; Graham, 2008). In addition, it was recently shown that the peroxisomal hydroxyl pyruvate reductase 1 (HPR1) plays a role in oxidizing NADH for functional  $\beta$ -oxidation (Pracharoenwattana *et al.*, 2010).

The NAD<sup>+</sup> level of *pxn* seedlings was determined to investigate if PXN generated a peroxisomal NAD<sup>+</sup> pool and if the NAD<sup>+</sup> metabolism is altered in plants lacking functional PXN expression. In addition, the redundancy of PXN was analyzed by generating mutant plants missing PXN expression and the expression of both PNC, both pMDH, required for the malate/OAA shuttle, or both pMDH and HPR1 proteins.

#### 3.8.1 NAD<sup>+</sup> level of *pxn* seedlings

To confirm the hypothesis that PXN generated a peroxisomal NAD<sup>+</sup> pool for functional metabolism, the NAD<sup>+</sup> and NADH levels of WT and *pxn-1* seedlings were measured. Total extract from Arabidopsis seedlings was used to determine the NAD<sup>+</sup> and NADH levels. The NAD<sup>+</sup> and NADH concentrations were measured using a phenazine ethosulfate/3-(4,5-dimethylthiazolyl-2)-2,5-diphenyltetrazolium bromide (PES/MTT) assay (section 2.3.15; Gibon and Larher, 1997). The total NAD<sup>+</sup> content of four-day-old *pxn-1* seedlings grown

under short-day conditions ( $18.6 \pm 3.2$  pmol NAD<sup>+</sup> mg freshweight<sup>-1</sup>) was significantly increased in comparison to WT seedlings ( $10.0 \pm 1.6$  pmol NAD<sup>+</sup> mg freshweight<sup>-1</sup>; Figure 3.25; Trippelsdorf, 2012). The NADH level could not be tested due to a quenching effect of the leaf extract.

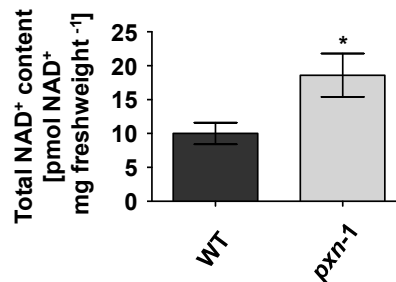


**Figure 3.25 Total NAD<sup>+</sup> content of WT and *pxn-1* seedlings**

The total NAD<sup>+</sup> content of four-day-old WT and *pxn-1* seedlings grown under short-day conditions was measured using a PES/MTT assay (Trippelsdorf, 2012). The NAD<sup>+</sup> level of *pxn-1* seedlings was significantly increased in comparison to WT. An unpaired t-test was performed. Asterisk indicate significance levels. \*P < 0.05 (significant).

### 3.8.2 PNC gene silencing using siRNAi approach in *pxn* mutants

It was analyzed if the PNC proteins can adopt the transport function of PXN when it is absent. Therefore, constructs to silence the PNC1 and PNC2 expression via small interfering siRNAs driven under the control of a constitutive promoter (p35S::siR-*PNC1/2*) or an ethanol inducible promoter (pAlcA::siR-*PNC1/2*) was used as described in Linka *et al.* (2008b). These constructs were transformed into *pxn-1* mutant plants and positive transformants were selected on agar plates containing the appropriate antibiotic (section 2.3.3). Seeds of the T<sub>2</sub> generation were collected. The T-DNA insertions expressing the PNC1/2 siRNAs were verified on gDNA using construct specific primers (Figure 3.26; section 2.3.3 and 2.3.5). p35S::siR-*PNC1/2* *pxn* plants did not exhibit an obvious phenotype. Because of time-limitation it could not be tested if the PNC1/2 siRNAs expression is induced upon ethanol treatment in pAlcA::siR-*PNC1/2* *pxn* plants.

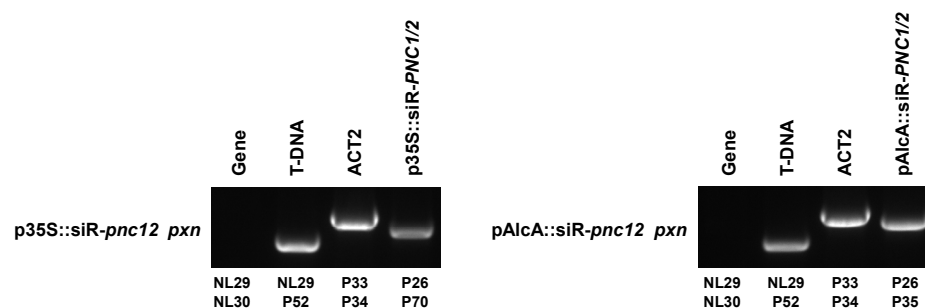


**Figure 3.26 Genotype of artificial PNC1/2 siRNAi lines in *pxn* background**

To silence both *pnc* genes, an artificial siRNAi construct was transformed into a *pxn-1* mutant line. p35S::siR-*PNC1/2* is driven under the control of the constitutive 35S promoter and pAlcA::siR-*PNC1/2* under an ethanol inducible promoter. A PCR-based screening with gene and T-DNA specific primers was performed. ACT2 specific primers were used as positive control for gDNA isolation. Expected PCR products: see section 2.3.5.

### 3.8.3 Redox equivalent exchange by the malate/oxaloacetate shuttle

It was hypothesized that PXN acts as a NAD<sup>+</sup>/NADH carrier and is therefore redundant to the malate/OAA shuttle mediated by the peroxisomal and cytosolic MDHs. To test if both systems act as redox shuttle, it was analyzed if a knock-down of PXN expression in these mutant backgrounds gained a severe phenotype as it is assumed that the peroxisomal supply of NAD<sup>+</sup> is essential.

To examine the redundancy of PXN and the malate/OAA shuttle, the *pmdh1 pm dh2* and *pmdh1 pm dh2 hpr1* mutant lines were crossed with the *pxn-1* mutant line. The obtained seedlings from the crossed siliques were grown on agar-plates and verified by PCR analysis. The T<sub>0</sub> lines were heterozygous for the T-DNA insertions in the *pxn*, *pmdh1*, *pmdh2*, and *hpr1* gene (Figure 3.27; section 2.3.5). Further, selfing of the heterozygous lines and selection of homozygous lines has to be performed.

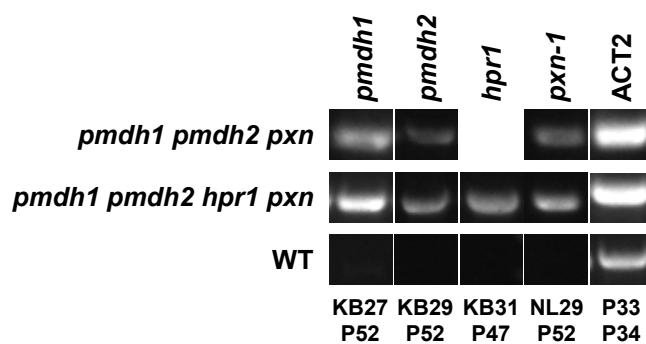


**Figure 3.27 Genotype of generated *pmdh1 pm dh2 pxn* and *pmdh1 pm dh2 hpr1 pxn* mutant lines**

*pmdh1 pm dh2 pxn* and *pmdh1 pm dh2 hpr1 pxn* mutant lines were created by crossing the single *pxn-1* mutant with the corresponding double or triple mutants. PCR analysis on genomic DNA was performed with T-DNA specific primer. ACT2 specific primers were used as positive control for gDNA isolation. Expected PCR products: see section 2.3.5. The plants of the first generation after crossing are heterozygous in all T-DNA insertions.

Alternatively approach to silence the *pxn* gene expression in the mutant plants lacking the malate/OAA shuttle was done by using an artificial microRNA for PXN. The prospective PXN amiRNA constructs, either driven by a constitutive UBQ10 promoter (pUBQ::amiR-*PXN*) or an estradiol inducible LexA promoter (pLexA::ami-*pxn*; section 2.3.8) was transformed into the *pmdh1 pm dh2* and *pmdh1 pm dh2 hpr1* background as well in WT (section 2.3.3).

After transformation, the T<sub>0</sub> seeds were selected on agar plates containing the corresponding antibiotic (section 2.3.3). Due to low transformation efficiency only few mutant plants could be verified by PCR on gDNA containing the T-DNA of the PXN amiRNA (Figure 3.28; section 2.3.5). No obvious growth phenotypes for these mutant lines (pUBQ::amiR-*PXN*, pUBQ::amiR-*PXN pm dh1 pm dh2 hpr1*, pUBQ10::amiR-*PXN pm dh1 pm dh2*, pLexA::amiR-*PXN*, and pLexA::amiR-*PXN pm dh1 pm dh2 hpr1*) were observed under standard growth conditions.



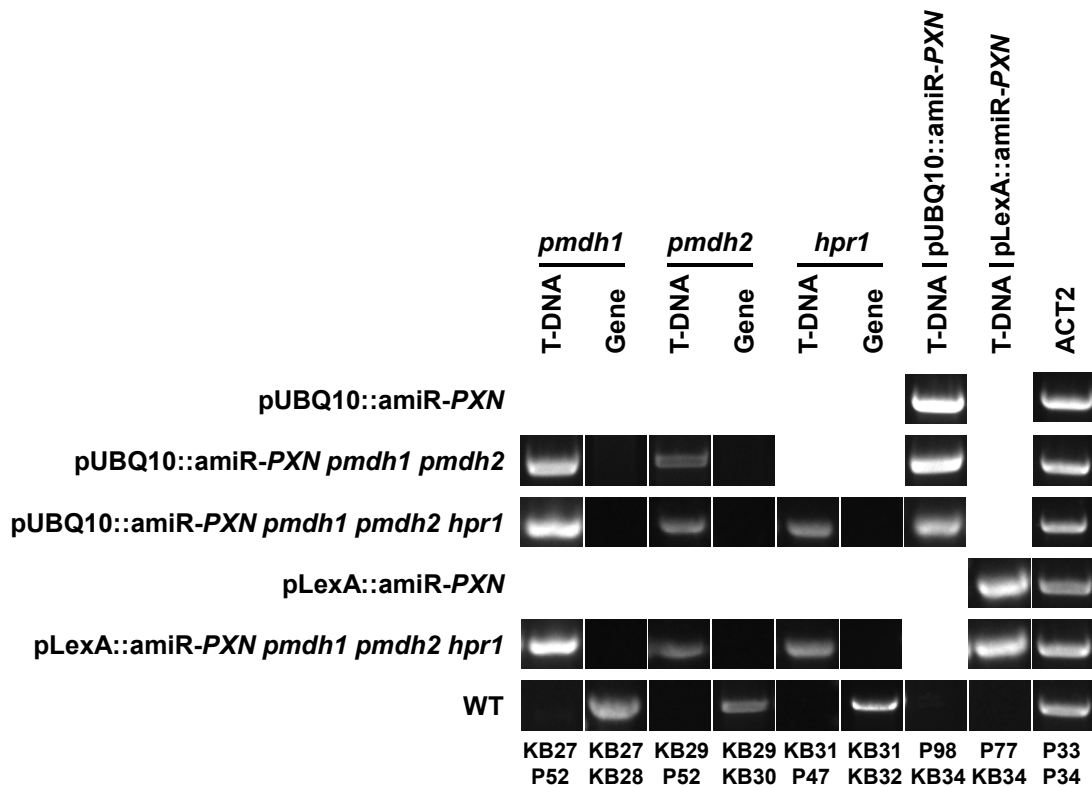


**Figure 3.28 Genotype of artificial miRNA *PXN* lines**

PCR analysis on gDNA of WT, *pmdh1 pmdh2*, and *pmdh1 pmdh2 hpr1* plants transformed with pUQ10::amiR-*PXN* and pLexA::amiR-*PXN* constructs for *pxn* gene silencing. Gene and T-DNA specific primers were used. ACT2 specific primers were used as positive control for gDNA isolation. Expected PCR products: see section 2.3.5.

### 3.9 Function of the unique loop region of *PXN*

In comparison to other members of the MCF family, *PXN* possesses a unique expanded loop region between transmembrane domain three and four (Figure 3.1; Figure 3.29). In addition, two independent proteomic studies performed with isolated peroxisomes of cell culture tissue detected a phosphorylation site at serine 155, which is localized in the loop region (data were obtained from the PhosPhAt 3.0 database, Eubel *et al.* (2008), Heazlewood *et al.* (2008), Ito *et al.* (2009), and Durek *et al.* (2010)). It is known that specific phosphorylation sites regulated the activity of transport proteins and the function of metabolic enzymes (Kaiser and Huber, 2001; Durek *et al.*, 2010; Lanquar and Frommer, 2010).

In this thesis, it was analyzed if the hydrophilic loop and the phosphorylation site of the *PXN* protein facilitated an impact on peroxisomal targeting or transport activity. For this purpose constructs with a complete loop deletion (named *PXN*  $\Delta$ loop) and amino acid exchanges of S155 were produced (section 2.4.4). S155 was exchanged to alanine (S155A), cysteine (S155C) and aspartate (S155D). Alanine was used as neutral amino acid. Cysteine, carrying a sulphur group, mimics the dephosphorylated state of S155. Aspartate imitates the phosphorylated state of S155 with the negative charged carboxyl group.

```

PXN      : VNVLMTNPIWVIVTRMQTHRKMTKDQTAAPESPSSNAEALVAVEPRPYGTFTNTIREVYDEAGITGFWKGV : 193
NDT1     : ATTIATNPLWVVKTRLQTQG-----MRVGIVPYKSTFSALRRIAYEEGIRGLYSGL : 176
NDT2     : ATSIATNPLWVVKTRLMTQG-----IRPGVVPYKSVMSAFSRICHEEGVRGLYSGL : 180
Ndt1p    : ASTTLLTNPIWVVKTRLMLQSN-----LGEHPHXYKGTFDFAFRKLFYQEGFKALYAGL : 240
Ndt2p    : ISTVATNPIWVVKTRLMLQTG-----IGKYSTHYKGTIDTFRKIIQQEGAKALYAGL : 202
SLC25A17 : VNVLLTTPPLWVVNTRLKLGAK-----FRNEDIVPTNYKGIIDAFHQIIRDEGISALWNGT : 169
PNC1     : CTSVLIQPLDTASSRMQTSE-----FGESKGLWKTLTEGSWADAFDGL : 161
PNC2     : CTSVLTQPLDTASSRMQTSE-----FGKSKGLWKTLTDGSGNAFDGL : 163
Ant1p    : ISQLFTSEPMVVATRQQTVHS-----AESAKFTNVIKDIYREN-NGDITAFWKGL : 185

```

**Figure 3.29** Section of an alignment of PXN and other MCF members focused on the unique loop region of PXN

Amino acid alignment of PXN and other Arabidopsis, yeast, and human NAD<sup>+</sup> carriers (NDT1, chloroplast; NDT2, Ndt1p, and Ndt2p, mitochondria; SLC25A14, peroxisome) and ATP carriers (PNC1, PNC2, Ant1p, peroxisome). Transmembrane domains (TMD) are indicated by black lines. Shaded in yellow is the unique loop region which is completely deleted in the PXN  $\Delta$ loop constructs. S155, labelled in red, was shown to be phosphorylated by proteomic studies (Eubel *et al.*, 2008; Ito *et al.*, 2009).

### 3.9.1 Impact of the loop region and phosphorylation site S155 on peroxisomal targeting

To establish if the hydrophilic loop region or the phosphorylation site at S155 of PXN is required for peroxisomal targeting, N-terminal yellow fluorescent protein (YFP)-fusion proteins of PXN, PXN S155A, PXN S155C, PXN S155D, and PXN  $\Delta$ loop were generated for co-localization analysis (section 2.3.11). Mediated by agrobacteria-infiltration, these constructs were transiently expressed in stable transformed tobacco leaves expressing a cyan fluorescent protein (CFP) fused to a peroxisomal targeting signal 1 (PTS1; section 2.3.11). Leaves were analyzed using laser scanning confocal microscopy. Fluorescence of YFP-PXN and all mutated YFP-PXN fusion proteins were detected in a punctuated pattern and co-localized to the signal of the peroxisomal CFP-PTS1 marker, indicating peroxisomal localization of all PXN variants (Figure 3.30).

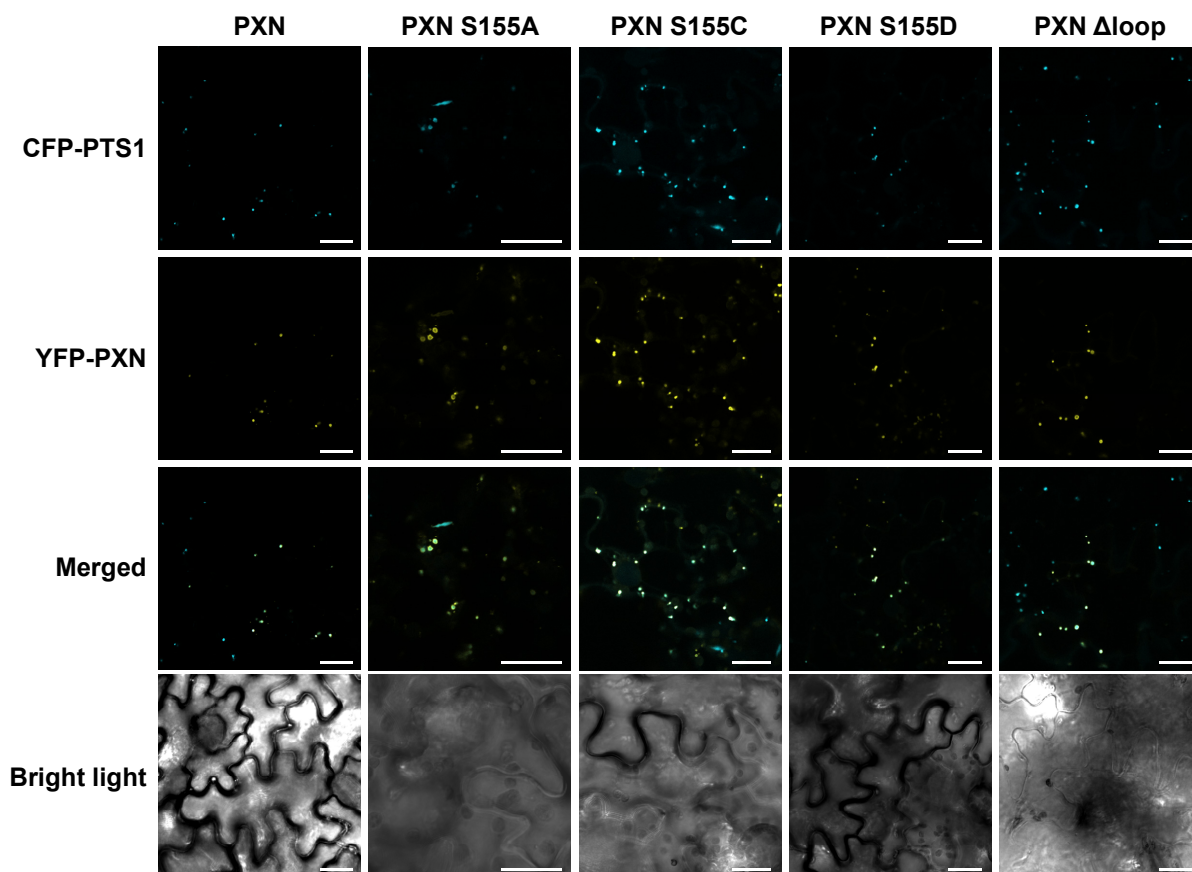


**Figure 3.30 Co-localization of YFP fused PXN, PXN S155A, PXN S155C, PXN S155D, and PXN  $\Delta$ loop proteins**

Constructs of N-terminal YFP fusions proteins of PXN, PXN S155A, PXN S155C, PXN S155D, and PXN  $\Delta$ loop were infiltrated using agrobacteria-mediated transformation of CFP-PTS1 expressing tobacco leaves. All proteins are co-localized with the peroxisomal marker CFP-PTS1. Scale bars: 10  $\mu$ M.

### 3.9.2 Impact of the loop region and phosphorylation site S155 on transport activity

To investigate if the unique loop region or the phosphorylation of S155 regulates the PXN transport function, uptake experiments with mutated PXN proteins were performed. Thus, constructs for cell-free expression of the mutated PXN-His proteins (PXN S155A, PXN S155C, PXN S155D, and PXN  $\Delta$ loop) were generated (section 2.4.1 and 2.4.4). Immunoblot analysis using anti-His antibody detected the cell-free expressed mutated PXN-His proteins with the calculated mass of 37.3 kDa for PXN, PXN S155A, PXN S155C, and S155D and of 33.4 kDa for PXN  $\Delta$ loop (Figure 3.31). The reduced size of the PXN  $\Delta$ loop protein due to the deletion could be visualized on both, the coomassie-stained SDS-PAGE and the immunoblot using an anti-His antibody (Figure 3.31).

Recombinant PXN-His and mutated PXN-His proteins were reconstituted into proteoliposomes preloaded with 30 mM  $\text{NAD}^+$ , NADH, or AMP (section 2.4.4) and time dependent uptake experiments with radioactively labelled  $[\alpha\text{-}^{32}\text{P}]\text{-NAD}^+$  (125  $\mu$ M) were performed (section 0).

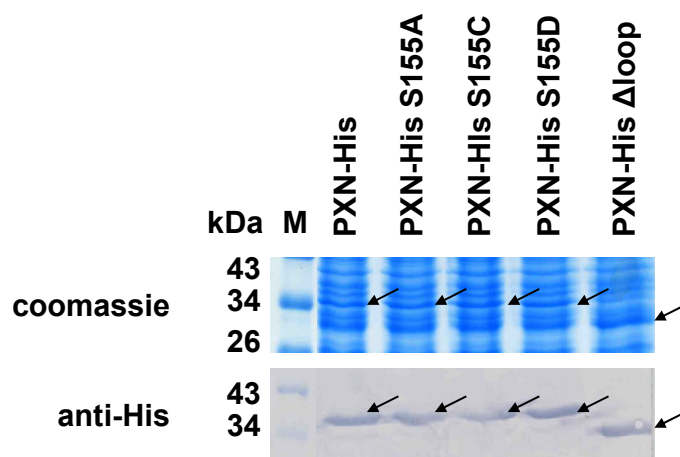


**Figure 3.31 Cell-free WGE expression of mutated PXN proteins**

Coomassie-stained SDS-PAGE and immunoblot analysis of recombinant PXN-His, PXN-His S155A, PXN-His S155C, PXN-His S155D, and PXN-His  $\Delta$ loop protein. Recombinant proteins were detected using an anti-His antibody. Arrows indicate recombinant proteins with the right molecular mass of 37.3 kDa for PXN-His and the mutated PXN-His S155 proteins and 33.4 kDa for PXN-His  $\Delta$ loop protein. M, marker proteins.

All mutated PXN-His proteins mediated  $\text{NAD}^+$  uptake and followed first-ordered kinetics (Figure 3.32 and Figure 7.3). The equilibrium plateau ( $V_{\max}$ ) and initial rate values were calculated of PXN-His and the mutated PXN-His proteins (Figure 3.32; Table 7.1).

The  $V_{\max}$  values were not significant different for  $\text{NAD}^+/\text{NAD}^+$  homo-exchange and  $\text{NAD}^+/\text{NADH}$  hetero-exchange (Figure 3.32, A; Table 7.1). But PXN-His S155C ( $83 \pm 5\%$ ) and PXN-His  $\Delta$ loop ( $68 \pm 10\%$ ) proteins exhibited a significant reduced  $V_{\max}$  for  $\text{NAD}^+/\text{AMP}$  exchange, whereas the  $V_{\max}$  values of PXN-His S155A ( $101 \pm 9\%$ ) and PXN-His S155D ( $119 \pm 16\%$ ) were similar to PXN-His protein ( $100 \pm 10\%$ ; Figure 3.32, A; Table 7.1). The initial rates possessed more differences between the divers PXN variants than the  $V_{\max}$  values. In comparison to PXN-His (set as 100%;  $\text{NAD}^+$ :  $100 \pm 14\%$ ;  $\text{NADH}$ :  $100 \pm 10\%$ ;  $\text{AMP}$ :  $100 \pm 2\%$ ), the initial rates of PXN-His S155C ( $\text{NAD}^+$ :  $73 \pm 3\%$ ;  $\text{NADH}$ :  $61 \pm 13\%$ ;  $\text{AMP}$ :  $71 \pm 1\%$ ) and PXN-His  $\Delta$ loop ( $\text{NAD}^+$ :  $67 \pm 14\%$ ;  $\text{NADH}$ :  $59 \pm 5\%$ ;  $\text{AMP}$ :  $47 \pm 2\%$ ) were significant reduced for  $\text{NAD}^+$  uptake in exchange with  $\text{NAD}^+$ ,  $\text{NADH}$ , and  $\text{AMP}$  (Figure 3.32, B; Table 7.1). The initial rates for  $\text{NAD}^+/\text{AMP}$  hetero-exchange were significant increased in comparison to  $\text{NAD}^+/\text{NAD}^+$  homo-exchange for PXN-His ( $155 \pm 3\%$ ) and all mutated PXN-His proteins (S155A:  $160 \pm 2\%$ ; S155C:  $152 \pm 1\%$ ; S155D:  $136 \pm 4\%$ ), beside for PXN-His  $\Delta$ loop protein ( $108 \pm 4\%$ ). In case for PXN-His S155D ( $106 \pm 3\%$ ), the initial rates for  $\text{NAD}^+/\text{AMP}$  hetero-exchange was increased in comparison to PXN-His ( $100 \pm 2\%$ ; Figure 3.32, B; Table 7.1). PXN-His S155A protein exhibited similar initial rate values like PXN-His for  $\text{NAD}^+$  uptake in exchange with  $\text{NAD}^+$  (PXN-His:  $100 \pm 14\%$ ; S155A:  $97 \pm 7\%$ ) and  $\text{AMP}$  (PXN-His:  $100 \pm 2\%$ ; S155A:  $100 \pm 1\%$ ), but it showed decreased values in exchange with  $\text{NADH}$  (PXN-His:  $100 \pm 10\%$ ; S155A:  $80 \pm 10\%$ ; Figure 3.32, B; Table 7.1).

It was analyzed if the recombinant PXN-His and mutated PXN-His proteins are phosphorylated if expressed using the WGE system. Therefore, a phosphoserine antibody

was used for immunoblot analysis (section 2.2.2) but no positive signal was observed (Figure 7.4). No conclusion could be assumed, because a positive control was missing.

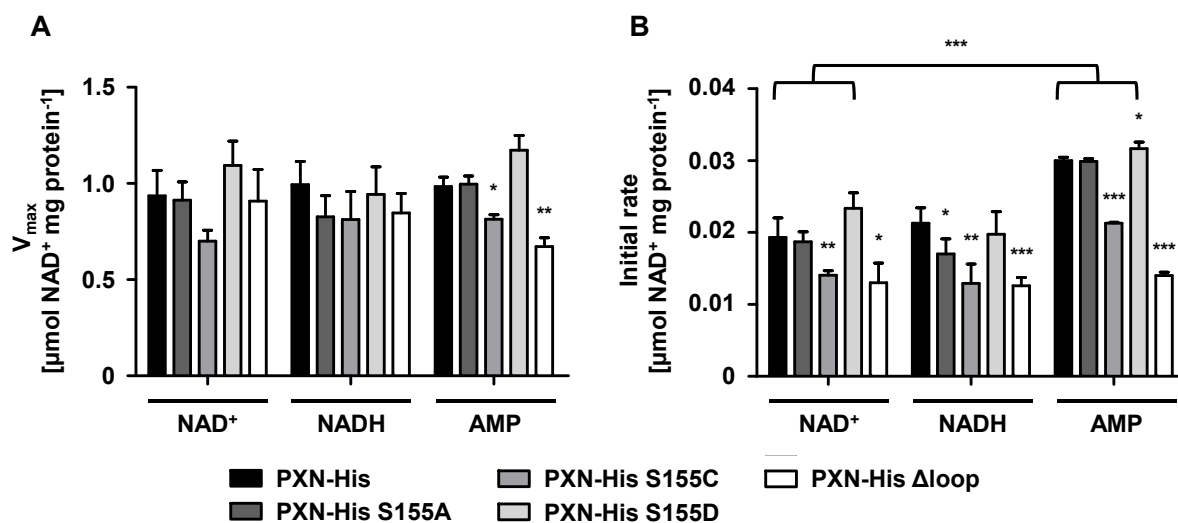


**Figure 3.32**  $[\alpha\text{-}^{32}\text{P}]\text{-NAD}^+$  uptake activity of PXN-His and mutated PXN-His proteins with  $\text{NAD}^+$ ,  $\text{NADH}$  and  $\text{AMP}$  exchange

Time dependent  $[\alpha\text{-}^{32}\text{P}]\text{-NAD}^+$  uptake was measured of  $\text{NAD}^+$ ,  $\text{NADH}$  or  $\text{AMP}$  preloaded proteoliposomes with reconstituted PXN-His, PXN-His S155A, PXN-His S155C, PXN-His S155D, and PXN-His  $\Delta\text{loop}$  protein. The calculated (A)  $V_{max}$  and (B) initial rate values are plotted in those graphs. Significance asterisks above the bars were calculated in comparison to PXN-His values and significance asterisks connected with the line were calculated in comparison to  $\text{NAD}^+/\text{NAD}^+$  homo-exchange. The data represents the arithmetic means  $\pm$  SEs of four independent experiments. Asterisks indicate significance levels.

### 3.10 The role of PEX19 in peroxisomal membrane protein targeting

Up to now it was not investigated how MCF-type PMPs are targeted to plant peroxisomes. Based on previous studies, the receptor protein PEX19 interacted with other PMPs and mediated the targeting of these PMPs to the peroxisomal membrane (section 1.2.2; Sacksteder *et al.*, 2000). It was investigated if peroxisomal MCF members and other peroxisomal transport proteins are targeted to plant peroxisomes in a PEX19-dependent manner.

In this thesis, PEX19 interaction studies were performed with PXN, PNC1 and PNC2. Other known peroxisomal transport proteins were included, such as the channel-forming proteins PMP22 (Tugal *et al.*, 1999), PMP22-like (unknown function; Jan Wiese, Heinrich-Heine University (HHU) Düsseldorf, Germany; personal communication), and pseudo-halves of the ABC transporter CTS (Zolman *et al.*, 2001; Footitt *et al.*, 2002; Nyathi *et al.*, 2012). As controls, transport proteins from other organelles were used, including the mitochondrial mitoPMP22 (unknown function, Jan Wiese, HHU Düsseldorf, Germany; personal communication) and the chloroplastic mesophyll envelope protein 1 (MEP1, unknown function; Thea Pick, HHU Düsseldorf, Germany; personal communication and Bräutigam *et al.* (2008)). In addition, the impact of the unique loop region and the phosphorylated serine of

PXN on the PEX19 interaction were analyzed with mutated PXN proteins (section 3.8). The interaction of PXN and PEX19 was evidenced by the co-expression of PXN with both Arabidopsis PEX19 proteins, PEX19.1 and PEX19.2, and the PMP targeting receptor PEX3 (Table 3.4). The interactions of PEX19 with the different transport proteins were tested by an *in vitro* PEX19 pull-down assay (section 2.5) and an *in vivo* mis-localization assay (section 2.5).

### 3.10.1 *In vitro* PEX19 pull-down assay

The two Arabidopsis PEX19 proteins PEX19.1 and PEX19.2 were used for *in vitro* PEX19 interaction studies (Nyathi *et al.*, 2012). Recombinant N-terminal tagged glutathione S-transferase (GST)-PEX19 fusion proteins and GST alone were expressed in *E. coli*, purified, and immobilized on glutathione magnetic beads (section 2.5). All examined transport proteins (PXN, PXN S155A, PXN S155C, PXN S155D, PXN  $\Delta$ loop, PNC1, PNC2, CTS-N, CTS-C, PMP22, mitoPMP22, and MEP1) were C-terminal His-tagged and expressed using the WGE system (section 2.4.2). After incubation of the recombinant transport proteins with the *E. coli* expressed PEX19 proteins, the PEX19 interacting proteins were eluted and analyzed by SDS-PAGE and immunoblot analysis using anti-His antibody (Figure 3.33). Each transport protein could be expressed *in vitro* (Figure 3.33, 20% input).

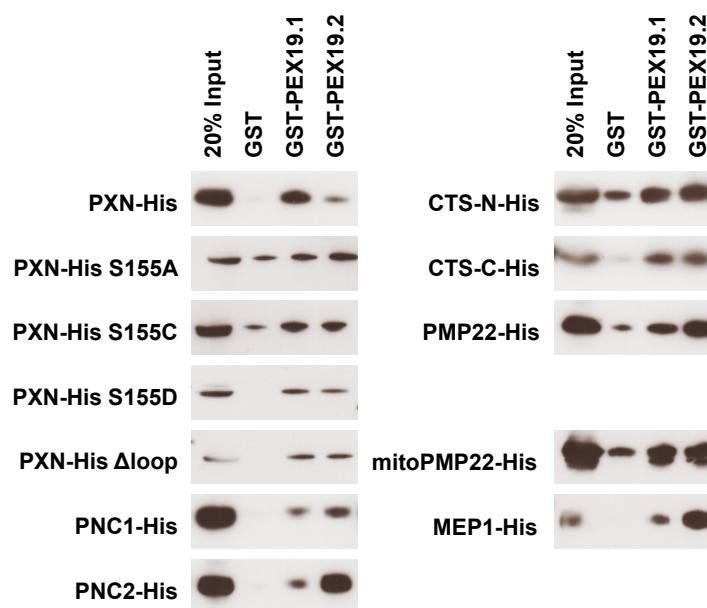


**Figure 3.33 *In vitro* PEX19.1 and PEX19.2 pull-down assay with recombinant transport proteins**

GST-PEX19 fusion protein and GST alone (as negative control) were expressed in *E. coli*, purified, immobilized on glutathione magnetic beads, and incubated with different *in vitro* translated C-terminal His-tagged transport proteins. Interacted proteins were eluted and analyzed by SDS-Page and immunoblot analysis. His-tagged proteins were detected using anti-His antibody. 20% input, 20% of the His-tagged proteins used in the pull-down experiment; GST, pull-down with GST alone; GST-PEX19.1, pull-down with PEX19.1; GST-PEX19.2, pull-down with PEX19.2. Peroxisomal proteins: PXN, PXN S155A, PXN S155C, PXN S155D, PXN  $\Delta$ loop, PNC1, PNC2, CTS-N, CTS-C, PMP22 and PMP22 like. Mitochondrial protein: mitoPMP22. Chloroplastic protein: MEP1. All transport proteins interacted with PEX19.1 and PEX19.2.

The PMP-His proteins exhibited stronger interaction signals with GST-PEX19.1 or GST-PEX19.2 than with GST alone (Figure 3.33), indicating an interaction of PXN-His, PXN-His S155A, PXN-His S155C, PXN-His S155D, PXN-His  $\Delta$ loop, PNC1-His, PNC2-His, CTS-N-His, CTS-C-His, and PMP22-His with both PEX19 proteins. Unexpectedly, the mitochondrial mitoPMP22-His and the chloroplastic MEP1-His protein exhibited the same interaction pattern as the PMPs, indicating an interaction with both PEX19 proteins (Figure 3.33).

### 3.10.2 *In vivo* PEX19 mis-localization assay

Alternatively, the interaction of PEX19 with PMPs was studied by using an *in vivo* approach. Therefore plant peroxisomal transport proteins were either N-terminal (PXN, PXN S155A, PXN S155C, PXN S155D, and PXN  $\Delta$ loop) or C-terminal fused to YFP (PNC1, PNC2, PMP22, and PMP22-like). As control the human peroxisomal ABC transporter ALDP (adrenoleukodystrophy protein) and ALDR (adrenoleukodystrophy-related protein) were C-terminal fused to YFP. Arabidopsis PEX19.1 was N-terminal fused to a nuclear localization signal (NLS). The YFP-fused PMPs and the NLS-PEX19.1 protein were transient co-expressed using agrobacteria-mediated transformation in tobacco leaves that stable expressed the peroxisomal marker CFP-PTS1 (section 2.3.11). Within this approach, a nuclear localization of the YFP fluorescence was expected if the YFP-fused PMPs interacted with the NLS-PEX19.1 protein, as the interacted proteins are targeted to the nucleus because of the NLS. It was shown before that ALDP-YFP and ALDR-YFP are localized to the nucleus by co-expression with NLS-PEX19 fusion protein in tobacco leaves and was used therefore as positive control (Zhang *et al.*, 2011).

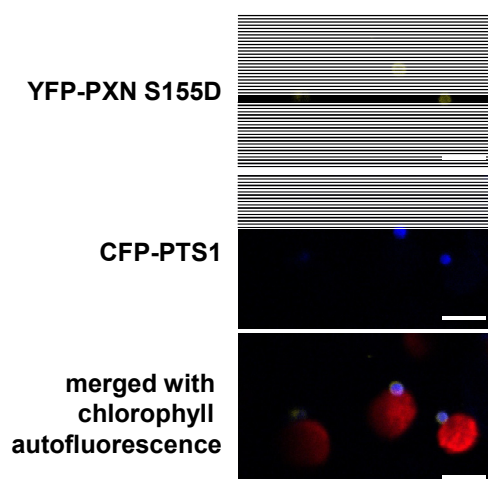


**Figure 3.34** Transient expression of PXN S155D in tobacco leaves

YFP-PXN S155D protein was transient expressed in stable transformed CFP-PTS1 tobacco leaves. The ring-like YFP fluorescence around the peroxisomal matrix marker CFP-PTS1 indicated the peroxisomal membrane localization of YFP-PXN S155D. Scale bars: 5  $\mu$ M. These pictures are representative for all tested YFP-PMP proteins. This experiment was repeated several times and the same outcome was always observed.

All tested YFP-fused PMPs showed a ring-like structure of the YFP fluorescence, which bordered the CFP fluorescence of the peroxisomal matrix localized CFP-PTS1 protein (YFP-PXN S155D is given as example in Figure 3.34), indicating the localization of all PMPs to the peroxisomal membrane. In these experiments, all tested YFP-fused PMPs were localized to peroxisomes in the presence or absence of NLS-PEX19.1. The expected nuclear localization of the positive controls, ALDP-YFP and ALDR-YFP, if co-expressed with the NLS-PEX19.1 protein was not observed.

### 3.10.3 *In silico* analysis of PEX19 binding sites

Furthermore, an *in silico* analysis using the PEX19 binding site predictor was performed that is online available with an algorithm of yeast and human PEX19 binding site motifs, identified as an integral part of the peroxisomal membrane targeting signal (mPTS; <http://www.peroxisomedb.org/>; Rottensteiner *et al.*, 2004; Halbach *et al.*, 2005).

Putative interactions with PEX19 were not exclusively predicted for peroxisomal proteins and the block E-values exhibited a bright spectrum from 0.014 for the chloroplastic MEP1 to 0.97 for the peroxisomal C-terminal half of CTS. The MCF members PXN (0.13), PNC1 (0.04), and PNC2 (0.053) exhibited a lower and more specific E-value as the ABC transporter CTS (0.66). In addition, the peroxisomal located PMP22 (0.023) and PMP22-like protein (0.021) exhibited a more specific E-value than the mitochondrial located mitoPMP22 (0.8) protein.

**Table 3.5 Predicted PEX19 binding site values of chosen transport proteins**

Block E-values for PEX19 binding site prediction of chosen transport proteins: PXN, PNC1, PNC2, CTS-FL, CTS-N, CTS-C, PMP22, PMP22 like, mitoPMP22, and MEP1. PEX19 binding site prediction was performed using PEX19 binding site predictor (Table 7.5). P, peroxisome; M, mitochondria; C, chloroplast.

Protein	Block E-value	Organelle
PXN	0.13	P
PNC1	0.04	P
PNC2	0.053	P
CTS-FL	0.66	P
CTS-N	0.97	P
CTS-C	0.33	P
PMP22	0.023	P
PMP22 like	0.021	P
mitoPMP22	0.8	M
MEP1	0.014	C



## 4 Discussion

Plant peroxisomes are essential organelles that fulfil several metabolic pathways essential for plant development and resistance against abiotic and biotic stresses (Hu *et al.*, 2012). Three main metabolic pathways, the fatty acid  $\beta$ -oxidation, photorespiratory  $C_2$  cycle, and  $H_2O_2$  detoxification are dependent on the cofactor  $NAD^+$  (Figure 1.1; section 1.3; Graham, 2008; Hu *et al.*, 2012). For decades, the existence of a specific peroxisomal  $NAD^+$  transport system was controversially discussed (Rottensteiner and Theodoulou, 2006). Because  $NAD^+$  biosynthesis exclusively takes places in the cytosol (section 1.4; Noctor *et al.*, 2006; Hashida *et al.*, 2009) and the peroxisomal membrane is impermeable for “bulky” substrates like  $NAD^+$  and other cofactors (section 1.5.1; Donaldson, 1981; Antonenkov and Hiltunen, 2012), a  $NAD^+$  import system has to exist to set up and maintain a peroxisomal  $NAD^+$  pool for functional metabolism.

In this thesis, the candidate gene At2g39970, encoding for a MCF member, was identified as peroxisomal  $NAD^+$  carrier, called PXN (section 1.5.3 and 3.1). The peroxisomal localization of PXN was confirmed by co-localization studies and immunoblot analysis before (Fukao *et al.*, 2001; Linka *et al.*, 2008b; Wilkinson, 2009). Because of its close homology to the peroxisomal ATP transporter PNC1 and PNC2, PXN was predicted to mediate ATP import (Linka *et al.*, 2008b). Nevertheless, it was shown that PXN could not complement a yeast strain missing the endogenous peroxisomal ATP carrier Ant1p (Linka *et al.*, 2008b). PXN represents a prime candidate for the peroxisomal  $NAD^+$  carrier as it exhibited close amino acid sequence homology to other  $NAD^+$  transporters of the MCF from Arabidopsis, yeast, and human (Figure 3.2 and Figure 3.1; section 3.1).

### 4.1 PXN is the first characterized peroxisomal $NAD^+$ carrier of plants

#### 4.1.1 PXN catalyzed *in vitro* the uptake of $NAD^+$ , NADH and CoA

This work demonstrated that cell-free expressed PXN protein catalyzed the transport of  $NAD^+$  with broad substrate specificity by performing uptake studies using radioactively labelled [ $\alpha$ - $^{32}P$ ]- $NAD^+$  (section 3.2). PXN mediated  $NAD^+$  transport activity followed first-order kinetics with a high affinity ( $K_M$ ) value of  $246 \pm 64 \mu M$   $NAD^+$  that is comparable to chloroplastic and mitochondrial  $NAD^+$  carrier from plant and yeast (Table 3.3).

It was postulated that most of the intracellular pyridine nucleotides are bound to proteins, presumably dehydrogenases. Therefore, the total concentration of both free and bound  $NAD^+$  was determined in various studies (Mettler and Beevers, 1980; Heineke *et al.*, 1991; Igamberdiev and Gardestrom, 2003; Queval and Noctor, 2007; Wang and Pichersky, 2007; Quettier *et al.*, 2008). A cytosolic concentration of  $600 \mu M$  free  $NAD^+$  was estimated from the concentrations of metabolites and enzyme activities from spinach leaves (Heineke *et al.*, 1991). In addition, in pea leaf protoplasts a cytosolic concentration of  $520 \mu M$  free

NAD<sup>+</sup> and 55 μM free NADH was determined by direct measurements (Igamberdiev and Gardestrom, 2003). Several independent studies confirmed the oxidized state of the cytosolic pyrimidine nucleotide pool (Mettler and Beevers, 1980; Heineke *et al.*, 1991; Igamberdiev and Gardestrom, 2003; Queval and Noctor, 2007; Wang and Pichersky, 2007; Quettier *et al.*, 2008). The fact that the K<sub>M</sub> value of PXN for NAD<sup>+</sup> is lower than the cytosolic free NAD<sup>+</sup> levels in plants, the import of NAD<sup>+</sup> from the cytosol into peroxisomes via PXN is conceivable.

The measured substrate specificity and inhibitor constants (Figure 3.4; Table 3.1) revealed that AMP, ADP, NADH, and CoA are putative counter substrates for PXN mediated NAD<sup>+</sup> transport. The precursor of NAD<sup>+</sup> biosynthesis, NaAD, is excluded as transport substrate. First, NaAD exhibited a low inhibitory affect on the NAD<sup>+</sup>/NAD<sup>+</sup> homo-exchange. Second, the NAD<sup>+</sup> biosynthesis exclusively takes place in the cytosol and the enzymes that convert NaAD to NAD<sup>+</sup> are not present in peroxisomes (Noctor *et al.*, 2006; Hashida *et al.*, 2009). FAD, ATP, GDP, GTP, NADP<sup>+</sup>, NADPH, NMN, and Nam are also excluded as putative substrate because these compounds did not mediated relevant NAD<sup>+</sup> uptake (Figure 3.4). Recently, Agrimi and co-worker confirmed the NAD<sup>+</sup> transport function of PXN using *E. coli* expressed PXN protein (Agrimi *et al.*, 2012b). They performed uptake assays using radioactively labelled [<sup>3</sup>H]-NAD<sup>+</sup> and [<sup>14</sup>C]-AMP and showed that PXN catalyzed the transport of NAD<sup>+</sup> or AMP in exchange with NAD<sup>+</sup>, NADH, AMP, ADP, CoA and dephospho-CoA (

Table 7.2; Agrimi *et al.*, 2012b). In addition, they characterized the close homologue of PXN, the human peroxisomal SLC25A17, also known as PMP34, as peroxisomal CoA and FAD carrier with a low NAD<sup>+</sup> uptake efficiency (Agrimi *et al.*, 2012a).

In this thesis, uptake studies were performed using PXN protein fused to a C-terminal His-tag because recombinant protein could be easily detected by immunoblot analysis using an anti-His antibody. The activity of PXN-His is slightly increased in comparison to PXN without His-tag (Figure 3.4), which could be explained by different protein concentrations expressed in the WGE system. Agrimi and co-workers expressed the PXN protein without tag and confirmed our results (Agrimi *et al.*, 2012b).

In comparison to other NAD<sup>+</sup> carrier of the MCF, PXN is the first characterized peroxisomal transport protein that mediated NADH uptake in plants. A bacterial member of the nucleotide transporter (NTT) family, NTT4, accepts NAD<sup>+</sup>, ATP and NADH (Haferkamp *et al.*, 2004). Recently, two Arabidopsis NAD<sup>+</sup> carrier located in the chloroplast (NDT1) and mitochondrion (NDT2) were identified (Palmieri *et al.*, 2009). Both proteins, expressed in *E. Coli*, facilitated an NAD<sup>+</sup> counter-exchange with ADP and AMP and not with NADH, NADP<sup>+</sup>, NADPH, Nam, and Na (Palmieri *et al.*, 2009). In this thesis, it was tested if the NDT proteins, expressed using the WGE expression systems, exhibited NADH uptake activity and if the unique NADH affinity of PXN was due to the different expression systems (section 3.2.2). NDT1 could not be functional expressed in WGE (section 3.2.2). NDT2 was functional

expressed in the WGE system (section 3.2.2) and mediated a low uptake activity of  $\text{NAD}^+$  that was extremely reduced in comparison to the transport activity of recombinant PXN protein (section 3.2.2). To define the transport function of NDT1 and NDT2 regarding the  $\text{NAD}^+/\text{NADH}$  hetero-exchange, the uptake studies has to be repeated with more active protein. On the other hand, PXN protein expressed in yeast verified the transport of  $\text{NAD}^+$  in exchange with AMP and NADH (Figure 3.5) and Agrimi and co-workers showed that *E. coli* expressed PXN protein mediated the unique  $\text{NAD}^+/\text{NADH}$  hetero-exchange (Agrimi *et al.*, 2012b). Therefore the  $\text{NAD}^+/\text{NADH}$  hetero-exchange can be stated as putative physiological function of PXN. The peroxisomal matrix of the yeast *Pichia pastoris* is more reductive than the cytosol under induced fatty acid oxidation (Yano *et al.*, 2010), reinforcing the possible export of NADH in exchange with  $\text{NAD}^+$  from the peroxisomes to the cytosol during fatty acid  $\beta$ -oxidation in plants.

Besides, it was shown that the only MCF-type transporter in yeast, the peroxisomal ATP carrier Ant1p, does not mediated the uptake of  $\text{NAD}^+$  in exchange with AMP or NADH (Figure 3.5). This raises the question how yeast peroxisomes are supplied with  $\text{NAD}^+$  as no  $\text{NAD}^+$  carrier was identified in yeast, to date. One possibility for the  $\text{NAD}^+/\text{NADH}$  redox shuttle is the malate/OAA shuttle, as yeasts lacking peroxisomal Mdh3p are impaired in  $\beta$ -oxidation of fatty acids (van Roermund *et al.*, 1995). Another possibility is the existence of a yet unknown  $\text{NAD}^+$  transporter in yeast peroxisomes.

#### 4.1.2 Putative *in vivo* functions of PXN

From the observed *in vitro* catalyzed transport function, the following possible transport modes for PXN are assumed.

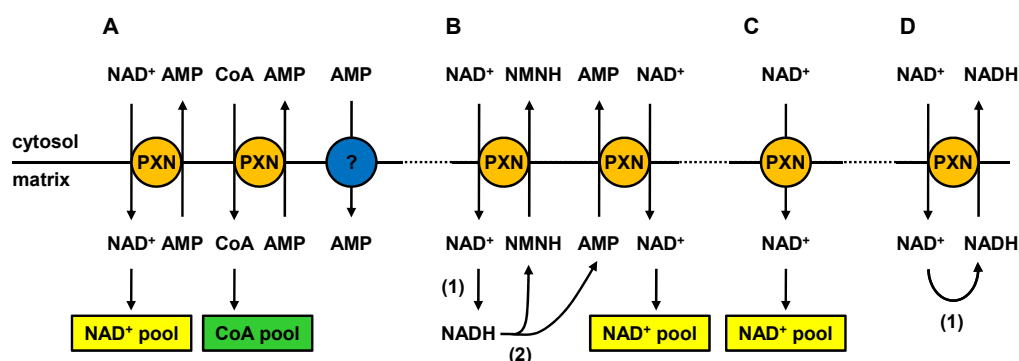


**Figure 4.1 Schematic transport mechanism of PXN**

(A) Two-transport model: PXN mediated  $\text{NAD}^+/\text{AMP}$  and  $\text{CoA}/\text{AMP}$  exchange is coupled to an unknown AMP transporter that catalyzed a unidirectional AMP transport to set-up or maintain the peroxisomal  $\text{NAD}^+$  and CoA pool. (B) Three-substrate model: To generate a peroxisomal  $\text{NAD}^+$  pool, PXN mediated the import of two molecules  $\text{NAD}^+$  in exchange with one AMP and NMNH molecule, both derived from the NUDT7 or NUDT19-catalyzed hydrolysis of one NADH molecule. (C) Uniport model: PXN mediated the import of  $\text{NAD}^+$  in a uniport mechanism to generate a peroxisomal  $\text{NAD}^+$  pool. (D) Redox model: PXN mediated  $\text{NAD}^+/\text{NADH}$  exchange generated a redox shuttle over the peroxisomal membrane. (1) Reduction of  $\text{NAD}^+$  to NADH via peroxisomal metabolism. (2) Peroxisomal nudix hydrolases NUDT7 and NUDT19.

(i) The two-transport model (Figure 4.1 A) assumed that PXN mediated the import of  $\text{NAD}^+$  and CoA in exchange with AMP for generating an  $\text{NAD}^+$  or CoA pool. For this scenario a carrier that catalyses the unidirectional AMP transport is required to balance the loss of AMP. To date, such an AMP uniporter was identified for the plastidic inner membrane (Leroch *et al.*, 2005; Kirchberger *et al.*, 2008). The exchange of  $\text{NAD}^+$  with AMP is favoured of PXN as the *in vitro* uptake studies revealed the highest  $\text{NAD}^+$  uptake activity in exchange with AMP. Agrimi and co-workers confirmed the results present in this work (Agrimi *et al.*, 2012b). The  $\text{NAD}^+/\text{AMP}$  exchange is also characteristic for the peroxisomal, mitochondrial and chloroplastic  $\text{NAD}^+$  carrier from human, Arabidopsis and yeast (Todisco *et al.*, 2006; Palmieri *et al.*, 2009; Agrimi *et al.*, 2012a). The chloroplastic  $\text{NAD}^+$  import in exchange with AMP via NDT1 is enabled by the adenylate pool synthesized in the stroma (Palmieri *et al.*, 2009). In mitochondria, the AMP efflux is coupled to the mitochondrial adenine nucleotide carrier ADNT1 that imports cytosolic AMP in exchange with ATP that is synthesized in the mitochondrial matrix (Palmieri *et al.*, 2008).

(ii) The second model for generating a peroxisomal  $\text{NAD}^+$  pool is the three-substrate model (Figure 4.1 B). PXN mediated the import of two molecules  $\text{NAD}^+$  in exchange with one molecule of AMP and NMNH. Both molecules are products of the NADH hydrolysis catalyzed by nudix hydrolases (NUDT). The NUDT7 is predicted to be peroxisomal (Reumann *et al.*, 2004) and NUDT19 was proven to be peroxisomal (Lingner *et al.*, 2011). The acceptance of NMNH as counter-substrate of PXN is required for this model. The exchange of  $\text{NAD}^+$  with NMNH could not be tested by uptake measurements in this thesis, because this compound is not commercial available. The three-substrate model might be function during oxidative stress, because NUDT7 is involved in maintaining the optimal cellular  $\text{NAD}^+/\text{NADH}$  balance and regulates the cellular antioxidant system during oxidative stress (Robertson *et al.*, 1995; Ge *et al.*, 2007; Ishikawa *et al.*, 2009; Jambunathan *et al.*, 2010).

(iii) An alternatively transport mechanism for PXN is as  $\text{NAD}^+$  uniport (Uniport model, Figure 4.1 C). Our experimental set-up exhibited PXN mediated  $\text{NAD}^+$  uptake in a strict exchange with other substrates (Figure 3.4), meaning that PXN functions as antiporter. To test the uniport function, uptake experiments using proteoliposomes without internal substrates were performed and no  $\text{NAD}^+$  uptake was mediated by PXN. In contrast, Agrimi and co-workers measured a low efflux of  $\text{NAD}^+$  and AMP from liposomes preloaded with radioactively labelled  $[^3\text{H}]\text{-NAD}^+$  or  $[^{14}\text{C}]\text{-AMP}$ , indicating a slow but existing uniport mechanism of PXN (Agrimi *et al.*, 2012b). Such a  $\text{NAD}^+$  uniport transport activity was also observed for the yeast orthologue Ndt1p to set up the mitochondrial  $\text{NAD}^+$  pool (Todisco *et al.*, 2006; Agrimi *et al.*, 2011).

(iv) Furthermore PXN could function as redox shuttle over the peroxisomal membrane by importing  $\text{NAD}^+$  in exchange with NADH (Figure 4.1 D). The impaired but not blocked  $\beta$ -oxidation in *pxn* mutants could be explained by the redundancy to the malate/OAA shuttle

as both transfer reductive equivalents in terms of  $\text{NAD}^+/\text{NADH}$  over the peroxisomal membrane (Mettler and Beevers, 1980) and exhibited the same  $\beta$ -oxidation phenotypes (section 4.6.2). In matters of the PXN functions as redox shuttle, the cellular  $\text{NAD}^+$  and  $\text{NADH}$  level has to be measured as well as the redox state of peroxisomes from the *pxn* mutant should be analyzed (section 4.6.2). The cellular  $\text{NAD}^+/\text{NADH}$  balance regulates the antioxidant system during oxidative stress (Robertson *et al.*, 1995; Ge *et al.*, 2007; Ishikawa *et al.*, 2009; Jambunathan *et al.*, 2010). To determine the peroxisomal  $\text{NAD}^+$  and  $\text{NADH}$  levels of WT and *pxn* mutants would be interesting to confirm that PXN functions as  $\text{NAD}^+/\text{NADH}$  shuttle. But until now, no experimental set-up are established for the determination of peroxisomal pyridine nucleotides contents, because metabolites and cofactors are sensitive to the peroxisome isolation process and no steady-state level can be measured.

#### 4.1.3 Phosphorylation of S155 regulates PXN activity

Two independent proteomic studies detected a phosphorylation site at serine 155 of PXN (Eubel *et al.*, 2008; Ito *et al.*, 2009) that is located in the unique loop region of the PXN protein between the third and fourth transmembrane domains (Figure 3.29). This putative phosphorylation site of PXN at S155 is conserved to those from the yeast mitochondria ATP/ADP transporter (AAC1p), which exhibited a phosphorylation site at S155/T156 or S157 (Reinders *et al.*, 2007). It was assumed that this phosphorylation sites could possibly regulates the protein activity or substrate specificity due to a phosphorylation or dephosphorylation event (Eubel *et al.*, 2008).

In this thesis, it was tested if the unique loop region or the phosphorylation site at S155 of PXN plays a role in the transport activity and substrate specificity (section 3.9.2). Therefore PXN was mutated by a complete deletion of the unique loop region (PXN  $\Delta$ loop) and by the exchange of S155 to alanine (PXN S155A) as control, to cysteine (PXN S155C) to mimic the dephosphorylated state, and to aspartate (PXN S155D) to imitate the phosphorylation state of PXN. By co-localization studies using agrobacteria-mediated transient transformation of tobacco leaves, it was shown that the loop region and the phosphorylation state of S155 does not interfere the correct targeting of PXN to the peroxisomal membrane (Figure 3.30).

Uptake studies exhibited  $\text{NAD}^+$  transport activity followed first-ordered kinetics of the mutated PXN versions (Figure 3.32 and Figure 7.3). The dephosphorylated S155, mimicked by S155C and PXN  $\Delta$ loop, maintained a decrease in  $\text{NAD}^+/\text{NAD}^+$  homo-exchange and  $\text{NAD}^+/\text{NADH}$  and  $\text{NAD}^+/\text{AMP}$  hetero-exchange activity, whereas the phosphorylation of S155, mimicked by S155D, leads to an increase of  $\text{NAD}^+/\text{AMP}$  hetero-exchange activity. This indicated that the PXN activity, especially the  $\text{NAD}^+$  uptake in exchange with AMP, is positively affected by a phosphorylation event at S155. The influence of the phosphorylation

on NAD<sup>+</sup>/CoA and CoA/AMP hetero-exchange has to be analyzed by uptake experiments using radioactively labelled [ $\alpha$ -<sup>32</sup>P]-NAD<sup>+</sup> and [<sup>14</sup>C]-AMP.

To investigate if the recombinant PXN protein is phosphorylated at S155, a phosphoserine antibody was used for immunoblot analyzes using PXN and modified PXN proteins. However, no concrete result could be confirmed so far (Figure 7.4). In a future experiment the addition of different kinases to the translation reaction are required to enable the phosphorylation of PXN as appropriate positive control. The *in vivo* role of phosphorylated PXN protein should be proven by complementation of the *pxn* mutants with the different mutated PXN proteins. As well as it is interesting if the phosphorylation level of PXN is regulated during different developmental stages and different stress conditions.

In case the PXN activity is regulated by phosphorylation, it is interesting to know if the PXN loop is orientated to the cytosol or the peroxisomal matrix to gain access to a peroxisomal or cytosolic kinase. An *in vivo* fluorescence protease protection (FPP) assay, developed in mammalian cells (Lorenz *et al.*, 2006), could be performed to investigate the topology of PXN in the peroxisomal membrane (Held *et al.*, 2008). Therefore GFP is fused to PXN at the N- or C-terminus and the fusion proteins were expressed in plant cells, which were treated with the protease trypsin. If GFP is orientated to the cytosol and not to the peroxisomal matrix, the GFP protein could be cleaved by trypsin, indicating the topology of PXN and that the loop region is orientated to the peroxisomal matrix.

#### **4.2 *pxn* mutant plants are delayed in fatty acid degradation during seedling establishment**

*In vitro* expressed PXN protein catalyzed the import of NAD<sup>+</sup> and CoA, essential cofactors for functional fatty acid  $\beta$ -oxidation in plants (Theodoulou and Eastmond, 2012). The NAD<sup>+</sup>-dependent MFP2 and the CoA-dependent LACS6 and LACS7 proteins are co-expressed with PXN (section 3.4), indicating a correlation of PXN and the fatty acid metabolism. In addition, transcript levels of enzymes required for  $\beta$ -oxidation are increased during germination and seedling establishment like the expression of PXN (section 3.4; Eastmond and Graham, 2000).

This work demonstrated that the import of NAD<sup>+</sup> and CoA, mediated by PXN, is required but not essential for fatty acid degradation during seedling establishment (section 3.6). Three independent PXN T-DNA insertion lines, two loss-of-function mutants (*pxn-1* and *pxn-3*) and one knock-down mutant (*pxn-2*), were used as tool to examine the function of PXN during seedling establishment (section 3.5). Even though plants lacking PXN are not affected in germination (Figure 3.20) or sucrose-dependent seedling establishment (Figure 3.15), they were impaired in peroxisomal fatty acid  $\beta$ -oxidation, indicated by less sensitivity to 2,4-DB, a precursor of the root growth inhibitor 2,4-D that is metabolized via  $\beta$ -oxidation

(Figure 3.16). In addition, *pxn* seedlings are delayed in storage oil breakdown. An increased TAG content was confirmed by high C20:1 levels (Figure 3.17) and the retention of oil bodies (Figure 3.18 and Figure 3.19) during post-germinative growth.

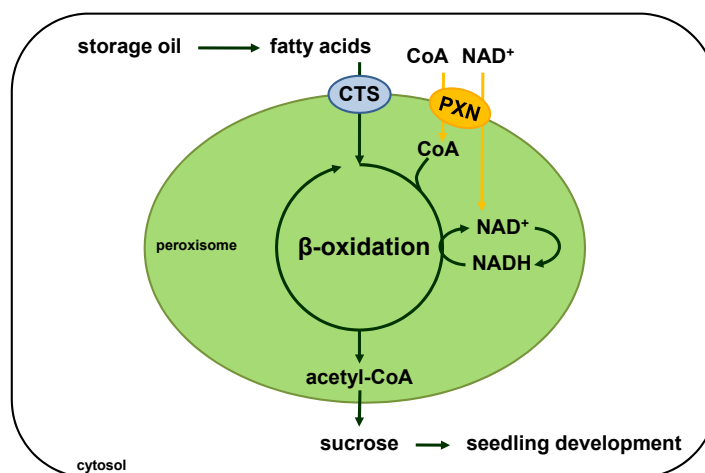


**Figure 4.2 Model of the new peroxisomal NAD<sup>+</sup> carrier**

Peroxisomal  $\beta$ -oxidation is supplied with NAD<sup>+</sup> and CoA by the peroxisomal NAD<sup>+</sup> carrier PXN. CTS imports the fatty acids for degradation to acetyl-CoA via  $\beta$ -oxidation.

The affect in germination of *pxn* seedlings was investigated to indicate that the delayed fatty acid degradation rate was not caused by a slower germination rate. The fact that storage oil mobilization is not essential for germination and that the major period of fatty acid breakdown occurs during post-germinative seedling growth (Graham, 2008) explained the absence of a germination phenotype of *pxn* seeds (section 3.6.4). The same phenotype, no germination affect but an increased C20:1 content was observed in seedlings missing the acyl-CoA oxidase 2 (ACX2) activity that mediated the first step of  $\beta$ -oxidation (Pinfield-Wells *et al.*, 2005).

Interestingly, it was recently shown that *pxn* mutant plants contained enlarged peroxisomes (Mano *et al.*, 2011). The same abnormal morphology of peroxisomes was observed in two  $\beta$ -oxidation mutants, the *mfp2* mutant lacking the NAD<sup>+</sup>-dependent multifunctional protein (Rylott *et al.*, 2006) and the *ped1* mutant deficient in the CoA-dependent 3-ketoacyl-CoA thiolase (KAT; Germain *et al.*, 2001; Hayashi *et al.*, 2001). It was proposed that the accumulation of intermediates of fatty acid  $\beta$ -oxidation regulates the peroxisome size and abundance (Mano *et al.*, 2011). So far, the real reason why peroxisomal  $\beta$ -oxidation mutants revealed enlarged peroxisomes is still unknown.

The role of PXN during natural senescence has to be verified as the  $\beta$ -oxidation is required for the turnover of membrane lipids. It was demonstrated that the PXN expression was increased during natural and induced senescence (section 3.4.1). The phenotype of *pxn* mutants during senescence should be observed. The chlorophyll and fatty acid content of excised leaves and whole darkened plants that induces senescence could be examined as described in Castillo and Leon (2008). A delayed senescence process is predicted for *pxn* mutants because the  $\beta$ -oxidation rate is reduced if PXN is missing.

### 4.3 Putative role of PXN in jasmonic acid and auxin biosynthesis

Peroxisomal  $\beta$ -oxidation is involved in many other processes throughout the plant life, beside fatty acid degradation for seedling establishment, like in metabolism of hormones and amino acids (Baker *et al.*, 2006). Phytohormone biosynthesis of jasmonic acid (JA), auxin, and salicylic acid (SA) is dependent on peroxisomal  $\beta$ -oxidation (Hu *et al.*, 2012).

To analyze the function of PXN during seedling establishment and other  $\beta$ -oxidation-dependent pathways, the PXN expression pattern was examined using PXN promoter-GUS activity staining in homozygous Arabidopsis WT plants, expressing the  $\beta$ -glucuronidase gene under the control of the PXN promoter (section 3.4.3). PXN is expressed in the whole leaf area with a stronger expression in the vascular tissue of leaves and root of seedlings and rosette leaves, in the transition zone from hypocotyl to root, and in the shoot and root meristem of seedlings (Figure 3.11), indicating the importance of PXN not only during seedling establishment. The PXN promoter activity pattern was confirmed by Mano *et al.* (2011). PXN expression in the leaf and in the hypocotyl-root junction correlates with the expression pattern of the NAD<sup>+</sup>-dependent multifunctional protein AIM1 (Richmond and Bleecker, 1999), indicated the importance of NAD<sup>+</sup> supply for functional fatty acid  $\beta$ -oxidation.

The vascular tissue specific PXN expression suggested a role of PXN in biosynthesis of the phytohormone JA that takes place in the sieve elements for long-distance transport (Hause *et al.*, 2003). The final steps of JA biosynthesis from  $\alpha$ -linolenic acid are the  $\beta$ -oxidation of 12-oxo-phytoenoic acid by AIM1 (Delker *et al.*, 2007; Arent *et al.*, 2010). The *aim1* mutant exhibited reduced JA levels upon wounding (Delker *et al.*, 2007). JA plays important roles as signalling molecule during seed germination, reproductive development, senescence, and plant defence, primary against insect herbivores and necrotrophic pathogens (Schaller and Stintzi, 2008). To investigate the role of PXN as NAD<sup>+</sup> and CoA supplier for functional  $\beta$ -oxidation in JA biosynthesis, the response of *pxn* seedlings to JA could be determined as a decreased response to JA is assumed. Additional, the JA content of wounded *pxn* mutants could be measured as a decrease in JA level and in increase in the content of precursors from JA biosynthesis are expected.

In addition, PXN is expressed in the shoot and root meristem where the  $\beta$ -oxidation dependent auxin biosynthesis takes place (Ljung *et al.*, 2005). The impact of PXN in auxin biosynthesis was confirmed with the impaired conversion of the synthetic auxin precursor 2,4-DB to 2,4-D in *pxn* seedlings (3.6.2). Indole-3-acetic acid (IAA) is the most abundant naturally occurring auxin (Bartel, 1997) and is derived from indole-3-butyric acid (IBA) via  $\beta$ -oxidation (Strader *et al.*, 2010). IAA plays a major role in lateral root initiation, cotyledon expansion, seedling establishment, vascular development, apical dominance, phototropism, and gravitropism (Zolman *et al.*, 2000; Strader *et al.*, 2010). NAD<sup>+</sup>-dependent AIM1 is



required for the conversion of IAA from IBA as *aim1* mutants are resistant to IBA (Zolman *et al.*, 2008).

#### 4.4 **PXN expression is altered during oxidative stress**

The APX/MDAR system depends on peroxisomal  $\text{NAD}^+$  to detoxify  $\text{H}_2\text{O}_2$ , which is produced in peroxisomes during  $\beta$ -oxidation, photorespiration, and oxidative stress (Hu *et al.*, 2012).  $\text{H}_2\text{O}_2$  plays a major role in controlling the response to abiotic and biotic stresses (Dat *et al.*, 2000; Mittler, 2002; del Rio *et al.*, 2006; Schrader and Fahimi, 2006). ROS production and breakdown are linked to the intracellular metabolic changes (Babourina *et al.*, 2006). It is known that an accumulation of cytosolic  $\text{H}_2\text{O}_2$  inhibits seedling establishment (Eastmond, 2007) and primary root growth (Dunand *et al.*, 2007). In plants, ROS production takes place in the peroxisome, chloroplast, mitochondria, plasma membrane, and the apoplastic space (Corpas *et al.*, 2001). The main peroxisomal  $\text{H}_2\text{O}_2$  pool is produced by superoxide dismutase (SOD) that converts superoxide radicals ( $\text{O}_2^{\cdot-}$ ) to  $\text{H}_2\text{O}_2$  and  $\text{O}_2$  (Palma *et al.*, 2009).  $\text{O}_2^{\cdot-}$  is produced by converting xanthine to uric acid via xanthine oxidase (XOD; Palma *et al.*, 2009). In this thesis it was investigated whether PXN supplies the APX/MDAR system with  $\text{NAD}^+$  (Figure 4.3).

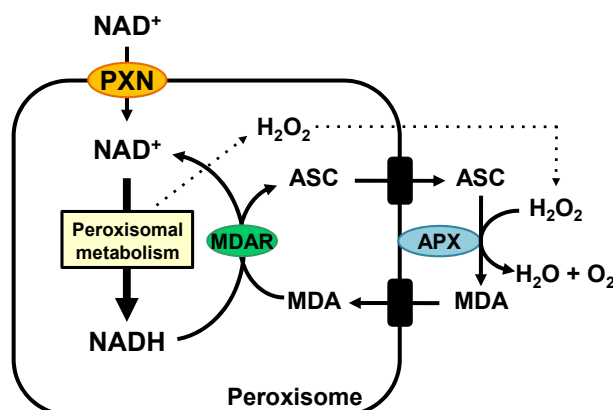


**Figure 4.3 Model of supporting the APX/MDAR system with  $\text{NAD}^+$  by PXN for  $\text{H}_2\text{O}_2$  detoxification**

PXN mediated the import of  $\text{NAD}^+$  that is metabolized by the peroxisomal metabolism to  $\text{NADH}$ .  $\text{H}_2\text{O}_2$  is generated by the peroxisomal metabolism and diffuses to the cytosol. Scavenging  $\text{H}_2\text{O}_2$  is degraded by the ascorbate peroxidase (APX) and monodehydroascorbate reductase (MDAR) shuttle using peroxisomal  $\text{NADH}$  as cofactor. ASC, ascorbate; MDA, monodehydroascorbate

Microarray analyses revealed that PXN is co-expressed with APX and MDAR (section 3.4.2). This might propose a role of PXN for ROS degradation. Therefore, *pxn* mutant lines were subjected to oxidative stress (section 3.7) and the effect of external  $\text{H}_2\text{O}_2$  on the root growth in the mutant seedlings were studied. However, the *pxn* plants did not response to exogenous  $\text{H}_2\text{O}_2$  (Figure 3.21) as well as the PXN expression level is not altered by oxidative stress induced by methylviologen (Figure 3.22), indicating that PXN is maybe not directly

---

influenced by H<sub>2</sub>O<sub>2</sub> than through indirect regulation by metabolic changes during oxidative stress.

The expression of PXN was increased by low pH and *P. syringae* treatment (section 3.7.2 and 3.7.3). It is known that both stress conditions trigger ROS production (Babourina *et al.*, 2006; Grosskinsky *et al.*, 2012). During pathogen infection, H<sub>2</sub>O<sub>2</sub> accumulates inside the plant cells for a hypersensitive response or by pathogen itself to kill the host tissue and toxic components (Grosskinsky *et al.*, 2012). Peroxisomes are involved in stress signalling and activation of plant defense by releasing H<sub>2</sub>O<sub>2</sub> to the cytosol where it can trigger defense gene expression (Grosskinsky *et al.*, 2012). *P. syringae* treated plants accumulates ascorbate and glutathione as antioxidants (Grosskinsky *et al.*, 2012). It is assumed that PXN is up-regulated during pathogen infection and low pH treatment to support the H<sub>2</sub>O<sub>2</sub> detoxification via APX/MDAR system as high H<sub>2</sub>O<sub>2</sub> levels induce programmed cell death and is toxic for the plant (Quan *et al.*, 2008).

However, several physiological experiments have to be performed to confirm this hypothesis. Therefore, *pxn* mutant and PXN over-expression plants have to be treated with the different oxidative stress conditions (e.g. low pH, heat, cold, salt, pathogen infection) to proof if they respond different like WT. Additional, the NAD<sup>+</sup>, NADH and H<sub>2</sub>O<sub>2</sub> levels should be determined of *pxn* and PXN over-expression plants that were treated with different oxidative stress circumstances to examine if they contained different concentrations than WT. Cellular H<sub>2</sub>O<sub>2</sub> levels could be determined using xylenol orange (Jiang *et al.*, 1990) and the NAD<sup>+</sup> and NADH level as described in this work. Besides, it would be interesting if the redox level is altered in *pxn* plants, which could be tested by using a peroxisomal fluorescent redox sensor as described in Yano *et al.* (2010).

A strict regulated cytosolic NAD<sup>+</sup>(H) level is required for signalling in the response to oxidative stress (Noctor *et al.*, 2006; Wang and Pichersky, 2007; Jambunathan *et al.*, 2010). Plants exposed to oxidative stress exhibited decreased cellular NAD<sup>+</sup> contents, linked to poly(ADP-ribose) polymerase (PARP) activity that degraded NAD<sup>+</sup> for protein post-translational modification (Noctor *et al.*, 2006; Xie *et al.*, 2009). Furthermore, the cytosolic NAD<sup>+</sup>/NADH and NADP<sup>+</sup>/NADPH ratios are important for the redox homeostasis. A change in the NAD<sup>+</sup>(H) levels during stress can lead to a redox imbalance, triggering the production of ROS and the activation of defence, phytohormone, and cell death signalling pathways, which is important to regulate the cellular antioxidant system (Jambunathan *et al.*, 2010; Waller *et al.*, 2010). As well as the peroxisomal NADH level is essential for the response to oxidative stress. The peroxisomal NADH kinase NADK3 (Waller *et al.*, 2010) is required under oxidative stress conditions to maintain the peroxisomal NADH/NADPH redox balance (Chai *et al.*, 2006). The fact that PXN could regulate the peroxisomal NAD<sup>+</sup>(H) level by adapting it to the cytosolic NAD<sup>+</sup> homeostasis would also explain the higher NAD<sup>+</sup> level in *pxn* seedlings during post-germinative growth (section 3.8.1).

#### **4.5 Is PXN required for the photorespiratory C<sub>2</sub> cycle?**

The relevance of PXN during the photorespiratory C<sub>2</sub> cycle, the third NAD<sup>+</sup>-dependent peroxisomal pathway, was not analyzed in this thesis. During photorespiration, the degradation of toxic 2-phosphoglycolate is separated in chloroplasts, peroxisomes, and mitochondria. The peroxisomal HPR1 requires NADH as cofactor for the detoxification of the photorespiratory compound (Timm *et al.*, 2011). *pxn* mutants growing under ambient air conditions (Figure 7.2) did not show a typical photorespiratory phenotype as described in (Somerville and Ogren, 1980). To test if *pxn* mutants exhibited an intermediate photorespiratory phenotype, the *pxn* plants could be analyzed using a CO<sub>2</sub> shift assay and detection of changes of specific photorespiratory metabolite concentrations (e.g. glycerate, glycolate, glycine, hydroxypyruvate, and serine) and enzyme activities (e.g. hydroxypyruvate- and glyoxylate-reducing enzymes) as described in Lisec *et al.* (2006), Voll *et al.* (2006), Timm *et al.* (2008), Bräutigam *et al.* (2010), and Pick *et al.* (2011).

NADH is needed for functional reduction of hydroxypyruvate to glycerate via HPR proteins during photorespiration (Timm *et al.*, 2011). It was shown before that the cytoplasmic HPR2 and chloroplastic HPR3 could bypass the peroxisomal HPR1 reaction (Timm *et al.*, 2008; Timm *et al.*, 2011) and that HRP2 is active when peroxisomal NADH generation is limited (Bauwe *et al.*, 2010). A *hpr1 hpr2 hpr3* triple mutant shows impaired growth, decreased photochemical efficiency and strongly affected gas exchange parameters (Timm *et al.*, 2011). An *hpr2 hpr3* double mutant displays no growth defect. It would be interesting to study whether an *hpr2 hpr3 pxn* triple mutant exhibits the same photorespiratory phenotype than the *hpr1 hpr2 hpr3* triple mutant, expecting that the peroxisomal NAD<sup>+</sup> supply is blocked for efficient HPR1 function. To confirm this hypothesis, the corresponding mutants have to be generated, either by crossing or by down-regulating the PXN expression using the artificial microRNA approach. This photorespiratory approach would examine if PXN mediates CoA import, as CoA has no impact on the photorespiratory C<sub>2</sub> cycle.

#### **4.6 Redundant systems for PXN function**

The intermediate phenotype of *pxn* seedlings (section 3.6) raises the question for a redundant system to supply peroxisomes with NAD<sup>+</sup> and CoA.

##### **4.6.1 PNC1 and PNC2 are candidates for a redundant system for PXN**

If PXN mediates the import of NAD<sup>+</sup> in exchange with AMP, we suggested that both PNCs could complement this transport process when PXN is absent (Figure 4.4), because NAD<sup>+</sup> and ATP are similar in structure and all three proteins used AMP as counter substrate (Arai *et al.*, 2008; Linka *et al.*, 2008b).

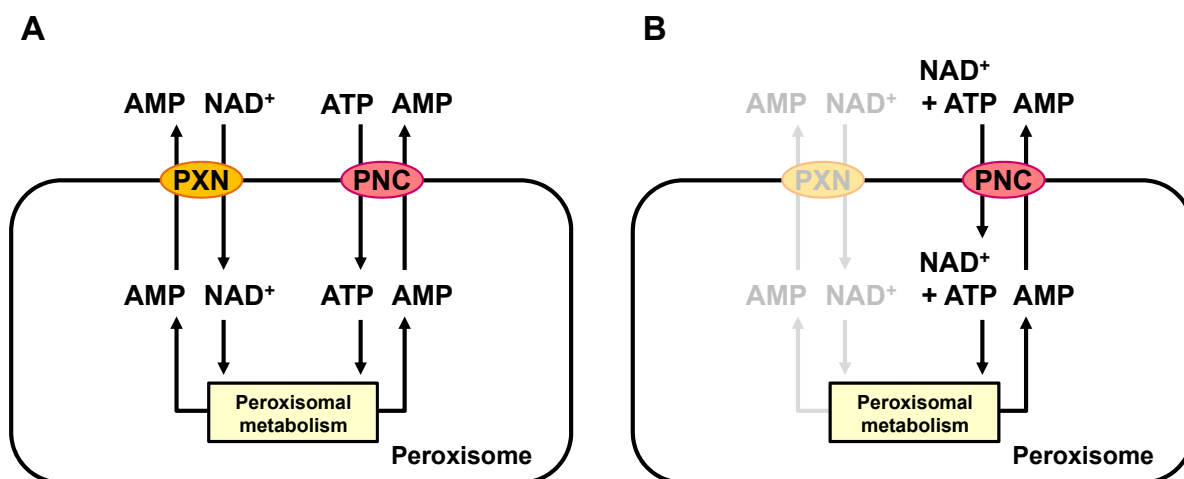


**Figure 4.4 Model of redundant systems for NAD<sup>+</sup>/AMP exchange mediated by PXN and PNC**

(A) Under normal conditions, PXN imports NAD<sup>+</sup> in exchange with AMP and both PNCs ATP in exchange with AMP for optimal peroxisomal metabolism. (B) If PXN is absent, both PNCs could complement the NAD<sup>+</sup> transport activity.

In this thesis, functional expressed PNC1-His and PNC2 protein did not mediated the uptake of NAD<sup>+</sup>/NAD<sup>+</sup> homo-exchange (section 3.2.3). Recently it was shown that both PNCs mediate the exchange of [ $\alpha$ -<sup>32</sup>P]-ATP with NAD<sup>+</sup> and NADH but not with CoA (Vigelius, 2009). The exchange of adenine nucleotides with pyridine nucleotides should be examined for both PNCs. The NAD<sup>+</sup>/AMP hetero-exchange either with radioactively labelled [ $\alpha$ -<sup>32</sup>P]-NAD<sup>+</sup> in exchange with AMP or with radioactively labelled [<sup>14</sup>C]-AMP in exchange with NAD<sup>+</sup> should be performed. In addition, it should be tested if both PNCs could mediate the exchange of CoA with AMP to completely complement the PXN function. To test the complete redundancy, uptake of [<sup>14</sup>C]-AMP in exchange with CoA and NADH should be assayed, because radioactive labelled CoA and NADH are not commercially available.

To address this hypothesis *in vivo*, a small interfering RNA was used to down regulate the expression of both PNC proteins in the *pxn* mutant background (section 3.8.2). In previous studies, the p35S::siR-*PNC1/2* construct was transformed into WT plants and no positive survivors could be selected, indicating the lethality of mutants lacking both peroxisomal ATP carriers (Linka *et al.*, 2008b). In this thesis, *pxn* mutants carrying the p35S::siR-*PNC1/2* T-DNA were selected, but no obvious phenotype was observed. A severe phenotype was expected and consequently the expression level of PNC1 and PNC2 has to be proven, because it could be that only these plants were selected that still expressed both PNC and that the strong repressor lines were lethal. Therefore, the expression of the siRNA has to be induced in the positive selected pAlcA::siR-*PNC1/2 pxn* mutants. It was shown before that an ethanol induced expression of siR-*PNC1/2* leads to a reduced PNC1 and PNC2 expression and a  $\beta$ -oxidation phenotype in the corresponding lines (Linka *et al.*, 2008b; Reinke, 2010).

Another approach to confirm the redundancy of PXN and both PNC proteins would be

the crossing of *pxn* with either single *pnc1* and *pnc2* mutant plant or with the recent established *pnc1 pnc2* double mutant (Sarah Vigelius, HHU Düsseldorf, Germany; personal communication). The *pnc1 pnc2* line exhibit a severe  $\beta$ -oxidation phenotype but is not lethal like the 35S-RNAi lines, because the *pnc1* line still expressed truncated *PNC1* transcript for functional  $\beta$ -oxidation (Linka *et al.*, 2008b).

All lines, simultaneous repressing the expression of PXN, PNC1, and PNC2, have to be checked for the expression level and different physiological experiments corresponding to peroxisomal fatty acid  $\beta$ -oxidation have to be performed. As the repression of both PNC proteins leads to a sucrose dependent phenotype (Linka *et al.*, 2008b), it is assumed that the triple mutant of both PNCs and PXN exhibited a more severe phenotype. The sucrose dependent phenotype, fatty acid content, response to 2,4-DB, and germination frequency of the triple mutant should be analyzed.

#### 4.6.2 Malate/oxaloacetate shuttle redundancy to the PXN mediated $\text{NAD}^+/\text{NADH}$ transport

In the case that PXN functions as  $\text{NAD}^+/\text{NADH}$  carrier, the malate/OAA shuttle mediated by the peroxisomal and cytosolic MDH (Pracharoenwattana *et al.*, 2007) would be redundant for generation a redox shuttle (Figure 4.5). In addition, Pracharoenwattana and co-worker could show that the photorespiratory enzyme HPR1 contributes in the regeneration of  $\text{NAD}^+$  for  $\beta$ -oxidation at early seedling growth in Arabidopsis (Pracharoenwattana *et al.*, 2010).

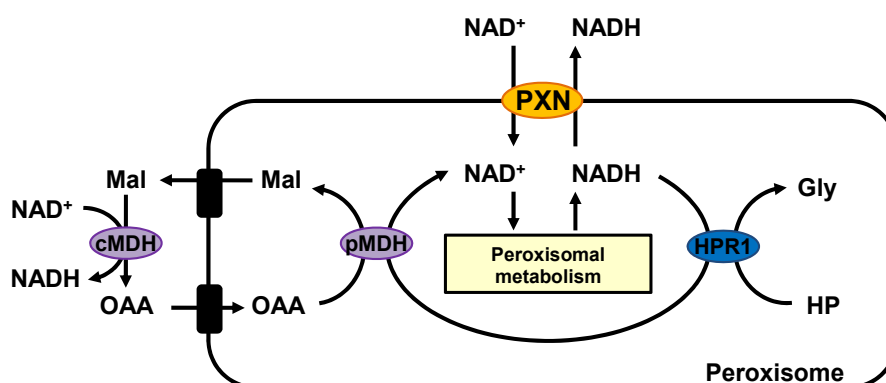


**Figure 4.5 Model of redundant systems for  $\text{NAD}^+/\text{NADH}$  exchange mediated by PXN, the malate/OAA shuttle and HPR1**

$\text{NAD}^+$  gets reduced to NADH during peroxisomal metabolism. Therefore a system for re-oxidizing NADH is essential. One way could be mediated by the antiport mechanism of PXN, which imports  $\text{NAD}^+$  and export NADH to re-oxidize NADH in the cytoplasm. Another known redox shuttle is the malate/OAA shuttle mediated by peroxisomal and cytosolic malate dehydrogenases (pMDH and cMDH). The peroxisomal hydroxypyruvate reductase 1 (HPR1) metabolized hydroxypyruvate (HP) to glycerate (Gly) by oxidizing NADH to  $\text{NAD}^+$ .

Arabidopsis double knock-out mutants of both pMDHs and a triple knock-out mutant of both pMDHs and HPR1 exhibited the same  $\beta$ -oxidation phenotype, whereas the phenotype of the *pmdh1 pm dh2 hpr1* triple mutant is strengthened. Both mutants exhibited a reduced germination efficiency, a sucrose dependent phenotype and less sensitivity to 2,4-DB

(Pracharoenwattana et al., 2007; Pracharoenwattana et al., 2010). A complete block in germination was supposed for the *pmdh1 pmdh2 hpr1* triple mutant if this is the only way to generate a redox shuttle over the peroxisomal membrane (Pracharoenwattana et al., 2010). The low germination rate of the triple mutant indicated that a  $\text{NAD}^+/\text{NADH}$  exchange is still present, maybe generated by PXN.

To analyse the redundancy of PXN and the redox shuttle mediated by the pMDHs and HPR1, the following experiments were designed in this thesis:

(i) It was assumed that the PXN expression level is increased in *pmdh1 pmdh2* and *pmdh1 pmdh2 hpr1* mutant to maintain the redox shuttle. However, micro array data of the *pmdh1 pmdh2* double mutant did not reveal changes in the PXN expression compared to WT (Pracharoenwattana et al., 2007). Co-expression analysis using quantitative real-time PCR (qRT-PCR) needs to be performed to verify an up-regulation of PXN in these mutant plants, indicating that PXN might complement the loss of the malate/OAA redox shuttle.

(ii) The germination and seedling establishment phenotype of the *pmdh1 pmdh2* and *pmdh1 pmdh2 hpr1* mutants could be rescued via an increased  $\text{NAD}^+/\text{NADH}$  shuttle activity by PXN in these mutant backgrounds. Therefore, an over-expression construct was generated in this thesis and was transformed into WT and the *pxn* mutant lines for complementation (section 3.5.3). For further experiments, this construct needs to be transformed into the *pmdh1 pmdh2* and *pmdh1 pmdh2 hpr1* mutants to enable the analysis of the assumed redundancy.

(iii) The *pmdh1 pmdh2* and *pmdh1 pmdh2 hpr1* mutants are strongly impaired in the germination rate and the seedling growth compared to the single mutants and WT, indicating that a  $\text{NAD}^+/\text{NADH}$  exchange is still present to support the peroxisomal  $\beta$ -oxidation (Pracharoenwattana et al., 2010). We hypothesized a severe germination and seedling establishment phenotype of plants deficient in PXN, pMDH1, pMDH2, and HPR1. Therefore *pmdh1 pmdh2 pxn* and *pmdh1 pmdh2 hpr1 pxn* lines were generated by crossing (section 3.8.3). Up to now, the first generation of plants could be selected after crossing which are heterozygous for each corresponding gene. Homozygous lines have to be generated before studying the germination and seedling establishment.

(iv) An alternatively approach to generate the corresponding triple and quadruple mutants was performed by using an artificial micro RNA to down-regulate the PXN expression controlled by either a constitutive or inducible promoter in the corresponding mutants. These constructs were transformed in WT, *pmdh1 pmdh2*, and *pmdh1 pmdh2 hpr1* lines (section 3.8.3). The Arabidopsis transformation has to be repeated to gain more independent lines expressing the amiR-PXN under the control of the constitutive and inducible promoters in the WT, *pmdh1 pmdh2*, and *pmdh1 pmdh2 hpr1* background. The PXN transcript level and the number and localization of the T-DNA insertions have to be analyzed of all generated mutants. In addition, the effect of the amiR-PXN in the different

backgrounds has to be analyzed by inducing the expression via estradiol of the corresponding lines transformed with the pLexA::amiR-*PXN* construct.

To date, no direct statement for the redundancy of *PXN*, *pMDH1*, *pMDH2*, and *HPR1* could be made due to missing results.

#### **4.6.3 *NAD*<sup>+</sup> is imported by cofactor-bound enzymes**

The peroxisomal importomer enables the import of folded, cofactor-bound, and oligomeric proteins across the peroxisomal membrane and does not affect the peroxisomal permeability barrier (Léon *et al.*, 2006; Meinecke *et al.*, 2010). The yeast peroxisomal importomer consisting of Pex5p and Pex14p generated a channel that can be opened to a diameter of 9 nm and mediated the import of PTS1 carrying enzymes (Meinecke *et al.*, 2010). The yeast peroxisomal acyl-CoA oxidase Aox is imported as heteropentameric complex bound to its cofactor FAD (Titorenko *et al.*, 2002). It was assumed that *NAD*<sup>+</sup> is imported in association with holoenzymes (Pracharoenwattana *et al.*, 2010), as shown for Aox, to generate a peroxisomal *NAD*<sup>+</sup> pool. If the main route of *NAD*<sup>+</sup> import is mediated by imported holoenzymes, *PXN* could be involved in maintaining the *NAD*<sup>+</sup> homeostasis during different physiological conditions.

#### **4.7 Peroxisomal members of the MCF are targeted to peroxisomes via PEX19**

For the first time, it was investigated how peroxisomal members of the MCF-type transporters from Arabidopsis are targeted to peroxisomes. Based on previous studies, a peroxin protein called PEX19 interacts with PMPs and mediated the transport to the peroxisomal membrane (Hadden *et al.*, 2006; Platta and Erdmann, 2007a). The PEX19/PMP complex interacts with the PEX3 receptor to release the PMP to the peroxisomal membrane (Hadden *et al.*, 2006; Platta and Erdmann, 2007a). The putative interaction of *PXN* with the PMP receptor complex was indicated by the co-expression of *PXN* with PEX19 and PEX3 (Table 3.4). The human homologue of *PXN*, SLC25A17 and the yeast homologue of PNC1 and PNC2, Ant1p, are targeted via PEX19 and ER-derived vesicles to the peroxisomal membrane (Sacksteder *et al.*, 2000; Palmieri *et al.*, 2001; Kim *et al.*, 2006; van der Zand *et al.*, 2010). The PEX19 interaction with the known peroxisomal MCF members *PXN*, PNC1, and PNC2 was verified in this thesis via an *in vitro* PEX19 pull-down assay (section 3.10.1). The phosphorylation site and unique loop region of *PXN* did not affect the peroxisomal targeting, as the mutated *PXN* proteins interacted with PEX19 (section 3.10.1) and are located to tobacco peroxisomes when transiently co-expressed with a peroxisomal marker (section 3.9.1). Other Arabidopsis PMPs were in addition tested for PEX19: PMP22 (section 3.10.1) and pseudo-halves of the ABC transporter CTS (section 3.10.1) interact with the

PMP receptor. Unexpectedly, an interaction of PEX19 with the mitochondrial mitoPMP22 and the chloroplastic MEP1 protein was verified (section 3.10.1). *In silico* analysis using the PEX19 binding site predictor exhibited putative interactions with PEX19 and peroxisomal, mitochondrial, and chloroplastic proteins (section 3.10.3). This prediction software was programmed based on an algorithm of yeast and human PEX19 binding site motifs. This algorithm might be not sufficient for a precise PEX19 interaction prediction for plant proteins. Alternatively, PEX19 acts as a general chaperone for peroxisomal as well as for other intracellular membrane proteins.

To verify *in vivo* the PEX19 interaction, a PEX19 mis-localization assay was performed (section 3.10.2). The expected nuclear localization of the NLS-PEX19.1/PMP-YFP interaction was not observed; neither with the positive control ALDP-YFP and ALDR-YFP. Because the positive controls did not exhibit the expected results, this experiment has to be redesigned or the components have to be checked for right expression vectors and expression in tobacco cells.

To confirm the PEX19 interaction results, a yeast two-hybrid assay could be performed as described in Sacksteder *et al.* (2000). They fused PEX19 to a GAL4 transcription activator domain and the PMP to a GAL4 DNA binding domain. Both fusion proteins were expressed in yeast strains and the LacZ activity was analyzed using X-Gal. In addition, the PMP of interest could be expressed in a yeast strain missing the expression of Pex19p or Pex3p as it was described for the yeast ATP transporter Ant1p (Palmieri *et al.*, 2001).

PMP targeting could also be dependent on ER-derived vesicles. To test if the targeting of the PMPs candidates is dependent on the ER, the same experiments as described in Sparkes *et al.* (2005) could be performed. They analyzed the targeting of PEX2 and PEX10 by transiently expressing PMP-YFP in tobacco leaves and blocking the ER transport routes using the fungal metabolite Brefeldin A or by co-expressing dominant negative mutants of Sar1 or RabD2a (Sparkes *et al.*, 2005).



## 5 Summary

### 5.1 Summary

NAD<sup>+</sup> is an essential cofactor for several metabolic processes. In plants, the NAD<sup>+</sup> biosynthesis takes exclusively place in the cytosol (Noctor *et al.*, 2006; Hashida *et al.*, 2009) whereas NAD<sup>+</sup>-dependent enzymes are located in the cytosol and other cell compartments, including peroxisomes. Earlier evidences assume that the peroxisomal membrane is impermeable for “bulky” cofactors like NAD<sup>+</sup> and CoA (Donaldson, 1981; Antonenkov and Hiltunen, 2012). However, the fact that peroxisomal metabolism require these molecules (e.g. for fatty acid  $\beta$ -oxidation, photorespiration, and H<sub>2</sub>O<sub>2</sub> detoxification; Hu *et al.*, 2012) necessitates the need for a NAD<sup>+</sup> import. For decades, the existence of such a peroxisomal NAD<sup>+</sup> transport protein was controversially discussed. In this thesis, the first peroxisomal NAD<sup>+</sup> carrier, named PXN, was characterized in the model plant *Arabidopsis thaliana*. The carrier encoded by the gene At2g39970 is a member of the mitochondrial carrier family (MCF) and closely related in sequence to peroxisomal, chloroplastic, and mitochondrial ATP and NAD<sup>+</sup> transporters from Arabidopsis, yeast, and human. Interaction studies confirmed that PXN is targeted to peroxisomes via interaction with PEX19 that is known to act as chaperone for PMP targeting (Jones *et al.*, 2004; Van Ael and Fransen, 2006).

Performing uptake assays, it was demonstrated that recombinant PXN protein catalyzed the transport of NAD<sup>+</sup> and CoA in exchange with AMP, which was recently confirmed by Agrimi *et al.* (2012b). Furthermore, cell-free expressed PXN protein mediated the exchange of NAD<sup>+</sup> with NADH and acts thereby as reduction/oxidation (redox) shuttle. The NADH transport activity is unique compared to the other known MCF-type NAD<sup>+</sup> transporter from Arabidopsis, yeast, and human. This thesis indicated first evidences that the PXN activity is positively regulated via phosphorylation. The phosphorylation site at serine 155 was detected in two independent phosphoproteomic studies (Eubel *et al.*, 2008; Ito *et al.*, 2009). Here, it was in addition shown that the phosphorylation site at S155 and the unique loop region of the PXN protein did not influence the PEX19-dependent peroxisomal targeting, indicating that the PEX19 binding site is not located at the loop region.

Three independent Arabidopsis *pxn* T-DNA insertion lines illustrated the requirement of peroxisomal NAD<sup>+</sup> and CoA supply mediated by PXN for optimal fatty acid  $\beta$ -oxidation. *pxn* seedlings were delayed in breakdown of fatty acids released from storage oil, which was visualized by higher levels of storage fatty acids and the retention of oil bodies. However, germination was not impaired in plants deficient in PXN. The *pxn*  $\beta$ -oxidation phenotype correlated with the increased PXN expression during  $\beta$ -oxidation-dependent seedling establishment and the PXN co-expression with proteins involved in  $\beta$ -oxidation. Furthermore, the link between PXN function and the  $\beta$ -oxidation-dependent processes (e.g. mobilization of

storage oil and biosynthesis of phytohormones) was exhibited by the expression pattern using PXN promoter-GUS studies in stable transformed Arabidopsis seedlings.

A redundant system for PXN was predicted, because *pxn* mutants exhibited an impaired but not complete block of  $\beta$ -oxidation, as expected for plants lacking the  $\text{NAD}^+$  and CoA supply via PXN. Two redundant systems were assumed. (i) The  $\text{NAD}^+$ /AMP shuttle could be taken over by the peroxisomal adenine nucleotide carriers PNC1 and PNC2 when PXN is absent, because both transport substrates, ATP and  $\text{NAD}^+$ , are similar in structure. To address this, mutant lines repressing both *pnc* genes and *pxn* were generated by using a small interfering RNA approach. The obtained transgenic plants need to be investigated in the future. (ii) The  $\text{NAD}^+$ /NADH exchange function of PXN could be redundant to the malate/oxaloacetate (malate/OAA) shuttle that transfers reducing equivalents across the peroxisomal membrane (Pracharoenwattana *et al.*, 2007). Furthermore, the peroxisomal hydroxypyruvate reductase 1 (HPR1) is proposed to play a role in regeneration  $\text{NAD}^+$  for  $\beta$ -oxidation and thus also functions as redox shuttle during early seedling growth (Pracharoenwattana *et al.*, 2010). To test this hypothesis, different Arabidopsis plants were generated in this work by crossing the *pxn* lines with the mutant defective in both *pmdh*s and HPR1 and by repressing the PXN expression using an PXN specific artificial microRNA in the *pmdh* and *hpr1* mutant lines. However, the resulted transgenic plants need to be further investigated regarding the impact on  $\beta$ -oxidation for storage oil mobilization.

*In silico* analysis revealed that PXN is co-expressed with the ascorbate peroxidase (APX) and the NADH-dependent monodehydroascorbate reductase (MDAR), which are required for  $\text{H}_2\text{O}_2$  detoxification (Graham, 2008). PXN expression is altered during oxidative stress, when  $\text{H}_2\text{O}_2$  accumulated inside the cells. This implicated a role of PXN in supplying  $\text{NAD}^+$  for peroxisomal  $\text{H}_2\text{O}_2$  detoxification via the APX/MDAR system. This hypothesis has to be verified by examining *pxn* mutants under oxidative stress conditions.

In sum, this thesis described the characterization and the function of a peroxisomal  $\text{NAD}^+$  and CoA carrier during seedling establishment and oxidative stress. Site-directed mutagenesis of the PXN protein revealed that the transport activity is regulated by phosphorylation. Regarding the PMP import, it was demonstrated that the PEX19 receptor is involved in the peroxisomal targeting of PXN and several other PMPs.

## 5.2 Zusammenfassung

NAD<sup>+</sup> ist ein essentieller Cofaktor für viele metabolische Prozesse und dessen Biosynthese findet ausschließlich im Zytosol statt (Noctor *et al.*, 2006; Hashida *et al.*, 2009). Eine subzelluläre Verteilung von NAD<sup>+</sup> muss gewährleistet sein da NAD<sup>+</sup>-abhängige Enzyme nicht nur im Zytosol, sondern auch in den anderen Zellkompartimenten, wie z.B. den Peroxisomen lokalisiert sind. Da die Membranen der Organellen impermeabel für NAD<sup>+</sup> sind, ist die Notwendigkeit eines NAD<sup>+</sup>-Transportsystems unabkömmlich. Die Existenz eines peroxisomalen NAD<sup>+</sup>-Transporters wurde über Jahrzehnte kontrovers diskutiert (Donaldson, 1981; Antonenkov and Hiltunen, 2012). Zu Beginn dieser Arbeit war nicht geklärt wie die NAD<sup>+</sup>-abhängigen Prozesse, wie z.B.  $\beta$ -Oxidation, Photorespiration und H<sub>2</sub>O<sub>2</sub> Abbau (Hu *et al.*, 2012) mit dem Cofaktor in den Peroxisomen versorgt werden.

In dieser Arbeit wurde erstmals ein peroxisomaler NAD<sup>+</sup>-Transporter aus der Modellpflanze *Arabidopsis thaliana* charakterisiert, der als *peroxisomal NAD<sup>+</sup> carrier* (PXN) bezeichnet wurde. Dieses Transportprotein, das durch das Gen At2g39970 kodiert wird, gehört als Mitglied der mitochondrialen Transportfamilie (*mitochondrial carrier family*; MCF) zur Gruppe der bereits bekannten peroxisomalen, mitochondrialen und chloroplastidären ATP- und NAD<sup>+</sup>-Transportern aus der Pflanze, Hefe und des Menschen an. Mit Hilfe von Protein-Interaktionsstudien konnte gezeigt werden, dass PXN mit dem Peroxin PEX19 interagiert, einem Hilfsprotein das peroxisomale Membranproteine zu den Peroxisomes geleitet (Jones *et al.*, 2004; Van Ael and Fransen, 2006).

Durch NAD<sup>+</sup>-Aufnahmemessungen an Liposomen konnte demonstriert werden, dass das rekombinante PXN-Protein den Transport von NAD<sup>+</sup> im Austausch mit AMP katalysiert. Zudem konnte gezeigt werden, dass ebenfalls CoA und NADH als Substrat für PXN fungieren. Gezielte Mutationen im PXN-Protein zeigten, dass die Transportaktivität über eine Phosphorylierung am Serin 155 reguliert wird, die durch zwei unabhängige Phosphoproteomic-Studien als Phosphorylierungsstelle verifiziert wurde (Eubel *et al.*, 2008; Ito *et al.*, 2009). In dieser Arbeit konnte darüber hinaus bestätigt werden, dass der Phosphorylierungszustand von S155 und die einzigartige Loop-Region von PXN keinen Einfluss auf das peroxisomale Targeting und die Bindung an PEX19 haben.

Drei unabhängige *Arabidopsis* T-DNA-Insertionslinien für das *pxn*-Gen zeigten, dass PXN für einen optimalen Ablauf der  $\beta$ -Oxidation notwendig ist. In diesen Mutanten ist der oxidative Abbau von Fettsäuren mittels der  $\beta$ -Oxidation während der Speicherlipid-Mobilisierung verzögert. Dies wurde durch die erhöhten Mengen an Speicherfettsäuren und an dem Verbleiben von Ölkörpern in den Mutanten-Keimlingen verifiziert. Der  $\beta$ -Oxidationsphänotyp von *pxn*-Keimlingen korreliert mit der erhöhten PXN-Expression während  $\beta$ -Oxidation-abhängiger Keimlingsentwicklung. Des Weiterem sind  $\beta$ -Oxidation-spezifische Gene mit PXN co-exprimiert.

Durch PXN Promotor-GUS Studien von stabil transformierten Arabidopsis-Keimlingen konnte der Zusammenhang zwischen PXN und der  $\beta$ -Oxidation während des Abbaus von Speicherlipiden und der Biosynthese von Pflanzenhormonen unterstützt werden.

Auf Grund des schwachen  $\beta$ -Oxidationsphänotyps von *pxn*-Keimlingen wurde die Existenz eines redundanten Systems angenommen, da in Abwesenheit von PXN eine vollständige Blockierung der  $\beta$ -Oxidation erwartet wurde. Es wurden daher die folgenden redundante Systeme angenommen: (i) Die  $\text{NAD}^+$ /AMP-Funktion von PXN könnte durch die peroxisomalen ATP Transportproteine PNC1 und PNC2 übernommen werden, da ATP und  $\text{NAD}^+$  eine ähnlichen Molekülstruktur aufweisen. Um dies zu testen, wurden Dreifachmutanten hergestellt, die in der Expression von PXN, PNC1 und PNC2 defekt sind. Zukünftige Analysen werden zeigen, ob der Defekt von PXN durch die PNCs aufgehoben werden kann. (ii) Im Fall dass PXN einen  $\text{NAD}^+$ /NADH-Austausch katalysiert, ist diese Transportfunktion zu dem peroxisomalen Malat/Oxalacetat-Shuttle redundant (Pracharoenwattana *et al.*, 2007). Darüberhinaus konnte kürzlich gezeigt werden, dass die peroxisomale Hydroxypyruvatreduktase 1 (HPR1)  $\text{NAD}^+$  während der  $\beta$ -Oxidation regeneriert und somit ebenfalls als Redox-Shuttle fungiert (Pracharoenwattana *et al.*, 2010). In dieser Arbeit wurden Arabidopsis-Mutanten erzeugt, bei denen PXN, die beiden peroxisomalen MDHs sowie die HPR1 ausgeschaltet werden. Eine detaillierte Untersuchung der Mutanten bezüglich der Speicherlipid-Mobilisierung steht noch aus.

*In silico* Analysen konnten zeigen, dass PXN mit der Ascorbatperoxidase (APX) und der  $\text{NAD}^+$ -abhängigen Monodehydroascorbatreduktase (MDAR) co-exprimiert ist. Diese beiden Enzyme sind für den Abbau von giftigen  $\text{H}_2\text{O}_2$  in den Peroxisomen beteiligt (Graham, 2008). Zudem ist die Expression von PXN während oxidativen Stresses verändert, bei dem  $\text{H}_2\text{O}_2$  in der Zelle akkumuliert. Um zu zeigen, dass der PXN für den Abbau von  $\text{H}_2\text{O}_2$  mittels des APX/MDAR systems zuständig ist, sollten physiologische Experimente unter verschiedenen oxidativen Stressbedingungen mit Hilfe der *pxn* Mutanten durchgeführt werden.

Zusammenfassend beschreibt diese Arbeit die Charakterisierung und den Einfluss von PXN als einen peroxisomalen  $\text{NAD}^+$ - und CoA-Transporter während der Speicherlipid-Mobilisierung und oxidativen Stress. Darüber hinaus konnten erste Hinweise auf eine Regulation der PXN Transportaktivität über Phosphorylierung gezeigt werden. Zusätzlich wurde demonstriert, dass PXN und andere peroxisomale Membranproteine über eine Interaktion mit PEX19 zu der peroxisomalen Membran transportiert werden.

---

## 6 References

- Agrawal, G., Joshi, S., and Subramani, S.** (2011). Cell-free sorting of peroxisomal membrane proteins from the endoplasmic reticulum. *Proc Natl Acad Sci U S A* **108**, 9113-9118.
- Agrimi, G., Russo, A., Scarcia, P., and Palmieri, F.** (2012a). The human gene SLC25A17 encodes a peroxisomal transporter of coenzyme A, FAD and NAD<sup>+</sup>. *Biochem J* **443**, 241-247.
- Agrimi, G., Russo, A., Pierri, C.L., and Palmieri, F.** (2012b). The peroxisomal NAD<sup>(+)</sup> carrier of *Arabidopsis thaliana* transports coenzyme A and its derivatives. *J Bioenerg Biomembr*.
- Agrimi, G., Brambilla, L., Frascotti, G., Pisano, I., Porro, D., Vai, M., and Palmieri, L.** (2011). Deletion or overexpression of mitochondrial NAD<sup>+</sup> carriers in *Saccharomyces cerevisiae* alters cellular NAD and ATP contents and affects mitochondrial metabolism and the rate of glycolysis. *Appl Environ Microbiol* **77**, 2239-2246.
- Antonenkov, V.D., and Hiltunen, J.K.** (2006). Peroxisomal membrane permeability and solute transfer. *Biochimica et Biophysica Acta (BBA) - Molecular Cell Research* **1763**, 1697-1706.
- Antonenkov, V.D., and Hiltunen, J.K.** (2012). Transfer of metabolites across the peroxisomal membrane. *Biochim Biophys Acta*.
- Antonenkov, V.D., Sormunen, R.T., and Hiltunen, J.K.** (2004). The rat liver peroxisomal membrane forms a permeability barrier for cofactors but not for small metabolites in vitro. *J Cell Sci* **117**, 5633-5642.
- Arai, Y., Hayashi, M., and Nishimura, M.** (2008). Proteomic identification and characterization of a novel peroxisomal adenine nucleotide transporter supplying ATP for fatty acid beta-oxidation in soybean and *Arabidopsis*. *Plant Cell* **20**, 3227-3240.
- Arent, S., Christensen, C.E., Pye, V.E., Norgaard, A., and Henriksen, A.** (2010). The multifunctional protein in peroxisomal beta-oxidation: structure and substrate specificity of the *Arabidopsis thaliana* protein MFP2. *J Biol Chem* **285**, 24066-24077.
- Babourina, O., Ozturk, L., Cakmak, I., and Rengel, Z.** (2006). Reactive oxygen species production in wheat roots is not linked with changes in h fluxes during acidic and aluminium stresses. *Plant Signal Behav* **1**, 71-76.
- Baerends, R.J.S., Faber, K.N., Kiel, J.A.K.W., van der Klei, I.J., Harder, W., and Veenhuis, M.** (2000). Sorting and function of peroxisomal membrane proteins. *FEMS Microbiology Reviews* **24**, 291-301.

- Baker, A., Graham, I.A., Holdsworth, M., Smith, S.M., and Theodoulou, F.L.** (2006). Chewing the fat: beta-oxidation in signalling and development. *Trends Plant Sci* **11**, 124-132.
- Bartel, B.** (1997). Auxin Biosynthesis. *Annu Rev Plant Physiol Plant Mol Biol* **48**, 51-66.
- Bassel, G.W., Fung, P., Chow, T.-f.F., Foong, J.A., Provart, N.J., and Cutler, S.R.** (2008). Elucidating the Germination Transcriptional Program Using Small Molecules. *Plant Physiology* **147**, 143-155.
- Bauwe, H., Hagemann, M., and Fernie, A.R.** (2010). Photorespiration: players, partners and origin. *Trends Plant Sci* **15**, 330-336.
- Bauwe, H., Hagemann, M., Kern, R., and Timm, S.** (2012). Photorespiration has a dual origin and manifold links to central metabolism. *Current Opinion in Plant Biology*.
- Berendzen, K., Searle, I., Ravenscroft, D., Koncz, C., Batschauer, A., Coupland, G., Somssich, I.E., and Ulker, B.** (2005). A rapid and versatile combined DNA/RNA extraction protocol and its application to the analysis of a novel DNA marker set polymorphic between *Arabidopsis thaliana* ecotypes Col-0 and Landsberg erecta. *Plant Methods* **1**, 4.
- Bernhardt, K., Wilkinson, S., Weber, A.P.M., and Linka, N.** (2012a). A peroxisomal carrier delivers NAD<sup>+</sup> and contributes to optimal fatty acid degradation during storage oil mobilization. *The Plant Journal* **69**, 1-13.
- Bernhardt, K., Vigelius, S.K., Wiese, J., Linka, N., and Weber, A.P.** (2012b). *Agrobacterium*-mediated *Arabidopsis thaliana* transformation: An overview of T-DNA binary vectors, floral dip and screening for homozygous lines. *Journal of Endocytobiosis and Cell Research* **22**, 19-28.
- Bessman, M.J., Frick, D.N., and O'Handley, S.F.** (1996). The MutT proteins or "Nudix" hydrolases, a family of versatile, widely distributed, "housecleaning" enzymes. *J Biol Chem* **271**, 25059-25062.
- Bowsher, C.G., and Tobin, A.K.** (2001). Compartmentation of metabolism within mitochondria and plastids. *Journal of Experimental Botany* **52**, 513-527.
- Bräutigam, A., Hoffmann-Benning, S., and Weber, A.P.** (2008). Comparative proteomics of chloroplast envelopes from C3 and C4 plants reveals specific adaptations of the plastid envelope to C4 photosynthesis and candidate proteins required for maintaining C4 metabolite fluxes. *Plant Physiol* **148**, 568-579.

- Bräutigam, A., Kajala, K., Wullenweber, J., Sommer, M., Gagneul, D., Weber, K.L., Carr, K.M., Gowik, U., Mass, J., Lercher, M.J., Westhoff, P., Hibberd, J.M., and Weber, A.P.** (2010). An mRNA blueprint for C4 photosynthesis derived from comparative transcriptomics of closely related C3 and C4 species. *Plant Physiol* **155**, 142-156.
- Brosius, U., Dehmel, T., and Gartner, J.** (2002). Two different targeting signals direct human peroxisomal membrane protein 22 to peroxisomes. *J Biol Chem* **277**, 774-784.
- Brown, L.A., and Baker, A.** (2008). Shuttles and cycles: transport of proteins into the peroxisome matrix (review). *Mol Membr Biol* **25**, 363-375.
- Browse, J., McCourt, P.J., and Somerville, C.R.** (1986). Fatty acid composition of leaf lipids determined after combined digestion and fatty acid methyl ester formation from fresh tissue. *Anal Biochem* **152**, 141-145.
- Castillo, M.C., and Leon, J.** (2008). Expression of the beta-oxidation gene 3-ketoacyl-CoA thiolase 2 (KAT2) is required for the timely onset of natural and dark-induced leaf senescence in Arabidopsis. *J Exp Bot* **59**, 2171-2179.
- Chai, M.F., Wei, P.C., Chen, Q.J., An, R., Chen, J., Yang, S., and Wang, X.C.** (2006). NADK3, a novel cytoplasmic source of NADPH, is required under conditions of oxidative stress and modulates abscisic acid responses in Arabidopsis. *Plant J* **47**, 665-674.
- Chen, P.-Y., Wang, C.-K., Soong, S.-C., and To, K.-Y.** (2003). Complete sequence of the binary vector pBI121 and its application in cloning T-DNA insertion from transgenic plants. *Molecular Breeding* **11**, 287-293.
- Corpas, F.J., Barroso, J.B., and del Rio, L.A.** (2001). Peroxisomes as a source of reactive oxygen species and nitric oxide signal molecules in plant cells. *Trends Plant Sci* **6**, 145-150.
- Cousins, A.B., Pracharoenwattana, I., Zhou, W., Smith, S.M., and Badger, M.R.** (2008). Peroxisomal malate dehydrogenase is not essential for photorespiration in Arabidopsis but its absence causes an increase in the stoichiometry of photorespiratory CO<sub>2</sub> release. *Plant Physiol* **148**, 786-795.
- Cousins, A.B., Walker, B.J., Pracharoenwattana, I., Smith, S.M., and Badger, M.R.** (2011). Peroxisomal hydroxypyruvate reductase is not essential for photorespiration in Arabidopsis but its absence causes an increase in the stoichiometry of photorespiratory CO<sub>2</sub> release. *Photosynth Res* **108**, 91-100.
- Curtis, M.D., and Grossniklaus, U.** (2003). A gateway cloning vector set for high-throughput functional analysis of genes in planta. *Plant Physiol* **133**, 462-469.

- Dat, J., Vandenabeele, S., Vranova, E., Van Montagu, M., Inze, D., and Van Breusegem, F.** (2000). Dual action of the active oxygen species during plant stress responses. *Cell Mol Life Sci* **57**, 779-795.
- De Duve, C., and Baudhuin, P.** (1966). Peroxisomes (microbodies and related particles). *Physiol Rev* **46**, 323-357.
- del Rio, L.A., Sandalio, L.M., Palma, J.M., Bueno, P., and Corpas, F.J.** (1992). Metabolism of oxygen radicals in peroxisomes and cellular implications. *Free Radic Biol Med* **13**, 557-580.
- del Rio, L.A., Sandalio, L.M., Corpas, F.J., Palma, J.M., and Barroso, J.B.** (2006). Reactive oxygen species and reactive nitrogen species in peroxisomes. Production, scavenging, and role in cell signaling. *Plant Physiol* **141**, 330-335.
- Delker, C., Zolman, B.K., Miersch, O., and Wasternack, C.** (2007). Jasmonate biosynthesis in *Arabidopsis thaliana* requires peroxisomal beta-oxidation enzymes--additional proof by properties of *pex6* and *aim1*. *Phytochemistry* **68**, 1642-1650.
- Dereeper, A., Guignon, V., Blanc, G., Audic, S., Buffet, S., Chevenet, F., Dufayard, J.F., Guindon, S., Lefort, V., Lescot, M., Claverie, J.M., and Gascuel, O.** (2008). Phylogeny.fr: robust phylogenetic analysis for the non-specialist. *Nucleic Acids Res* **36**, W465-469.
- Donaldson, R.P.** (1981). Organelle Membranes from Germinating Castor Bean Endosperm: II. ENZYMES, CYTOCHROMES, AND PERMEABILITY OF THE GLYOXYSOME MEMBRANE. *Plant Physiol* **67**, 21-25.
- Dunand, C., Crevecoeur, M., and Penel, C.** (2007). Distribution of superoxide and hydrogen peroxide in *Arabidopsis* root and their influence on root development: possible interaction with peroxidases. *New Phytol* **174**, 332-341.
- Durek, P., Schmidt, R., Heazlewood, J.L., Jones, A., MacLean, D., Nagel, A., Kersten, B., and Schulze, W.X.** (2010). PhosPhAt: the *Arabidopsis thaliana* phosphorylation site database. An update. *Nucleic Acids Res* **38**, D828-834.
- Eastmond, P.J.** (2007). MONODEHYDROASCORBATE REDUCTASE4 is required for seed storage oil hydrolysis and postgerminative growth in *Arabidopsis*. *Plant Cell* **19**, 1376-1387.
- Eastmond, P.J., and Graham, I.A.** (2000). The multifunctional protein AtMFP2 is coordinately expressed with other genes of fatty acid beta-oxidation during seed germination in *Arabidopsis thaliana* (L.) Heynh. *Biochem Soc Trans* **28**, 95-99.
- Eastmond, P.J., Hooks, M., and Graham, I.A.** (2000). The *Arabidopsis* acyl-CoA oxidase gene family. *Biochem Soc Trans* **28**, 755-757.



- Eubel, H., Meyer, E.H., Taylor, N.L., Bussell, J.D., O'Toole, N., Heazlewood, J.L., Castleden, I., Small, I.D., Smith, S.M., and Millar, A.H.** (2008). Novel proteins, putative membrane transporters, and an integrated metabolic network are revealed by quantitative proteomic analysis of Arabidopsis cell culture peroxisomes. *Plant Physiol* **148**, 1809-1829.
- Fagarasanu, M., Fagarasanu, A., Tam, Y.Y., Aitchison, J.D., and Rachubinski, R.A.** (2005). Inp1p is a peroxisomal membrane protein required for peroxisome inheritance in *Saccharomyces cerevisiae*. *J Cell Biol* **169**, 765-775.
- Fan, J., Quan, S., Orth, T., Awai, C., Chory, J., and Hu, J.** (2005). The Arabidopsis PEX12 gene is required for peroxisome biogenesis and is essential for development. *Plant Physiol* **139**, 231-239.
- Finkelstein, R.R.** (1994). Mutations at two new Arabidopsis ABA response loci are similar to the *abi3* mutations. *The Plant Journal* **5**, 765-771.
- Footitt, S., Marquez, J., Schmutz, H., Baker, A., Theodoulou, F.L., and Holdsworth, M.** (2006). Analysis of the role of COMATOSE and peroxisomal beta-oxidation in the determination of germination potential in Arabidopsis. *J Exp Bot* **57**, 2805-2814.
- Footitt, S., Slocombe, S.P., Larner, V., Kurup, S., Wu, Y., Larson, T., Graham, I., Baker, A., and Holdsworth, M.** (2002). Control of germination and lipid mobilization by COMATOSE, the Arabidopsis homologue of human ALDP. *EMBO J* **21**, 2912-2922.
- Fransen, M., Wylin, T., Brees, C., Mannaerts, G.P., and Van Veldhoven, P.P.** (2001). Human pex19p binds peroxisomal integral membrane proteins at regions distinct from their sorting sequences. *Mol Cell Biol* **21**, 4413-4424.
- Fukao, Y., Hayashi, Y., Mano, S., Hayashi, M., and Nishimura, M.** (2001). Developmental analysis of a putative ATP/ADP carrier protein localized on glyoxysomal membranes during the peroxisome transition in pumpkin cotyledons. *Plant Cell Physiol* **42**, 835-841.
- Fulda, M., Schnurr, J., Abbadi, A., Heinz, E., and Browse, J.** (2004). Peroxisomal Acyl-CoA synthetase activity is essential for seedling development in Arabidopsis thaliana. *Plant Cell* **16**, 394-405.
- Ge, X., Li, G.J., Wang, S.B., Zhu, H., Zhu, T., Wang, X., and Xia, Y.** (2007). AtNUDT7, a negative regulator of basal immunity in Arabidopsis, modulates two distinct defense response pathways and is involved in maintaining redox homeostasis. *Plant Physiol* **145**, 204-215.

- Germain, V., Rylott, E.L., Larson, T.R., Sherson, S.M., Bechtold, N., Carde, J.P., Bryce, J.H., Graham, I.A., and Smith, S.M.** (2001). Requirement for 3-ketoacyl-CoA thiolase-2 in peroxisome development, fatty acid beta-oxidation and breakdown of triacylglycerol in lipid bodies of Arabidopsis seedlings. *Plant J* **28**, 1-12.
- Gibon, Y., and Larher, F.** (1997). Cycling assay for nicotinamide adenine dinucleotides: NaCl precipitation and ethanol solubilization of the reduced tetrazolium. *Anal Biochem* **251**, 153-157.
- Gossmann, T.I., Ziegler, M., Puntervoll, P., de Figueiredo, L.F., Schuster, S., and Heiland, I.** (2012). NAD(+) biosynthesis and salvage - a phylogenetic perspective. *FEBS J*.
- Graham, I.A.** (2008). Seed storage oil mobilization. *Annu Rev Plant Biol* **59**, 115-142.
- Grefen, C., Donald, N., Hashimoto, K., Kudla, J., Schumacher, K., and Blatt, M.R.** (2010). A ubiquitin-10 promoter-based vector set for fluorescent protein tagging facilitates temporal stability and native protein distribution in transient and stable expression studies. *The Plant Journal* **64**, 355-365.
- Grosskinsky, D.K., Koffler, B.E., Roitsch, T., Maier, R., and Zechmann, B.** (2012). Compartment-Specific Antioxidative Defense in Arabidopsis Against Virulent and Avirulent *Pseudomonas syringae*. *Phytopathology* **102**, 662-673.
- Hadden, D.A., Phillipson, B.A., Johnston, K.A., Brown, L.A., Manfield, I.W., El-Shami, M., Sparkes, I.A., and Baker, A.** (2006). Arabidopsis PEX19 is a dimeric protein that binds the peroxin PEX10. *Mol Membr Biol* **23**, 325-336.
- Haferkamp, I., and Schmitz-Esser, S.** (2012). The plant mitochondrial carrier family: functional and evolutionary aspects. *Front Plant Sci* **3**, 2.
- Haferkamp, I., Schmitz-Esser, S., Linka, N., Urbany, C., Collingro, A., Wagner, M., Horn, M., and Neuhaus, H.E.** (2004). A candidate NAD<sup>+</sup> transporter in an intracellular bacterial symbiont related to Chlamydiae. *Nature* **432**, 622-625.
- Halbach, A., Lorenzen, S., Landgraf, C., Volkmer-Engert, R., Erdmann, R., and Rottensteiner, H.** (2005). Function of the PEX19-binding site of human adrenoleukodystrophy protein as targeting motif in man and yeast. PMP targeting is evolutionarily conserved. *J Biol Chem* **280**, 21176-21182.
- Hanahan, D.** (1983). Studies on transformation of *Escherichia coli* with plasmids. *J Mol Biol* **166**, 557-580.
- Hashida, S.N., Takahashi, H., and Uchimiya, H.** (2009). The role of NAD biosynthesis in plant development and stress responses. *Ann Bot* **103**, 819-824.

- Hause, B., Hause, G., Kutter, C., Miersch, O., and Wasternack, C.** (2003). Enzymes of jasmonate biosynthesis occur in tomato sieve elements. *Plant Cell Physiol* **44**, 643-648.
- Hayashi, M., and Nishimura, M.** (2006). *Arabidopsis thaliana* - A model organism to study plant peroxisomes. *Biochimica et Biophysica Acta (BBA) - Molecular Cell Research* **1763**, 1382-1391.
- Hayashi, M., Toriyama, K., Kondo, M., and Nishimura, M.** (1998). 2,4-Dichlorophenoxybutyric acid-resistant mutants of *Arabidopsis* have defects in glyoxysomal fatty acid beta-oxidation. *Plant Cell* **10**, 183-195.
- Hayashi, Y., Hayashi, M., Hayashi, H., Hara-Nishimura, I., and Nishimura, M.** (2001). Direct interaction between glyoxysomes and lipid bodies in cotyledons of the *Arabidopsis thaliana* ped1 mutant. *Protoplasma* **218**, 83-94.
- Heazlewood, J.L., Durek, P., Hummel, J., Selbig, J., Weckwerth, W., Walther, D., and Schulze, W.X.** (2008). PhosPhAt: a database of phosphorylation sites in *Arabidopsis thaliana* and a plant-specific phosphorylation site predictor. *Nucleic Acids Res* **36**, D1015-1021.
- Heineke, D., Riens, B., Grosse, H., Hoferichter, P., Peter, U., Flugge, U.I., and Heldt, H.W.** (1991). Redox Transfer across the Inner Chloroplast Envelope Membrane. *Plant Physiol* **95**, 1131-1137.
- Held, M.A., Boulaflous, A., and Brandizzi, F.** (2008). Advances in Fluorescent Protein-Based Imaging for the Analysis of Plant Endomembranes. *Plant Physiology* **147**, 1469-1481.
- Herrmann, J.M., Koll, H., Cook, R.A., Neupert, W., and Stuart, R.A.** (1995). Topogenesis of cytochrome oxidase subunit II. Mechanisms of protein export from the mitochondrial matrix. *J Biol Chem* **270**, 27079-27086.
- Hoepfner, D., Schildknecht, D., Braakman, I., Philippsen, P., and Tabak, H.F.** (2005). Contribution of the endoplasmic reticulum to peroxisome formation. *Cell* **122**, 85-95.
- Hu, J., Baker, A., Bartel, B., Linka, N., Mullen, R.T., Reumann, S., and Zolman, B.K.** (2012). *Plant Peroxisomes: Biogenesis and Function*. *Plant Cell*.
- Hunt, J.E., and Trelease, R.N.** (2004). Sorting pathway and molecular targeting signals for the *Arabidopsis* peroxin 3. *Biochem Biophys Res Commun* **314**, 586-596.
- Igamberdiev, A.U., and Gardestrom, P.** (2003). Regulation of NAD- and NADP-dependent isocitrate dehydrogenases by reduction levels of pyridine nucleotides in mitochondria and cytosol of pea leaves. *Biochim Biophys Acta* **1606**, 117-125.

- Ishikawa, K., Ogawa, T., Hirose, E., Nakayama, Y., Harada, K., Fukusaki, E., Yoshimura, K., and Shigeoka, S.** (2009). Modulation of the poly(ADP-ribosyl)ation reaction via the Arabidopsis ADP-ribose/NADH pyrophosphohydrolase, AtNUDX7, is involved in the response to oxidative stress. *Plant Physiol* **151**, 741-754.
- Islinger, M., Grille, S., Fahimi, H.D., and Schrader, M.** (2012). The peroxisome: an update on mysteries. *Histochem Cell Biol* **137**, 547-574.
- Ito, J., Taylor, N.L., Castleden, I., Weckwerth, W., Millar, A.H., and Heazlewood, J.L.** (2009). A survey of the Arabidopsis thaliana mitochondrial phosphoproteome. *Proteomics* **9**, 4229-4240.
- Iyer-Pascuzzi, A.S., Jackson, T., Cui, H., Petricka, J.J., Busch, W., Tsukagoshi, H., and Benfey, P.N.** (2011). Cell identity regulators link development and stress responses in the Arabidopsis root. *Dev Cell* **21**, 770-782.
- Jambunathan, N., and Mahalingam, R.** (2006). Analysis of Arabidopsis growth factor gene 1 (GFG1) encoding a nudix hydrolase during oxidative signaling. *Planta* **224**, 1-11.
- Jambunathan, N., Penaganti, A., Tang, Y., and Mahalingam, R.** (2010). Modulation of redox homeostasis under suboptimal conditions by Arabidopsis nudix hydrolase 7. *BMC Plant Biol* **10**, 173.
- Jiang, Z.Y., Woollard, A.C., and Wolff, S.P.** (1990). Hydrogen peroxide production during experimental protein glycation. *FEBS Lett* **268**, 69-71.
- Jones, J.M., Morrell, J.C., and Gould, S.J.** (2004). PEX19 is a predominantly cytosolic chaperone and import receptor for class 1 peroxisomal membrane proteins. *J Cell Biol* **164**, 57-67.
- Kaiser, W.M., and Huber, S.C.** (2001). Post-translational regulation of nitrate reductase: mechanism, physiological relevance and environmental triggers. *J Exp Bot* **52**, 1981-1989.
- Karnik, S.K., and Trelease, R.N.** (2007). Arabidopsis peroxin 16 trafficks through the ER and an intermediate compartment to pre-existing peroxisomes via overlapping molecular targeting signals. *J Exp Bot* **58**, 1677-1693.
- Kasahara, M., and Hinkle, P.C.** (1976). Reconstitution of D-glucose transport catalyzed by a protein fraction from human erythrocytes in sonicated liposomes. *Proc Natl Acad Sci U S A* **73**, 396-400.
- Kemp, S., Theodoulou, F.L., and Wanders, R.J.** (2011). Mammalian peroxisomal ABC transporters: from endogenous substrates to pathology and clinical significance. *Br J Pharmacol* **164**, 1753-1766.

- Kilian, J., Whitehead, D., Horak, J., Wanke, D., Weini, S., Batistic, O., D'Angelo, C., Bornberg-Bauer, E., Kudla, J., and Harter, K.** (2007). The AtGenExpress global stress expression data set: protocols, evaluation and model data analysis of UV-B light, drought and cold stress responses. *The Plant Journal* **50**, 347-363.
- Kim, P.K., Mullen, R.T., Schumann, U., and Lippincott-Schwartz, J.** (2006). The origin and maintenance of mammalian peroxisomes involves a de novo PEX16-dependent pathway from the ER. *J Cell Biol* **173**, 521-532.
- Kirchberger, S., Tjaden, J., and Neuhaus, H.E.** (2008). Characterization of the Arabidopsis Brittle1 transport protein and impact of reduced activity on plant metabolism. *Plant J* **56**, 51-63.
- Koncz, C., and Schell, J.** (1986). The promoter of T<sub>L</sub>-DNA gene 5 controls the tissue-specific expression of chimaeric genes carried by a novel type of *Agrobacterium* binary vector. *Molecular and General Genetics MGG* **204**, 383-396.
- Koyama, H., Toda, T., and Hara, T.** (2001). Brief exposure to low-pH stress causes irreversible damage to the growing root in *Arabidopsis thaliana*: pectin-Ca interaction may play an important role in proton rhizotoxicity. *Journal of Experimental Botany* **52**, 361-368.
- Kraszewska, E.** (2008). The plant Nudix hydrolase family. *Acta Biochim Pol* **55**, 663-671.
- Lam, S.K., Yoda, N., and Schekman, R.** (2010). A vesicle carrier that mediates peroxisome protein traffic from the endoplasmic reticulum. *Proc Natl Acad Sci U S A* **107**, 21523-21528.
- Lanquar, V., and Frommer, W.B.** (2010). Adjusting ammonium uptake via phosphorylation. *Plant Signal Behav* **5**, 736-738.
- Lanyon-Hogg, T., Warriner, S.L., and Baker, A.** (2010). Getting a camel through the eye of a needle: the import of folded proteins by peroxisomes. *Biol Cell* **102**, 245-263.
- Lazarow, P.B., and Fujiki, Y.** (1985). Biogenesis of peroxisomes. *Annu Rev Cell Biol* **1**, 489-530.
- Lemieux, B., Miquel, M., Somerville, C., and Browse, J.** (1990). Mutants of *Arabidopsis* with alterations in seed lipid fatty acid composition. *TAG Theoretical and Applied Genetics* **80**, 234-240.
- Léon, S., Goodman, J.M., and Subramani, S.** (2006). Uniqueness of the mechanism of protein import into the peroxisome matrix: Transport of folded, co-factor-bound and oligomeric proteins by shuttling receptors. *Biochimica et Biophysica Acta (BBA) - Molecular Cell Research* **1763**, 1552-1564.

- 
- Leonardi, R., Zhang, Y.M., Rock, C.O., and Jackowski, S.** (2005). Coenzyme A: back in action. *Prog Lipid Res* **44**, 125-153.
- Leroch, M., Kirchberger, S., Haferkamp, I., Wahl, M., Neuhaus, H.E., and Tjaden, J.** (2005). Identification and characterization of a novel plastidic adenine nucleotide uniporter from *Solanum tuberosum*. *J Biol Chem* **280**, 17992-18000.
- Leroch, M., Neuhaus, H.E., Kirchberger, S., Zimmermann, S., Melzer, M., Gerhold, J., and Tjaden, J.** (2008). Identification of a novel adenine nucleotide transporter in the endoplasmic reticulum of *Arabidopsis*. *Plant Cell* **20**, 438-451.
- Lingard, M.J., and Trelease, R.N.** (2006). Five *Arabidopsis* peroxin 11 homologs individually promote peroxisome elongation, duplication or aggregation. *J Cell Sci* **119**, 1961-1972.
- Lingner, T., Kataya, A.R., Antonicelli, G.E., Benichou, A., Nilssen, K., Chen, X.Y., Siemsen, T., Morgenstern, B., Meinicke, P., and Reumann, S.** (2011). Identification of novel plant peroxisomal targeting signals by a combination of machine learning methods and in vivo subcellular targeting analyses. *Plant Cell* **23**, 1556-1572.
- Linka, M., Jamai, A., and Weber, A.P.** (2008a). Functional characterization of the plastidic phosphate translocator gene family from the thermo-acidophilic red alga *Galdieria sulphuraria* reveals specific adaptations of primary carbon partitioning in green plants and red algae. *Plant Physiol* **148**, 1487-1496.
- Linka, N., and Esser, C.** (2012). Transport proteins regulate the flux of metabolites and cofactors across the membrane of plant peroxisomes. *Front Plant Sci* **3**, 3.
- Linka, N., Theodoulou, F.L., Haslam, R.P., Linka, M., Napier, J.A., Neuhaus, H.E., and Weber, A.P.** (2008b). Peroxisomal ATP import is essential for seedling development in *Arabidopsis thaliana*. *Plant Cell* **20**, 3241-3257.
- Lisec, J., Schauer, N., Kopka, J., Willmitzer, L., and Fernie, A.R.** (2006). Gas chromatography mass spectrometry-based metabolite profiling in plants. *Nat Protoc* **1**, 387-396.
- Lisenbee, C.S., Heinze, M., and Trelease, R.N.** (2003). Peroxisomal Ascorbate Peroxidase Resides within a Subdomain of Rough Endoplasmic Reticulum in Wild-Type *Arabidopsis* Cells. *Plant Physiology* **132**, 870-882.
- Lisenbee, C.S., Lingard, M.J., and Trelease, R.N.** (2005). *Arabidopsis* peroxisomes possess functionally redundant membrane and matrix isoforms of monodehydroascorbate reductase. *Plant J* **43**, 900-914.

- Ljung, K., Hull, A.K., Celenza, J., Yamada, M., Estelle, M., Normanly, J., and Sandberg, G.** (2005). Sites and regulation of auxin biosynthesis in Arabidopsis roots. *Plant Cell* **17**, 1090-1104.
- Lorenz, H., Hailey, D.W., and Lippincott-Schwartz, J.** (2006). Fluorescence protease protection of GFP chimeras to reveal protein topology and subcellular localization. *Nat Methods* **3**, 205-210.
- Ma, C., Agrawal, G., and Subramani, S.** (2011). Peroxisome assembly: matrix and membrane protein biogenesis. *J Cell Biol* **193**, 7-16.
- Mano, S., Nakamori, C., Fukao, Y., Araki, M., Matsuda, A., Kondo, M., and Nishimura, M.** (2011). A defect of peroxisomal membrane protein 38 causes enlargement of peroxisomes. *Plant Cell Physiol* **52**, 2157-2172.
- Meinecke, M., Cizmowski, C., Schliebs, W., Kruger, V., Beck, S., Wagner, R., and Erdmann, R.** (2010). The peroxisomal importomer constitutes a large and highly dynamic pore. *Nat Cell Biol* **12**, 273-277.
- Mettler, I.J., and Beevers, H.** (1980). Oxidation of NADH in Glyoxysomes by a Malate-Aspartate Shuttle. *Plant Physiol* **66**, 555-560.
- Mhamdi, A., Noctor, G., and Baker, A.** (2012). Plant catalases: Peroxisomal redox guardians. *Arch Biochem Biophys*.
- Mittler, R.** (2002). Oxidative stress, antioxidants and stress tolerance. *Trends Plant Sci* **7**, 405-410.
- Mullen, R.T., and Trelease, R.N.** (2006). The ER-peroxisome connection in plants: Development of the "ER semi-autonomous peroxisome maturation and replication" model for plant peroxisome biogenesis. *Biochimica et Biophysica Acta (BBA) - Molecular Cell Research* **1763**, 1655-1668.
- Murphy, M.A., Phillipson, B.A., Baker, A., and Mullen, R.T.** (2003). Characterization of the targeting signal of the Arabidopsis 22-kD integral peroxisomal membrane protein. *Plant Physiol* **133**, 813-828.
- Nakabayashi, K., Okamoto, M., Koshiba, T., Kamiya, Y., and Nambara, E.** (2005). Genome-wide profiling of stored mRNA in Arabidopsis thaliana seed germination: epigenetic and genetic regulation of transcription in seed. *Plant J* **41**, 697-709.
- Nakagawa, T., Imanaka, T., Morita, M., Ishiguro, K., Yurimoto, H., Yamashita, A., Kato, N., and Sakai, Y.** (2000). Peroxisomal membrane protein Pmp47 is essential in the metabolism of middle-chain fatty acid in yeast peroxisomes and is associated with peroxisome proliferation. *J Biol Chem* **275**, 3455-3461.

- Nito, K., Kamigaki, A., Kondo, M., Hayashi, M., and Nishimura, M.** (2007). Functional classification of Arabidopsis peroxisome biogenesis factors proposed from analyses of knockdown mutants. *Plant Cell Physiol* **48**, 763-774.
- Noctor, G., Queval, G., and Gakiere, B.** (2006). NAD(P) synthesis and pyridine nucleotide cycling in plants and their potential importance in stress conditions. *J Exp Bot* **57**, 1603-1620.
- Nyathi, Y., Zhang, X., Baldwin, J.M., Bernhardt, K., Johnson, B., Baldwin, S.A., Theodoulou, F.L., and Baker, A.** (2012). Pseudo half-molecules of the ABC transporter, COMATOSE, bind Pex19 and target to peroxisomes independently but are both required for activity. *FEBS letters* **586**, 2280-2286.
- Ogawa, T., Ueda, Y., Yoshimura, K., and Shigeoka, S.** (2005). Comprehensive analysis of cytosolic Nudix hydrolases in Arabidopsis thaliana. *J Biol Chem* **280**, 25277-25283.
- Ogawa, T., Yoshimura, K., Miyake, H., Ishikawa, K., Ito, D., Tanabe, N., and Shigeoka, S.** (2008). Molecular characterization of organelle-type Nudix hydrolases in Arabidopsis. *Plant Physiol* **148**, 1412-1424.
- Olejnik, K., Bucholc, M., Anielska-Mazur, A., Lipko, A., Kujawa, M., Modzelan, M., Augustyn, A., and Kraszewska, E.** (2011). Arabidopsis thaliana Nudix hydrolase AtNUDT7 forms complexes with the regulatory RACK1A protein and Ggamma subunits of the signal transducing heterotrimeric G protein. *Acta Biochim Pol* **58**, 609-616.
- Palma, J.M., Corpas, F.J., and del Rio, L.A.** (2009). Proteome of plant peroxisomes: new perspectives on the role of these organelles in cell biology. *Proteomics* **9**, 2301-2312.
- Palmieri, F., Pierri, C.L., De Grassi, A., Nunes-Nesi, A., and Fernie, A.R.** (2011). Evolution, structure and function of mitochondrial carriers: a review with new insights. *Plant J* **66**, 161-181.
- Palmieri, F., Rieder, B., Ventrella, A., Blanco, E., Do, P.T., Nunes-Nesi, A., Trauth, A.U., Fiermonte, G., Tjaden, J., Agrimi, G., Kirchberger, S., Paradies, E., Fernie, A.R., and Neuhaus, H.E.** (2009). Molecular identification and functional characterization of Arabidopsis thaliana mitochondrial and chloroplastic NAD<sup>+</sup> carrier proteins. *J Biol Chem* **284**, 31249-31259.
- Palmieri, L., Rottensteiner, H., Girzalsky, W., Scarcia, P., Palmieri, F., and Erdmann, R.** (2001). Identification and functional reconstitution of the yeast peroxisomal adenine nucleotide transporter. *EMBO J* **20**, 5049-5059.



- Palmieri, L., Santoro, A., Carrari, F., Blanco, E., Nunes-Nesi, A., Arrigoni, R., Genchi, F., Fernie, A.R., and Palmieri, F.** (2008). Identification and characterization of ADNT1, a novel mitochondrial adenine nucleotide transporter from Arabidopsis. *Plant Physiol* **148**, 1797-1808.
- Peterhansel, C., and Maurino, V.G.** (2011). Photorespiration redesigned. *Plant Physiol* **155**, 49-55.
- Philipp, F.** (2010). Die physiologische Rolle eines peroxisomalen NAD-Transportproteins in der Pflanze. Bachelor thesis.
- Picault, N., Hodges, M., Palmieri, L., and Palmieri, F.** (2004). The growing family of mitochondrial carriers in Arabidopsis. *Trends Plant Sci* **9**, 138-146.
- Pick, T.R., Brautigam, A., Schluter, U., Denton, A.K., Colmsee, C., Scholz, U., Fahnenstich, H., Pieruschka, R., Rascher, U., Sonnewald, U., and Weber, A.P.** (2011). Systems analysis of a maize leaf developmental gradient redefines the current C4 model and provides candidates for regulation. *Plant Cell* **23**, 4208-4220.
- Pinfield-Wells, H., Rylott, E.L., Gilday, A.D., Graham, S., Job, K., Larson, T.R., and Graham, I.A.** (2005). Sucrose rescues seedling establishment but not germination of Arabidopsis mutants disrupted in peroxisomal fatty acid catabolism. *Plant J* **43**, 861-872.
- Platta, H.W., and Erdmann, R.** (2007a). The peroxisomal protein import machinery. *FEBS Lett* **581**, 2811-2819.
- Platta, H.W., and Erdmann, R.** (2007b). Peroxisomal dynamics. *Trends Cell Biol* **17**, 474-484.
- Pracharoenwattana, I., Cornah, J.E., and Smith, S.M.** (2007). Arabidopsis peroxisomal malate dehydrogenase functions in beta-oxidation but not in the glyoxylate cycle. *Plant J* **50**, 381-390.
- Pracharoenwattana, I., Zhou, W., and Smith, S.M.** (2010). Fatty acid beta-oxidation in germinating Arabidopsis seeds is supported by peroxisomal hydroxypyruvate reductase when malate dehydrogenase is absent. *Plant Mol Biol* **72**, 101-109.
- Quan, L.J., Zhang, B., Shi, W.W., and Li, H.Y.** (2008). Hydrogen peroxide in plants: a versatile molecule of the reactive oxygen species network. *J Integr Plant Biol* **50**, 2-18.
- Quettier, A.L., and Eastmond, P.J.** (2009). Storage oil hydrolysis during early seedling growth. *Plant Physiol Biochem* **47**, 485-490.

- Quettier, A.L., Shaw, E., and Eastmond, P.J.** (2008). SUGAR-DEPENDENT6 encodes a mitochondrial flavin adenine dinucleotide-dependent glycerol-3-p dehydrogenase, which is required for glycerol catabolism and post germinative seedling growth in Arabidopsis. *Plant Physiol* **148**, 519-528.
- Queval, G., and Noctor, G.** (2007). A plate reader method for the measurement of NAD, NADP, glutathione, and ascorbate in tissue extracts: Application to redox profiling during Arabidopsis rosette development. *Anal Biochem* **363**, 58-69.
- Reinders, J.r., Wagner, K., Zahedi, R.P., Stojanovski, D., Eyrich, B., van der Laan, M., Rehling, P., Sickmann, A., Pfanner, N., and Meisinger, C.** (2007). Profiling Phosphoproteins of Yeast Mitochondria Reveals a Role of Phosphorylation in Assembly of the ATP Synthase. *Molecular & Cellular Proteomics* **6**, 1896-1906.
- Reinke, P.** (2010). Physiological impact of peroxisomal ATPimport into peroxisomes during the plant life cycle. Diploma thesis.
- Reumann, S., and Weber, A.P.** (2006). Plant peroxisomes respire in the light: some gaps of the photorespiratory C2 cycle have become filled--others remain. *Biochim Biophys Acta* **1763**, 1496-1510.
- Reumann, S., Maier, E., Benz, R., and Heldt, H.W.** (1995). The membrane of leaf peroxisomes contains a porin-like channel. *J Biol Chem* **270**, 17559-17565.
- Reumann, S., Ma, C., Lemke, S., and Babujee, L.** (2004). AraPeroX. A database of putative Arabidopsis proteins from plant peroxisomes. *Plant Physiol* **136**, 2587-2608.
- Reumann, S., Quan, S., Aung, K., Yang, P., Manandhar-Shrestha, K., Holbrook, D., Linka, N., Switzenberg, R., Wilkerson, C.G., Weber, A.P., Olsen, L.J., and Hu, J.** (2009). In-depth proteome analysis of Arabidopsis leaf peroxisomes combined with in vivo subcellular targeting verification indicates novel metabolic and regulatory functions of peroxisomes. *Plant Physiol* **150**, 125-143.
- Rhodin, J.** (1954). Correlation of ultrastructural organization and function in normal and experimentally changed proximal tubule cells of the mouse kidney. Ph.D. thesis, Karolinska Institute, Stockholm, Sweden.
- Richard, M., Muschalik, N., Grawe, F., Ozuyaman, S., and Knust, E.** (2009). A role for the extracellular domain of Crumbs in morphogenesis of Drosophila photoreceptor cells. *Eur J Cell Biol* **88**, 765-777.
- Richmond, T.A., and Bleecker, A.B.** (1999). A defect in beta-oxidation causes abnormal inflorescence development in Arabidopsis. *Plant Cell* **11**, 1911-1924.

- Rieder, B., and Neuhaus, H.E.** (2011). Identification of an Arabidopsis Plasma Membrane-located ATP Transporter Important for Anther Development. *The Plant Cell Online* **23**, 1932-1944.
- Robertson, D., Davies, D.R., Gerrish, C., Jupe, S.C., and Bolwell, G.P.** (1995). Rapid changes in oxidative metabolism as a consequence of elicitor treatment of suspension-cultured cells of French bean (*Phaseolus vulgaris* L.). *Plant Mol Biol* **27**, 59-67.
- Romeis, T., Ludwig, A.A., Martin, R., and Jones, J.D.** (2001). Calcium-dependent protein kinases play an essential role in a plant defence response. *EMBO J* **20**, 5556-5567.
- Rosar, C., Kanonenberg, K., Nanda, A.M., Mielewczik, M., Bräutigam, A., Novak, O., Strnad, M., Walter, A., and Weber, A.P.M.** (2012). The Leaf Reticulate Mutant *dov1* Is Impaired in the First Step of Purine Metabolism. *Molecular Plant*.
- Rottensteiner, H., and Theodoulou, F.L.** (2006). The ins and outs of peroxisomes: coordination of membrane transport and peroxisomal metabolism. *Biochim Biophys Acta* **1763**, 1527-1540.
- Rottensteiner, H., Kramer, A., Lorenzen, S., Stein, K., Landgraf, C., Volkmer-Engert, R., and Erdmann, R.** (2004). Peroxisomal membrane proteins contain common Pex19p-binding sites that are an integral part of their targeting signals. *Mol Biol Cell* **15**, 3406-3417.
- Rylott, E.L., Hooks, M.A., and Graham, I.A.** (2001). Co-ordinate regulation of genes involved in storage lipid mobilization in *Arabidopsis thaliana*. *Biochem Soc Trans* **29**, 283-287.
- Rylott, E.L., Eastmond, P.J., Gilday, A.D., Slocombe, S.P., Larson, T.R., Baker, A., and Graham, I.A.** (2006). The *Arabidopsis thaliana* multifunctional protein gene (MFP2) of peroxisomal beta-oxidation is essential for seedling establishment. *Plant J* **45**, 930-941.
- Sacksteder, K.A., Jones, J.M., South, S.T., Li, X., Liu, Y., and Gould, S.J.** (2000). PEX19 binds multiple peroxisomal membrane proteins, is predominantly cytoplasmic, and is required for peroxisome membrane synthesis. *J Cell Biol* **148**, 931-944.
- Sambrook, J., Fritsch, E.F., and Maniatis, T.** (1989). *Molecular cloning: a laboratory manual*, 3rd edn. (Cold Spring Harbor Laboratory Press).
- Sauer, N., and Stadler, R.** (1993). A sink-specific H<sup>+</sup>/monosaccharide co-transporter from *Nicotiana tabacum*: cloning and heterologous expression in baker's yeast. *Plant J* **4**, 601-610.

- Schaller, A., and Stintzi, A.** (2008). Jasmonate Biosynthesis and Signaling for Induced Plant Defense against Herbivory In *Induced Plant Resistance to Herbivory* (Springer Netherlands), pp. 349-366.
- Schluter, A., Fourcade, S., Ripp, R., Mandel, J.L., Poch, O., and Pujol, A.** (2006). The evolutionary origin of peroxisomes: an ER-peroxisome connection. *Mol Biol Evol* **23**, 838-845.
- Schmid, M., Davison, T.S., Henz, S.R., Pape, U.J., Demar, M., Vingron, M., Scholkopf, B., Weigel, D., and Lohmann, J.U.** (2005). A gene expression map of *Arabidopsis thaliana* development. *Nat Genet* **37**, 501-506.
- Schrader, M., and Fahimi, H.D.** (2006). Peroxisomes and oxidative stress. *Biochim Biophys Acta* **1763**, 1755-1766.
- Schrader, M., and Fahimi, H.D.** (2008). The peroxisome: still a mysterious organelle. *Histochem Cell Biol* **129**, 421-440.
- Schwab, R., Ossowski, S., Riester, M., Warthmann, N., and Weigel, D.** (2006). Highly specific gene silencing by artificial microRNAs in *Arabidopsis*. *Plant Cell* **18**, 1121-1133.
- Siloto, R.M.P., Findlay, K., Lopez-Villalobos, A., Yeung, E.C., Nykiforuk, C.L., and Moloney, M.M.** (2006). The Accumulation of Oleosins Determines the Size of Seed Oilbodies in *Arabidopsis*. *The Plant Cell Online* **18**, 1961-1974.
- Somerville, C.R., and Ogren, W.L.** (1980). Photorespiration mutants of *Arabidopsis thaliana* deficient in serine-glyoxylate aminotransferase activity. *Proc Natl Acad Sci U S A* **77**, 2684-2687.
- Sparkes, I.A., and Baker, A.** (2002). Peroxisome biogenesis and protein import in plants, animals and yeasts: enigma and variations? (Review). *Mol Membr Biol* **19**, 171-185.
- Sparkes, I.A., Hawes, C., and Baker, A.** (2005). AtPEX2 and AtPEX10 are targeted to peroxisomes independently of known endoplasmic reticulum trafficking routes. *Plant Physiol* **139**, 690-700.
- Sparkes, I.A., Brandizzi, F., Slocombe, S.P., El-Shami, M., Hawes, C., and Baker, A.** (2003). An *Arabidopsis* pex10 null mutant is embryo lethal, implicating peroxisomes in an essential role during plant embryogenesis. *Plant Physiol* **133**, 1809-1819.
- Strader, L.C., Culler, A.H., Cohen, J.D., and Bartel, B.** (2010). Conversion of endogenous indole-3-butyric acid to indole-3-acetic acid drives cell expansion in *Arabidopsis* seedlings. *Plant Physiol* **153**, 1577-1586.

- 
- Tabak, H.F., van der Zand, A., and Braakman, I.** (2008). Peroxisomes: minted by the ER. *Curr Opin Cell Biol* **20**, 393-400.
- Theodoulou, F.L., and Eastmond, P.J.** (2012). Seed storage oil catabolism: a story of give and take. *Curr Opin Plant Biol* **15**, 322-328.
- Timm, S., Florian, A., Jahnke, K., Nunes-Nesi, A., Fernie, A.R., and Bauwe, H.** (2011). The hydroxypyruvate-reducing system in Arabidopsis: multiple enzymes for the same end. *Plant Physiol* **155**, 694-705.
- Timm, S., Nunes-Nesi, A., Parnik, T., Morgenthal, K., Wienkoop, S., Keerberg, O., Weckwerth, W., Kleczkowski, L.A., Fernie, A.R., and Bauwe, H.** (2008). A cytosolic pathway for the conversion of hydroxypyruvate to glycerate during photorespiration in Arabidopsis. *Plant Cell* **20**, 2848-2859.
- Titorenko, V.I., Nicaud, J.M., Wang, H., Chan, H., and Rachubinski, R.A.** (2002). Acyl-CoA oxidase is imported as a heteropentameric, cofactor-containing complex into peroxisomes of *Yarrowia lipolytica*. *J Cell Biol* **156**, 481-494.
- Todisco, S., Agrimi, G., Castegna, A., and Palmieri, F.** (2006). Identification of the mitochondrial NAD<sup>+</sup> transporter in *Saccharomyces cerevisiae*. *J Biol Chem* **281**, 1524-1531.
- Toro, A.A., Araya, C.A., Cordova, G.J., Arredondo, C.A., Cardenas, H.G., Moreno, R.E., Venegas, A., Koenig, C.S., Cancino, J., Gonzalez, A., and Santos, M.J.** (2009). Pex3p-dependent peroxisomal biogenesis initiates in the endoplasmic reticulum of human fibroblasts. *J Cell Biochem* **107**, 1083-1096.
- Trippelsdorf, M.** (2012). The role of a peroxisomal NAD-transporter in plants. Bachelor thesis.
- Tugal, H.B., Pool, M., and Baker, A.** (1999). Arabidopsis 22-kilodalton peroxisomal membrane protein. Nucleotide sequence analysis and biochemical characterization. *Plant Physiol* **120**, 309-320.
- Usadel, B., Obayashi, T., Mutwil, M., Giorgi, F.M., Bassel, G.W., Tanimoto, M., Chow, A., Steinhauser, D., Persson, S., and Provart, N.J.** (2009). Co-expression tools for plant biology: opportunities for hypothesis generation and caveats. *Plant Cell Environ* **32**, 1633-1651.
- Van Ael, E., and Fransen, M.** (2006). Targeting signals in peroxisomal membrane proteins. *Biochimica et Biophysica Acta (BBA) - Molecular Cell Research* **1763**, 1629-1638.

- van der Graaff, E., Schwacke, R., Schneider, A., Desimone, M., Flugge, U.I., and Kunze, R.** (2006). Transcription analysis of arabidopsis membrane transporters and hormone pathways during developmental and induced leaf senescence. *Plant Physiol* **141**, 776-792.
- van der Zand, A., Braakman, I., and Tabak, H.F.** (2010). Peroxisomal membrane proteins insert into the endoplasmic reticulum. *Mol Biol Cell* **21**, 2057-2065.
- van Roermund, C.W., Elgersma, Y., Singh, N., Wanders, R.J., and Tabak, H.F.** (1995). The membrane of peroxisomes in *Saccharomyces cerevisiae* is impermeable to NAD(H) and acetyl-CoA under in vivo conditions. *EMBO J* **14**, 3480-3486.
- Van Veldhoven, P., Debeer, L.J., and Mannaerts, G.P.** (1983). Water- and solute-accessible spaces of purified peroxisomes. Evidence that peroxisomes are permeable to NAD<sup>+</sup>. *Biochem J* **210**, 685-693.
- Van Veldhoven, P.P., Just, W.W., and Mannaerts, G.P.** (1987). Permeability of the peroxisomal membrane to cofactors of beta-oxidation. Evidence for the presence of a pore-forming protein. *J Biol Chem* **262**, 4310-4318.
- Vigelius, S.K.** (2009). Dissecting the role of two adenine nucleotide carriers in *Arabidopsis thaliana*. Diploma thesis.
- Visser, W.F., van Roermund, C.W., Waterham, H.R., and Wanders, R.J.** (2002). Identification of human PMP34 as a peroxisomal ATP transporter. *Biochem Biophys Res Commun* **299**, 494-497.
- Voinnet, O., Rivas, S., Mestre, P., and Baulcombe, D.** (2003). An enhanced transient expression system in plants based on suppression of gene silencing by the p19 protein of tomato bushy stunt virus. *Plant J* **33**, 949-956.
- Voll, L.M., Jamai, A., Renne, P., Voll, H., McClung, C.R., and Weber, A.P.** (2006). The photorespiratory *Arabidopsis* shm1 mutant is deficient in SHM1. *Plant Physiol* **140**, 59-66.
- Waller, J.C., Dhanoa, P.K., Schumann, U., Mullen, R.T., and Snedden, W.A.** (2010). Subcellular and tissue localization of NAD kinases from *Arabidopsis*: compartmentalization of de novo NADP biosynthesis. *Planta* **231**, 305-317.
- Walton, P.A., and Pizzitelli, M.** (2012). Effects of peroxisomal catalase inhibition on mitochondrial function. *Front Physiol* **3**, 108.
- Wanders, R.J.** (2004). Peroxisomes, lipid metabolism, and peroxisomal disorders. *Mol Genet Metab* **83**, 16-27.

- Wanders, R.J., and Waterham, H.R.** (2006). Biochemistry of mammalian peroxisomes revisited. *Annu Rev Biochem* **75**, 295-332.
- Wang, G., and Pichersky, E.** (2007). Nicotinamidase participates in the salvage pathway of NAD biosynthesis in *Arabidopsis*. *Plant J* **49**, 1020-1029.
- Wilkinson, S.** (2009). Molekularbiologische, biochemische und physiologische Charakterisierung eines peroxisomalen Membranproteins aus *Arabidopsis thaliana* Diploma thesis.
- Winter, D., Vinegar, B., Nahal, H., Ammar, R., Wilson, G.V., and Provart, N.J.** (2007). An "Electronic Fluorescent Pictograph" browser for exploring and analyzing large-scale biological data sets. *PLoS One* **2**, e718.
- Xie, W., Xu, A., and Yeung, E.S.** (2009). Determination of NAD(+) and NADH in a single cell under hydrogen peroxide stress by capillary electrophoresis. *Anal Chem* **81**, 1280-1284.
- Yang, Z., and Ohlrogge, J.B.** (2009). Turnover of fatty acids during natural senescence of *Arabidopsis*, *Brachypodium*, and switchgrass and in *Arabidopsis* beta-oxidation mutants. *Plant Physiol* **150**, 1981-1989.
- Yano, T., Oku, M., Akeyama, N., Itoyama, A., Yurimoto, H., Kuge, S., Fujiki, Y., and Sakai, Y.** (2010). A novel fluorescent sensor protein for visualization of redox states in the cytoplasm and in peroxisomes. *Mol Cell Biol* **30**, 3758-3766.
- Zhang, X., De Marcos Lousa, C., Schutte-Lensink, N., Ofman, R., Wanders, R.J., Baldwin, S.A., Baker, A., Kemp, S., and Theodoulou, F.L.** (2011). Conservation of targeting but divergence in function and quality control of peroxisomal ABC transporters: an analysis using cross-kingdom expression. *Biochem J* **436**, 547-557.
- Zolman, B.K., Yoder, A., and Bartel, B.** (2000). Genetic analysis of indole-3-butyric acid responses in *Arabidopsis thaliana* reveals four mutant classes. *Genetics* **156**, 1323-1337.
- Zolman, B.K., Silva, I.D., and Bartel, B.** (2001). The *Arabidopsis* pxa1 mutant is defective in an ATP-binding cassette transporter-like protein required for peroxisomal fatty acid beta-oxidation. *Plant Physiol* **127**, 1266-1278.
- Zolman, B.K., Martinez, N., Millius, A., Adham, A.R., and Bartel, B.** (2008). Identification and characterization of *Arabidopsis* indole-3-butyric acid response mutants defective in novel peroxisomal enzymes. *Genetics* **180**, 237-251.

## 7 Appendix

### 7.1 Supplemental figures and tables

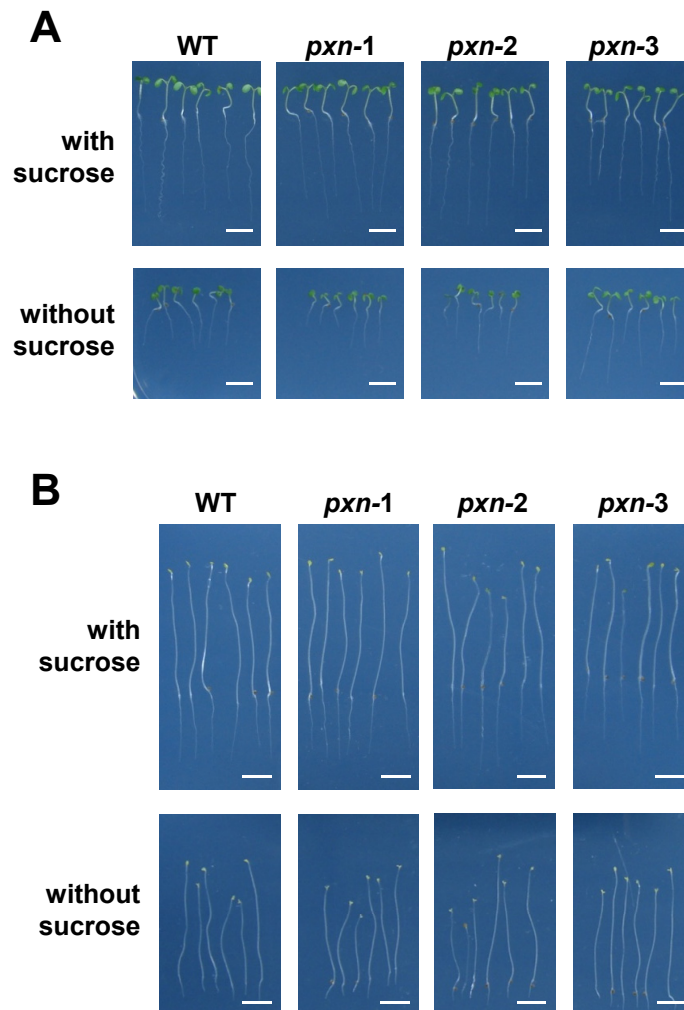


**Figure 7.1** *pxn* seedling establishment in dependency to sucrose

Representative six-day-old WT and *pxn* seedlings are shown, grown vertically on agar plates with or without sucrose addition. (A) Short-day condition. (B) Continuous darkness condition.

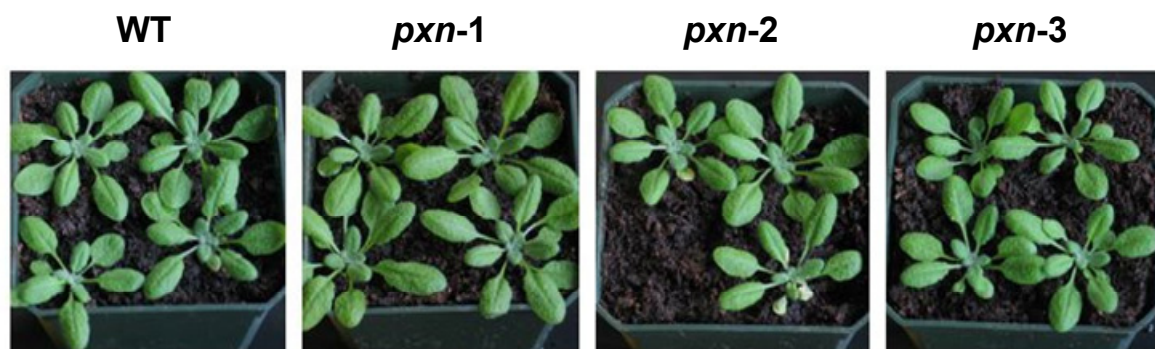


**Figure 7.2** Phenotype of eight-week-old WT and *pxn* mutant plants

WT and *pxn* mutant plants were grown under long-day conditions for eight weeks. All three *pxn* mutants look like WT and exhibited no photorespiratory phenotype.



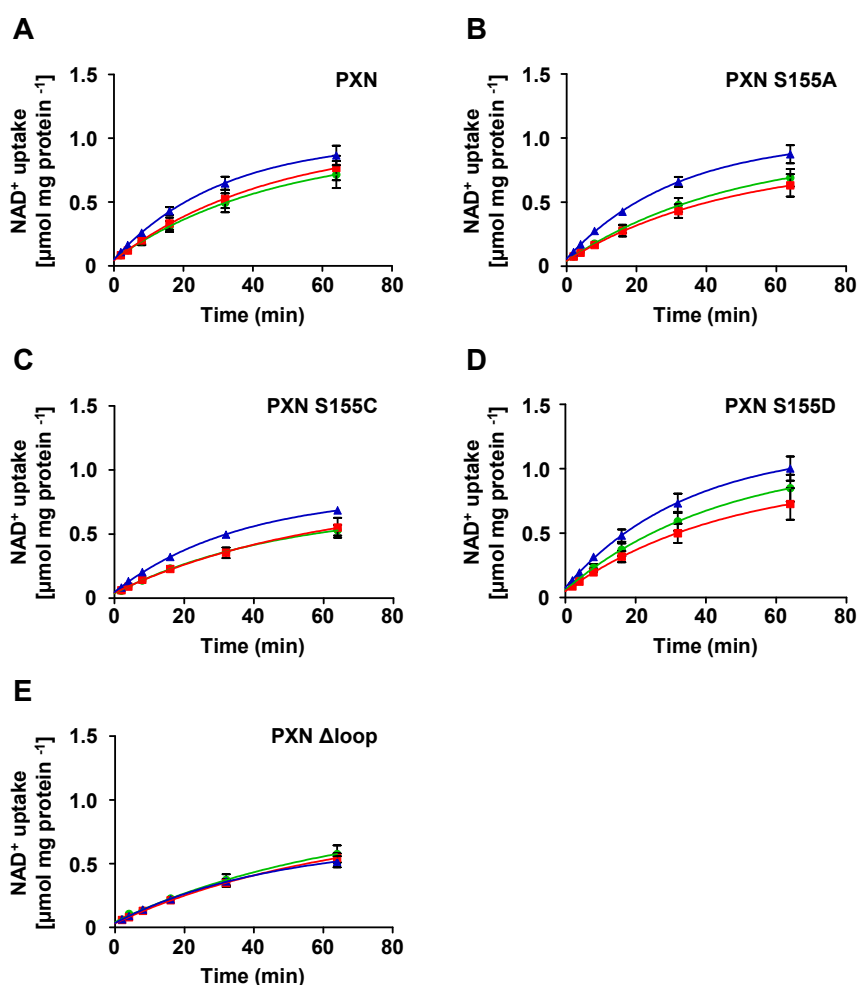


**Figure 7.3** Time dependent  $[\alpha\text{-}^{32}\text{P}]\text{-NAD}^+$  uptake of PXN and mutated PXN versions

*In vitro* expressed (A) PXN, (B) PXN S155A, (C) PXN S155C, (D) PXN S155D, and (E) PXN  $\Delta$ loop protein were reconstituted into proteoliposomes. Time-dependent  $[\alpha\text{-}^{32}\text{P}]\text{-NAD}^+$  (125  $\mu\text{M}$ ) uptake in exchange with 30 mM  $\text{NAD}^+$  (green), NAD (red) and AMP (blue) preloading was measured. The data represents the arithmetic means  $\pm$  SEs of four independent experiments.

**Table 7.1**  $V_{\max}$  and initial rate values for  $[\alpha\text{-}^{32}\text{P}]\text{-NAD}^+$  uptake activity of PXN and mutated PXN versions

Time-dependnet  $[\alpha\text{-}^{32}\text{P}]\text{-NAD}^+$  uptake was measured of recombinant PXN-His, PXN-His S155A, PXN-His S155C, PXN-His S155D, and PXN-His  $\Delta$ loop protein in exchange with  $\text{NAD}^+$ , NADH, and AMP. The  $V_{\max}$  and initial rate values were calculated. The data represents the arithmetic means  $\pm$  SEs of four independent experiments.

	NAD <sup>+</sup>				NADH				AMP			
	V <sub>max</sub>		Initial rate		V <sub>max</sub>		Initial rate		V <sub>max</sub>		Initial rate	
	$\mu\text{mol NAD}^+ \text{ mg protein}^{-1}$											
	mean	SE	mean	SE	mean	SE	mean	SE	mean	SE	mean	SE
PXN	0,94	0,27	0,0193	0,0027	0,99	0,24	0,0213	0,0021	0,98	0,10	0,0300	0,0005
PXN S155A	0,91	0,19	0,0187	0,0014	0,83	0,22	0,0170	0,0021	1,00	0,09	0,0299	0,0004
PXN S155C	0,70	0,11	0,0141	0,0006	0,81	0,29	0,0129	0,0027	0,81	0,05	0,0213	0,0001
PXN S155D	1,09	0,25	0,0233	0,0022	0,94	0,29	0,0198	0,0031	1,17	0,15	0,0316	0,0010
PXN $\Delta$ loop	0,91	0,33	0,0130	0,0028	0,85	0,20	0,0126	0,0012	0,67	0,09	0,0140	0,0005

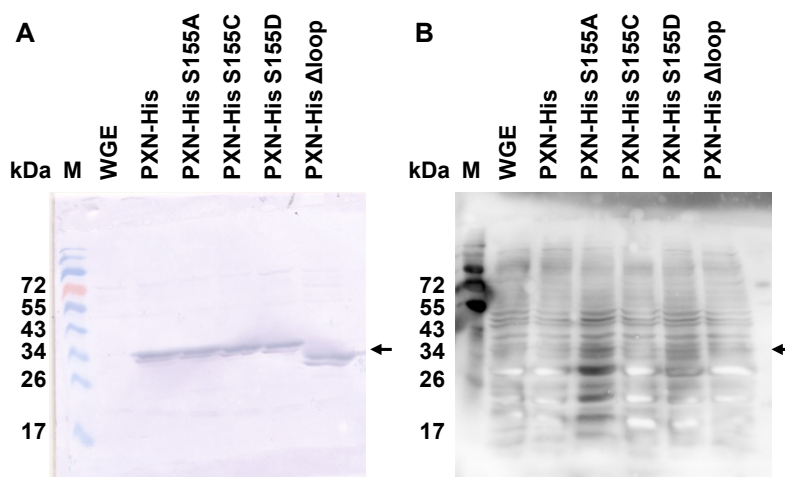


**Figure 7.4 Detection of phosphorylated serine of recombinant PXN-His protein using phosphoserine antibody**

Recombinant PXN-His, PXN-His S155A, PXN-His S155C, PXN-His S155D, PXN-His  $\Delta$ loop protein and WGE were analyzed by immunoblot analysis using (A) an anti-His antibody and (B) a phosphoserine antibody. Arrow indicates calculated molecular weight of PXN-His (37.3 kDa). M, marker proteins.

**Table 7.2 Substrate specificity of recombinant PXN protein**

Uptake activity of recombinant PXN protein reconstituted in proteoliposomes was measured with radioactively labeled  $\text{NAD}^+$  or AMP. In this thesis,  $[\alpha\text{-}^{32}\text{P}]\text{-NAD}^+$  was used and uptake assays were performed with cell-free expressed PXN-His using the WGE system. *E. coli* expressed PXN protein was used for uptake experiments using radioactively labeled  $[\text{}^3\text{H}]\text{-NAD}^+$  and  $[\text{}^{14}\text{C}]\text{-AMP}$  (Agrimi *et al.*, 2012b). Homo-exchange of  $\text{NAD}^+/\text{NAD}^+$  or AMP/AMP was set as 100% (grey shadowed). n.d., not determined; PAP, adenosine 3',5'-diphosphate.

Relative $\text{NAD}^+$ or AMP uptake [%]	this thesis	Agrimi <i>et al.</i> , 2012a	
	$[\alpha\text{-}^{32}\text{P}]\text{-NAD}^+$	$[\text{}^3\text{H}]\text{-NAD}^+$	$[\text{}^{14}\text{C}]\text{-AMP}$
$\text{NAD}^+$	100	100	48
NADH	69	51	42
AMP	90	108	100
ADP	56	97	40
ATP	10	7	8
FAD	11	13	15
CoA	32	65	39
dephospho-CoA	n.d.	87	45
PAP	n.d.	36	23

## 7.2 Abbreviations

Table 7.3 Abbreviations

Abbreviation	Meaning
2,4-D	2,4-dichlorophenoxyacetic acid
2,4-DB	2,4-dichlorophenoxybutyric acid
2',5'-ADP	2',5'-adenosine diphosphate
35S	cauliflower 35S mosaic virus promoter
3-AT	3-aminotriazole
ABA	abscisic acid
ABI	ABA insensitive
ACT	actin
ACX	acyl-CoA oxidase
ADP	adenosine diphosphate
AIM	abnormal inflorescence meristem
ALDP	adrenoleukodystrophy protein
ALDR	adrenoleukodystrophy-related protein
amiR	artificial micro RNA
AMP	adenosine monophosphate
AmpR	ampiciline
AP	alkaline phosphatase
APX	ascorbate peroxidase
ASC	ascorbate
ASP	aspartate
ATP	adenosine triphosphate
C20:1	Eicosenoic acid
cDNA	complementary DNA
CF Science	CellFree Science
CFP	cyan fluorescent protein
Cm <sup>R</sup>	chloramphenicol
cMDH	cytosolic malate dehydrogenase
CoA	coenzyme A
Col-0	Arabidopsis wild-type, Columbia-0 ecotype
CTS	comatose
CTS-C	C-terminal half of CTS
CTS-FL	full-length CTS
CTS-N	C-terminal half of CTS
DAI	day after imbibition
DET	detached dark-incubated leaves
DIS	shaded leaves still attached to the plant
DNA	deoxyribonucleic acid
ER	endoplasmic reticulum
FA	fatty acid
FAD	flavin adenine dinucleotide
FAME	fatty acid methyl ester
GAL	Galactose
gDNA	genomic DNA
GDP	guanosine diphosphate
GF-	germination frequency in the absence of sucrose

Abbreviation	Meaning
GF+	germination frequency in the presence of sucrose
GFP	yellow fluorescent protein
Gln	glutamine
Glu	glutamate
GlufR	Glufosinate ammonium (Basta)
Gly	glycerate
GOX	glycolate oxidase
GST	glutathione S-transferase
GTP	guanosine triphosphate
GUS	$\beta$ -glucuronidase
H <sub>2</sub> O <sub>2</sub>	hydrogen peroxide
HHU	Heinrich-Heine university
HP	hydroxypyruvate
HPR	hydroxypyruvate reductase
HRP	horseradish peroxidase
HygR	Hygromycin
IAA	indole-3-acetic acid
IBA	indole butyric acid
IDH	isocitrate dehydrogenase
JA	jasmonic acid
KanR	Kanamycine
KAT	3-ketoacyl-CoA thiolase
kDa	kilo Dalton
LACS	long chain acyl-CoA synthetase
LB	left border
LSM	Laser scanning microscope
Mal	malate
MCF	mitochondrial carrier family
MDA	monodehydroascorbate
MDAR	monodehydroascorbate reductase
MFP	multifunctional protein
MFP/DH	multifunctional protein/ L-3-hydroxyacyl-CoA dehydrogenase
MFP/HYD	multifunctional protein/ 2-trans-enoyl-CoA hydratase
mPTS	peroxisomal membrane targeting signal
MS medium	Murashige and Skoog medium
MTT	(3-[4,5-Dimethylthiazole-2-yl]-2,5-diphenyltetrazolium Bromide
Na	nicotinade
NaAD	nicotinate adenine dinucleotide
NaCl	sodium chloride
NAD <sup>+</sup>	oxidized nicotinamide adenine dinucleotide
NaDA	nicotinamide deamidase
NADH	reduced nicotinamide adenine dinucleotide
NADK	NAD kinase
NADP <sup>+</sup>	nicotinamide adenine dinucleotide phosphate
NADPH	reduced nicotinamide adenine dinucleotide phosphate
NADS	NAD synthase
NALD	neonatal adrenoleukodystrophy

Abbreviation	Meaning
Nam	nicotinamide
NaMN	nicotinade mononucleotide
NaPRT	nicotinate phosphoribosyltransferase
NDT	nicotinamide adenine dinucleotide carrier
Ni-NTA	Nickel-nitrilotriacetic acid
NLS	nuclear localization signal
NMN	nicotinamide mononucleotide
NMNAT	nicotinate/nicotinamide mononucleotide adenylyltransferase
NMNH	reduced nicotinamide mononucleotide
NS	developmental leaf senescence
nudix	nucleoside diphosphate linked to some moiety X
NUDT	Nudix hydrases
OAA	oxaloacetate
PCR	polymerase chain reaction
PES	Phenazine ethosulfate
PEX	peroxin
pMDH	peroxisomal malate dehydrogenase
PMP	peroxisomal membrane protein
PNC	peroxisomal adenine nucleotide carrier
PPi	pyrophosphate
PRPP	5'-phosphoribosyl-1'-pyrophosphate
PTS	peroxisomal targeting signal
PXA	peroxisomal ABC transporter
PXN	peroxisomal NAD carrier
QPT	quinolinate phosphoribosyltransferase
RB	right border
redox	reduction/oxidation
RifR	Rifampicin
RNA	ribonucleic acid
ROS	reactive oxygen species
RT-PCR	reverse transcription PCR
RubisCO	ribulose-1,5-bisphosphate carboxylase/oxygenase
S. spec.	substrate specificity
SA	salicylic acid
SD	standard deviation
SDH	succinate dehydrogenase
SDM	site directed mutagenesis
SDP	sugar dependent phenotype
SDS-PAGE	sodium dodecyl sulfate polyacrylamide gel electrophoresis
SE	standard error
siR	small interfering RNA
SOD	superoxide dismutase
SuIR	Sulfadiazine
TAG	triacylglycerol
TCA	tricaroxylic acid cycle
TEM	transmission electron microscope
UBQ	Ubiquitin
w	week

Abbreviation	Meaning
WGE	wheat germ expression
WT	wild type
XOD	xanthine oxidase
YFP	yellow fluorescent protein

### 7.3 Companies, websites and used softwares

**Table 7.4 Companies**

Company	Website
5PRIME	<a href="http://www.5prime.com">www.5prime.com</a>
ABRC Arabidopsis biological resource center	<a href="http://abrc.osu.edu/">http://abrc.osu.edu/</a>
Agilent Technologies	<a href="http://www.agilent.com">www.agilent.com</a>
Bio-Rad	<a href="http://www.bio-rad.com">www.bio-rad.com</a>
Carl Roth	<a href="http://www.carlroth.com">www.carlroth.com</a>
CellFree Science	<a href="http://www.cfsciences.com">www.cfsciences.com</a>
Duchefa	<a href="http://www.duchefa.com">www.duchefa.com</a>
Fermentas	<a href="http://www.fermentas.com">www.fermentas.com</a>
GATC Biotech	<a href="http://www.gatc-biotech.com">www.gatc-biotech.com</a>
GE Healthcare	<a href="http://www.gelifesciences.com">www.gelifesciences.com</a>
Hartmann Analytic	<a href="http://www.hartmann-analytic.de">www.hartmann-analytic.de</a>
Invitrogen	<a href="http://www.invitrogen.com">www.invitrogen.com</a>
Merck Biosciences	<a href="http://www.merck.com">www.merck.com</a>
NASC European Arabidopsis Stock Centre	<a href="http://arabidopsis.info">http://arabidopsis.info</a>
New England Biolabs	<a href="http://www.neb.com">www.neb.com</a>
Novagen	<a href="http://www.novagen.com">www.novagen.com</a>
Perkin Elmer	<a href="http://www.perkinelmer.com">www.perkinelmer.com</a>
Pineda Antikörper Service	<a href="http://www.pineda-abservice.de">www.pineda-abservice.de</a>
Promega	<a href="http://www.promega.com">www.promega.com</a>
Qiagen	<a href="http://www.qiagen.com">www.qiagen.com</a>
Roche	<a href="http://www.roche-applied-science.com">www.roche-applied-science.com</a>
Santa Cruz Biotechnology	<a href="http://www.scbt.com">www.scbt.com</a>
Sarstedt	<a href="http://www.sarstedt.com">www.sarstedt.com</a>
Sigma-Aldrich	<a href="http://www.sigmaaldrich.com">www.sigmaaldrich.com</a>
Stratagene	<a href="http://www.stratagene.com">www.stratagene.com</a>
ThermoFisher Scientific	<a href="http://www.thermofisher.com">www.thermofisher.com</a>
Zeiss	<a href="http://www.zeiss.com">www.zeiss.com</a>

**Table 7.5 Softwares and databases**

Software / database	Website
Adobe Photoshop CS3	<a href="http://www.adobe.com">www.adobe.com</a>
Arabidopsis eFP Browser	<a href="http://bar.utoronto.ca/efp/cgi-bin/efpWeb.cgi">http://bar.utoronto.ca/efp/cgi-bin/efpWeb.cgi</a>
Arabidopsis Co-Response Database (AthCoR)	<a href="http://csbdb.mpimp-golm.mpg.de/csbdb/dbcor/ath.html">http://csbdb.mpimp-golm.mpg.de/csbdb/dbcor/ath.html</a>
Aramemnon database	<a href="http://aramemnon.uni-koeln.de">http://aramemnon.uni-koeln.de</a>
AraPerox1.2 database	<a href="http://www3.uis.no/araperoxv1">www3.uis.no/araperoxv1</a>
ATTEDII	<a href="http://atted.jp">http://atted.jp</a>
CLUSTALW2	<a href="http://www.ebi.ac.uk/Tools/msa/clustalw2">www.ebi.ac.uk/Tools/msa/clustalw2</a>

Software / database	Website
GENEDOC	<a href="http://www.nrbsc.org/gfx/genedoc">www.nrbsc.org/gfx/genedoc</a>
GeneMANIA	<a href="http://genemania.org">http://genemania.org</a>
Genevestigator	<a href="http://www.genevestigator.com/gv/plant.jsp">www.genevestigator.com/gv/plant.jsp</a>
GraphPad PRISM	<a href="http://www.graphpad.com/prism/prism.htm">www.graphpad.com/prism/prism.htm</a>
Human gene database	<a href="http://www.genecards.org">www.genecards.org</a>
IMAGEJ	<a href="http://rsbweb.nih.gov/ij">http://rsbweb.nih.gov/ij</a>
Microsoft Office 2007	<a href="http://office.microsoft.com">http://office.microsoft.com</a>
PEX19 binding site predictor	<a href="http://www.peroxisomedb.org/diy_Pex19.html">www.peroxisomedb.org/diy_Pex19.html</a>
PhosPhAt 3.0	<a href="http://phosphat.mpimp-golm.mpg.de/">http://phosphat.mpimp-golm.mpg.de/</a>
Phylogenetic tree software	<a href="http://www.phylogeny.fr">www.phylogeny.fr</a>
PubMed	<a href="http://www.ncbi.nlm.nih.gov/pubmed">www.ncbi.nlm.nih.gov/pubmed</a>
QuickChange Primer Design Program	<a href="http://www.agilent.com/genomics/qcpd">www.agilent.com/genomics/qcpd</a>
Saccharomyces Genome Database (SGD)	<a href="http://www.yeastgenome.org">www.yeastgenome.org</a>
TAIR The Arabidopsis Information Resource	<a href="http://www.arabidopsis.org">www.arabidopsis.org</a>
VectorNTI Suite 9	<a href="http://www.invitrogen.com">www.invitrogen.com</a>
WMD3- Web MicroRNA Designer	<a href="http://wmd3.weigelworld.org">http://wmd3.weigelworld.org</a>
Zeiss LSM Image Browser	<a href="http://www.zeiss.com">www.zeiss.com</a>

## 7.4 Figures

Figure 1.1 The importance of NAD <sup>+</sup> in peroxisomal $\beta$ -oxidation, photorespiration and H <sub>2</sub> O <sub>2</sub> detoxification .....	4
Figure 1.2 peroxisomal fatty acid $\beta$ -oxidation pathway .....	6
Figure 1.3 Model of cytosolic NAD <sup>+</sup> biosynthesis, consumption, and recycling pathways .....	8
Figure 3.1 Amino acid sequence homology of PXN to NAD <sup>+</sup> and ATP carrier of the MCF ....	29
Figure 3.2 Phylogenetic tree of the NAD <sup>+</sup> and ATP carriers of the MCF of Arabidopsis, yeast and human .....	30
Figure 3.3 Recombinant PXN protein expressed in the cell-free WGE system .....	30
Figure 3.4 [ $\alpha$ - <sup>32</sup> P]-NAD <sup>+</sup> uptake activity and substrate specificity of recombinant PXN protein .....	31
Figure 3.5 Expression of PXN-His and Ant1p-His in yeast .....	33
Figure 3.6 Time-dependent [ $\alpha$ - <sup>32</sup> P]-NAD <sup>+</sup> and [ $\alpha$ - <sup>32</sup> P]-ATP uptake of recombinant PXN-His and Ant1p-His protein expressed in yeast.....	34
Figure 3.7 [ $\alpha$ - <sup>32</sup> P]-NAD <sup>+</sup> uptake activity of recombinant NDT1-His and NDT2-His protein expressed in WGE .....	36
Figure 3.8 [ $\alpha$ - <sup>32</sup> P]-ATP and [ $\alpha$ - <sup>32</sup> P]-NAD <sup>+</sup> uptake activity of recombinant PNC1-His and PNC2 protein .....	37
Figure 3.9 Anti-PXN antibody specificity on recombinant protein .....	38
Figure 3.10 PXN expression level during germination and senescence .....	40
Figure 3.11 PXN promoter-GUS activity in seedlings and rosette leaves .....	42
Figure 3.12 Genotype of three independent T-DNA insertion lines for PXN .....	43
Figure 3.13 PXN protein detection of isolated membranes from etiolated <i>pxn</i> seedlings .....	44
Figure 3.14 Genotype of PXN over-expression lines .....	44
Figure 3.15 Sucrose-dependent establishment of <i>pxn</i> seedlings.....	45
Figure 3.16 2,4-DB and 2,4-D assay of <i>pxn</i> seedlings.....	46
Figure 3.17 Fatty acid analysis of <i>pxn</i> seedlings.....	47
Figure 3.18 Nile red staining of oil bodies in WT, <i>pxn</i> and <i>pxa1</i> seedlings .....	48
Figure 3.19 TEM images of five-day-old etiolated cotyledon cells .....	48
Figure 3.20 Germination assay of WT, <i>pxn</i> , <i>abi4</i> , and <i>pmdh1 pmdh2</i> seeds .....	49
Figure 3.21 Root growth of seedlings in response to H <sub>2</sub> O <sub>2</sub> and 3-AT .....	51
Figure 3.22 <i>In silico</i> analysis of PXN expression level using eFP Browser – oxidative stress .....	51
Figure 3.23 <i>In silico</i> analysis of PXN expression level using eFP Browser – low pH.....	52
Figure 3.24 <i>In silico</i> analysis of PXN expression level using eFP Browser – <i>Pseudomonas syringae</i> .....	53
Figure 3.25 Total NAD <sup>+</sup> content of WT and <i>pxn-1</i> seedlings.....	54
Figure 3.26 Genotype of artificial PNC1/2 siRNAi lines in <i>pxn</i> background .....	54



Figure 3.27 Genotype of generated <i>pmdh1 pmdh2 pxn</i> and <i>pmdh1 pmdh2 hpr1 pxn</i> mutant lines .....	55
Figure 3.28 Genotype of artificial miRNA <i>PXN</i> lines .....	56
Figure 3.29 Section of an alignment of <i>PXN</i> and other MCF members focused on the unique loop region of <i>PXN</i> .....	57
Figure 3.30 Co-localization of YFP fused <i>PXN</i> , <i>PXN S155A</i> , <i>PXN S155C</i> , <i>PXN S155D</i> , and <i>PXN Δloop</i> proteins .....	58
Figure 3.31 Cell-free WGE expression of mutated <i>PXN</i> proteins .....	59
Figure 3.32 [ $\alpha$ - $^{32}$ P]- $\text{NAD}^+$ uptake activity of <i>PXN</i> -His and mutated <i>PXN</i> -His proteins with $\text{NAD}^+$ , $\text{NADH}$ and $\text{AMP}$ exchange .....	60
Figure 3.33 <i>In vitro</i> PEX19.1 and PEX19.2 pull-down assay with recombinant transport proteins.....	61
Figure 3.34 Transient expression of <i>PXN S155D</i> in tobacco leaves.....	62
Figure 4.1 Schematic transport mechanism of <i>PXN</i> .....	66
Figure 4.2 Model of the new peroxisomal $\text{NAD}^+$ carrier .....	70
Figure 4.3 Model of supporting the APX/MDAR system with $\text{NAD}^+$ by <i>PXN</i> for $\text{H}_2\text{O}_2$ detoxification .....	72
Figure 4.4 Model of redundant systems for $\text{NAD}^+$ /AMP exchange mediated by <i>PXN</i> and <i>PNC</i> .....	75
Figure 4.5 Model of redundant systems for $\text{NAD}^+$ /NADH exchange mediated by <i>PXN</i> , the malate/OAA shuttle and <i>HPR1</i> .....	76
Figure 7.1 <i>pxn</i> seedling establishment in dependency to sucrose.....	103
Figure 7.2 Phenotype of eight-week-old WT and <i>pxn</i> mutant plants.....	103
Figure 7.3 Time dependent [ $\alpha$ - $^{32}$ P]- $\text{NAD}^+$ uptake of <i>PXN</i> and mutated <i>PXN</i> versions.....	104
Figure 7.4 Detection of phosphorylated serine of recombinant <i>PXN</i> -His protein using phosphoserine antibody .....	105

## 7.5 Tables

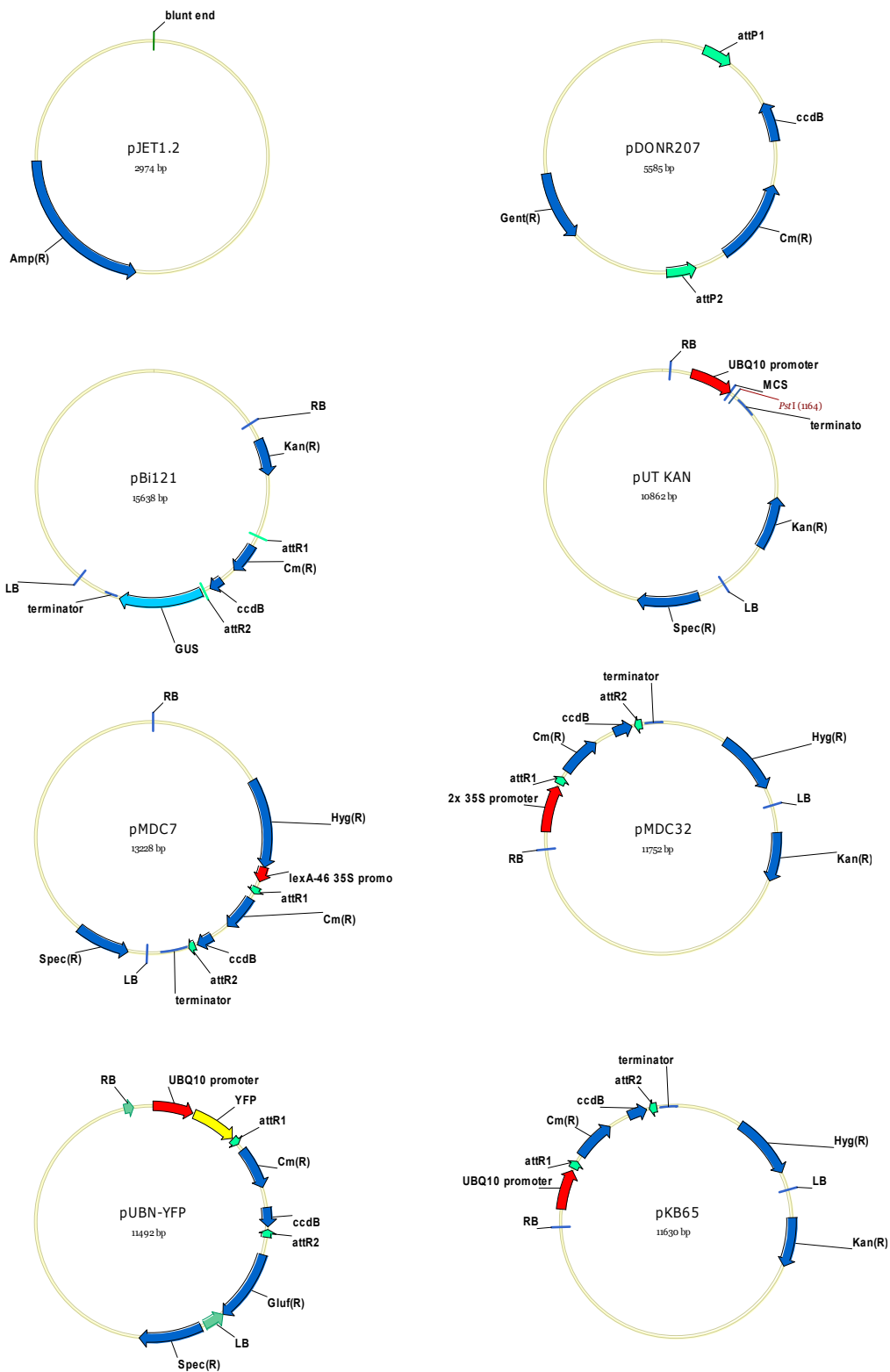
Table 2.1 <i>Escherichia coli</i> strains used for cloning .....	13
Table 2.2 Plasmids used for cloning .....	13
Table 2.3 Antibodies used for immunoblot analysis .....	14
Table 2.4 Arabidopsis mutant lines .....	15
Table 2.5 <i>Agrobacterium tumefaciens</i> strains .....	16
Table 2.6 Produced Arabidopsis mutant lines by agrobacteria-mediated transformation .....	16
Table 2.7 Produced Arabidopsis mutant lines by crossing.....	17
Table 2.8 Oligonucleotides used for gDNA screening of transgenic plants .....	18
Table 2.9 Oligonucleotides used for generating <i>PXN</i> microRNA expressing vectors .....	19
Table 2.10 Plasmids used for gene silencing.....	19

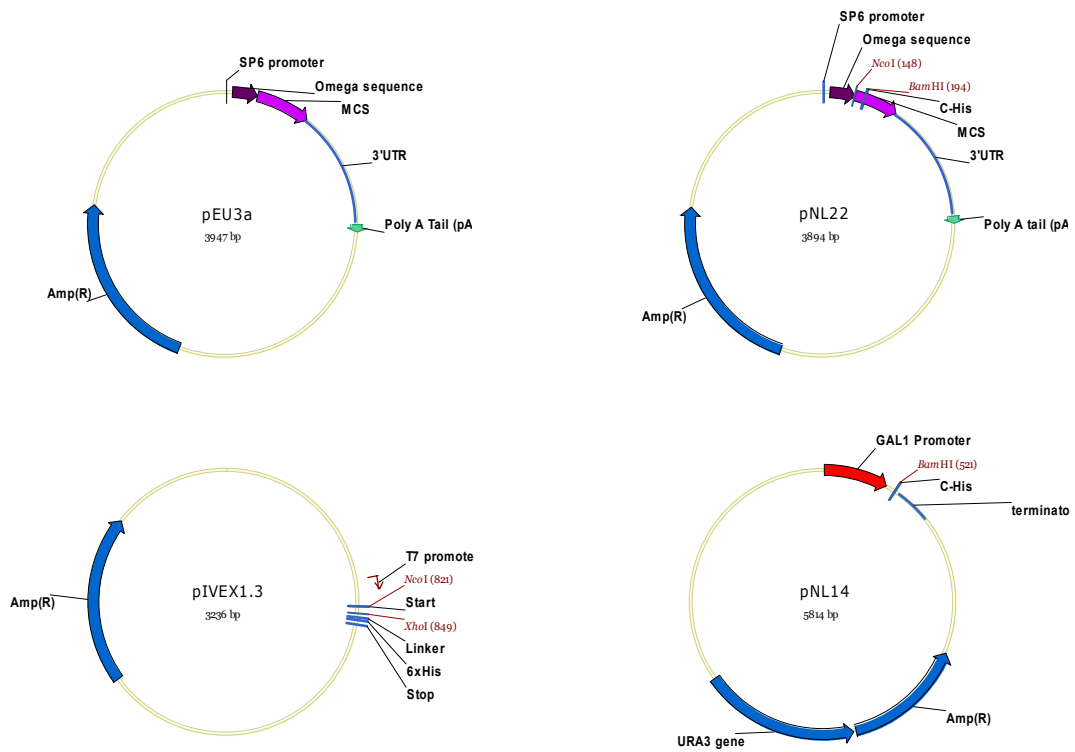
---

Table 2.11 Oligonucleotides used for creating PXN over-expression construct .....	20
Table 2.12 Oligonucleotides used for creating a PXN promoter GUS construct.....	20
Table 2.13 Tobacco plants used for transient transformation .....	21
Table 2.14 Oligonucleotides used for cloning YFP-PXN fusion protein .....	21
Table 2.15 Plasmids used for co-localization .....	21
Table 2.16 Oligonucleotides used for cloning vectors for two-step protein WGE expression	23
Table 2.17 Plasmids used for <i>in vitro</i> two-step WGE expression.....	23
Table 2.18 Oligonucleotides used for cloning of one-step WGE expression vectors.....	24
Table 2.19 Plasmids used for <i>in vitro</i> one-step WGE expression .....	24
Table 2.20 Plasmids used for protein expression in yeast .....	25
Table 2.21 Oligonucleotides used for generating of mutated PXN proteins.....	26
Table 3.1 $K_M$ ( $NAD^+$ ) and $K_i$ values of recombinant PXN-His protein for various metabolites	32
Table 3.2 Kinetic values of $[\alpha\text{-}^{32}\text{P}]\text{-}NAD^+$ and $[\alpha\text{-}^{32}\text{P}]\text{-}ATP$ uptake of recombinant PXN-His and Ant1p-His protein expressed in yeast.....	33
Table 3.3 Comparison of substrate specificity, $K_M$ and $K_i$ levels of plant and yeast $NAD^+$ carrier .....	35
Table 3.4 Co-expression analysis for PXN.....	41
Table 3.5 Predicted PEX19 binding site values of chosen transport proteins.....	63
Table 7.1 $V_{max}$ and initial rate values for $[\alpha\text{-}^{32}\text{P}]\text{-}NAD^+$ uptake activity of PXN and mutated PXN versions.....	104
Table 7.2 Substrate specificity of recombinant PXN protein .....	105
Table 7.3 Abbreviations.....	106
Table 7.4 Companies .....	109
Table 7.5 Softwares and databases.....	109

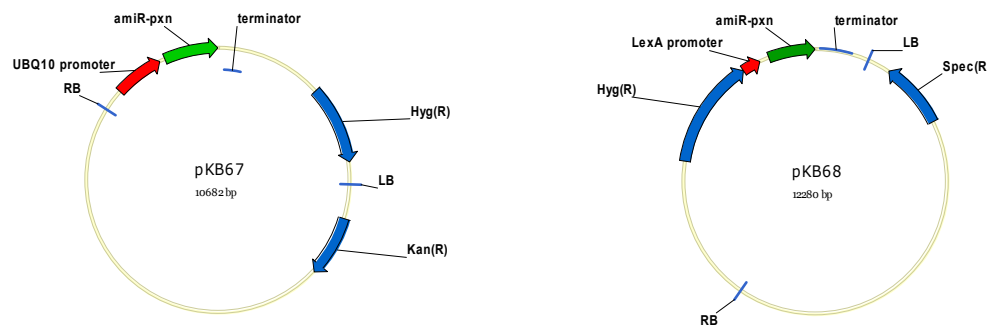
## 7.6 Vector and construct maps

### 7.6.1 Plasmids used for cloning

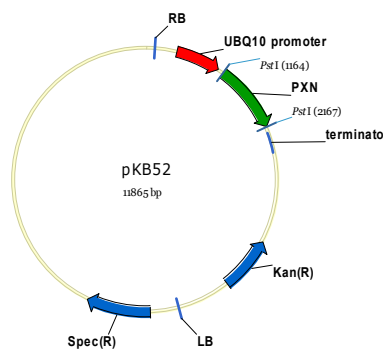




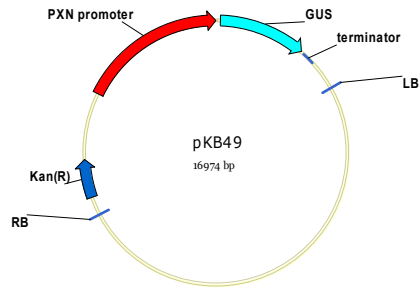
### 7.6.2 Plasmid used for gene silencing



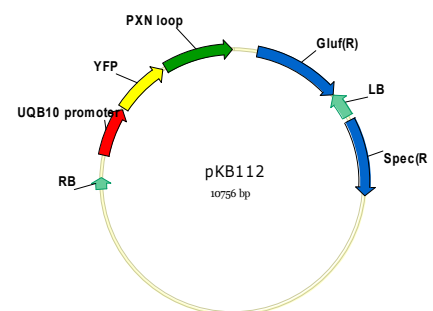
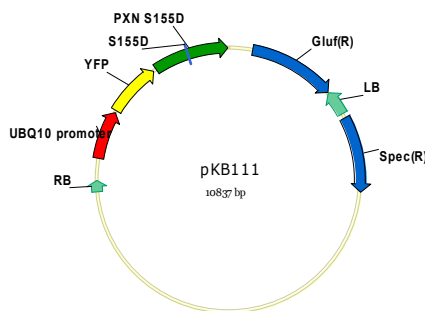
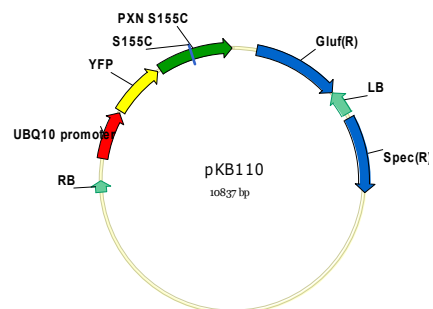
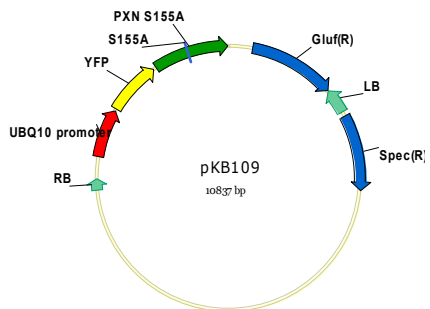
### 7.6.3 Plasmid used for PXN over-expression

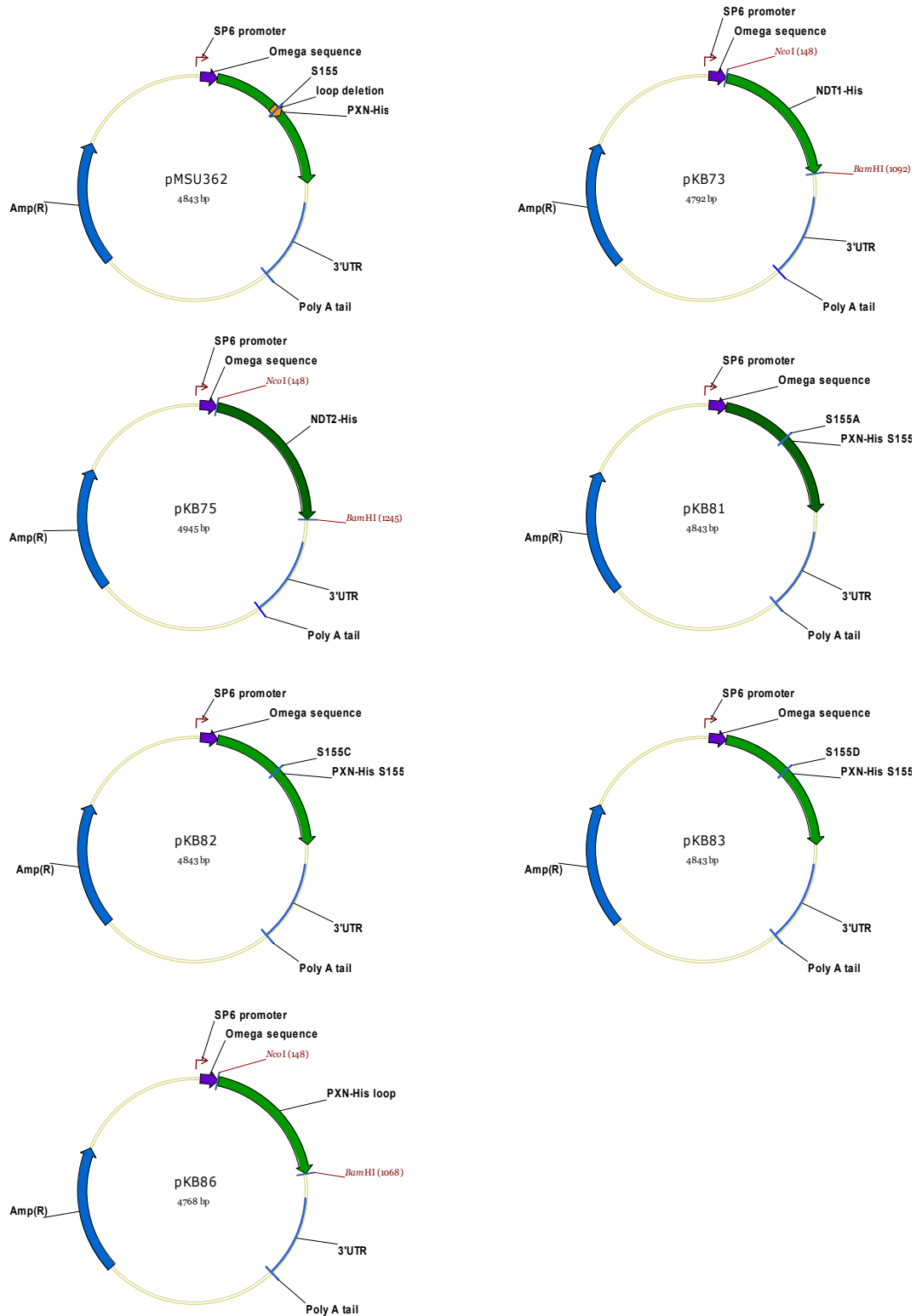


### 7.6.4 Plasmid used for PXN promoter GUS analysis



### 7.6.5 Plasmids used for co-localization



7.6.6 Plasmids used for *in vitro* two-step WGE expression

7.6.7 Plasmids used for *in vitro* one-step WGE expression

## 7.7 List of publications

Nyathi, Y., Zhang, X., Baldwin, J.M., **Bernhardt, K.**, Johnson, B., Baldwin, S.A., Theodoulou, F.L., and Baker, A. (2012). Pseudo half-molecules of the ABC transporter, COMATOSE, bind Pex19 and target to peroxisomes independently but are both required for activity. *FEBS letters* **586**, 2280-2286.

**Bernhardt, K.**, Vigelius, S.K., Wiese, J., Linka, N., and Weber, A.P. (2012). Agrobacterium-mediated *Arabidopsis thaliana* transformation: An overview of T-DNA binary vectors, floral dip and screening for homozygous lines. *Journal of Endocytobiosis and Cell Research* **22**, 19-28.

**Bernhardt, K.**, Wilkinson, S., Weber, A.P.M., and Linka, N. (2012). A peroxisomal carrier delivers NAD<sup>+</sup> and contributes to optimal fatty acid degradation during storage oil mobilization. *The Plant Journal* **69**, 1-13.



---

## 7.8 Curriculum vitae

### Personal data:

Name: Kristin Bernhardt  
Birth: February 22<sup>nd</sup>, 1984; Düsseldorf

### Education:

1990 - 1994 Primary school Knittkuhl, Düsseldorf

1994 - 2004 Secondary school  
Marie-Curie-Gymnasium Düsseldorf  
A-levels (Abitur)

### Academic studies:

10/2004 – 06/2009 Studies in biology at Friedrich-Alexander University Erlangen-Nuremberg (Diploma)

09/2008 – 06/2009 Diploma Thesis in the group of Prof. Dr. Sauer at the Institute of Molecular Plant Physiology, Friedrich-Alexander University Erlangen-Nuremberg: “Untersuchungen zur Entstehung sekundärer Plasmodesmata in *Arabidopsis thaliana*” (Formation of secondary plasmodesmata in *Arabidopsis thaliana*)”

### Doctorate:

Since 07/2009 PhD student at the Institute of Plant Biochemistry, Heinrich-Heine University Düsseldorf: “The role of a peroxisomal NAD<sup>+</sup> carrier in plants”. Project leaders: Dr. Nicole Linka and Prof. Dr. Andreas Weber.

Since 03/2010 Member of the international Graduate Program for Plant Science, iGRAD Plant, Heinrich-Heine University Düsseldorf

01/2012 – 04/2012 Research assistant at Rothamsted Research, Harpenden, UK. “How are peroxisomal membrane proteins targeted to peroxisomes in plants”. Project leader: Dr. Frederica Theodoulou

Düsseldorf, 09/10/2012

## 8 Acknowledgement

Ein großes Dankeschön geht an:

Dr. Nicole Linka. Du warst eine super "Doktormama", hast mir dieses spannende und fruchtbare Thema gegeben und mich immer unterstützt. Wenn ich mal wieder keinen Ausweg gefunden habe, hast du nur gesagt: „No Problem, wir finden schon eine Lösung“ und du hattest immer recht damit. Zudem hast du mir meinen Forschungsaufenthalt in England und viele Tagungen, besonders Dabringhausen und das Peroxisomen-Meeting in Minneapolis ermöglicht. Vielen Dank auch für die schönen Dinner bei dir.

Prof. Dr. Andreas Weber. Als ich das Bewerbungsgespräch bei Ihnen und Nicole hatte, hatte ich mich riesig gefreut als ich ein paar Tage später die Zusage für diese Doktorandenstelle bekommen hatte. Damals wusste ich noch nicht so recht was auf mich zu kommt, aber heute bin ich froh, dass Sie mich in ihr Institut geholt haben. Ich habe wahnsinnig viele neue Methoden gelernt, die Möglichkeit bekommen zu mehreren Tagungen zu fahren und konnte mit netten Kollegen zusammenarbeiten. Besser hätte es für mich nicht laufen können.

Prof. Dr. Rüdiger Simon. Vielen Dank, dass Sie das Zweitgutachten für diese Arbeit übernommen haben und dass Sie immer gute Ideen und Ratschläge für mein Projekt hatten.

Dr. Frederica Theodoulou. You gave me the wonderful possibility to join you at Rothamsted Research for three month. It was an amazing time with several new impressions and it was a successful time for me (private and work). Besides, special thanks go to all colleagues from the lab in the UK: It was a cordial atmosphere.

Ferdi Grawe und Dr. Ulla Neumann. Ihr habt mich bei der TEM unterstützt und es war spannend diese Methode zu erlernen.

Dr. Siegrun Wegener-Feldbrügge. Du hast mir und sicherlich allen anderen Studenten im iGRAD-Plant Programm das Leben durch deine Organisation erleichtert. Vielen Dank auch für die schönen und lustigen Weihnachtsfeiern bei euch zu Hause.

Dr. Sabine Schneider. Du hast diese Arbeit überhaupt möglich gemacht. Vielen vielen Dank noch einmal für dein Engagement, ich werde es nie vergessen.

Peroxisomen-Gruppe. Es war immer lustig mit euch und es war schön mit euch zu diskutieren und schöne Abende miteinander zu verbringen. Ich finde es war eine super Truppe.

Sarah Vigelius. Du hast mich von Anfang an „aufgenommen“ und ich konnte wirklich bei jedem Problem (Peroxisomen-, Methoden- und Privat-spezifisch) zu dir kommen und du hattest immer eine Antwort parat. Es hat viel Spaß gemacht mit dir zusammen zu arbeiten.

Weberlab. Ihr allesamt wart super. Ich werde nie vergessen, wie ich als dritte Doktorandin angefangen habe und mittlerweile 13 von uns im Labor rumgeistern und gute Laune verbreiten. Jeder von euch (TA, Doktorand, Postdoc) hatte immer ein offenes Ohr und hat mir geholfen. Ich hatte viel Spaß bei unseren BBQ-Abenden, jährlichen Rheinkirmes-Ausflügen und besonders den aktiven Betriebsausflügen. Vielen Dank auch für die leckere Sauerlandburger- und Knoblauchsoßen-Rezepte.

Maximilian Trippelsdorf. Es hat mir richtig viel Spaß gemacht dich in deiner Bachelorarbeit zu betreuen. Und falls du jemals diese Arbeit lesen wirst, dann wirst du ein paar deiner Ergebnisse wiederfinden.

Sabrina Wilkinson. Ich weiß, dass wir nicht im besten auseinandergegangen sind, aber ich möchte dir wirklich dafür danken, dass du diese Arbeit soweit gebracht hast. Ich weiß es echt zu schätzen, wie viel Vorarbeit du in dieses Projekt gesteckt hattest und ohne dies wäre meine Arbeit nicht möglich gewesen.

Dorien Engeländer. Du hast mich, gerade in letzter Zeit, wahnsinnig unterstützt und mir geholfen. Danke, dass du für mich da bist.

Esel, Hund, Katze und Knutschkugel. Schön das es euch gibt und ihr mich immer aufgenommen habt. Ihr seid wahre Freunde und die besten die man sich wünschen kann.

Bastian Szopinski. Du hast schon meinen Schulabschluss und mein Studium miterlebt. Jetzt haben wir sogar meine Promotion miteinander bewerkstelligt. Du hattest mich immer unterstützt und mir Rückhalt gegeben. Du weißt, dass du tief in meinem Herzen verankert bist.

Uta und Andrés Bernhardt, oder auch meine lieben Eltern. Hättet ihr das gedacht, als ihr mich vor mehr als 28 Jahren zum ersten Mal als kleines unbeholfenes Würmchen gesehen habt, das ich jetzt hier stehe und mich Dr. nennen kann? Ihr habt mir das überhaupt ermöglicht, indem ihr mir ein schönes Leben gegeben habt und ich zu dem werden konnte was ich bin und was ich wollte. Danke schön und eine dicke Umarmung auf diesem Wege.

Familie. Ich möchte mich auch bei dem Rest meiner Familie bedanken. Meiner Schwester, meinem Opa, meiner Oma und meinen Onkeln und Tanten. Schön das es euch gibt und ihr mir jederzeit Rückhalt gegeben habt.

---

## **Eidesstattliche Versicherung**

Ich versichere an Eides Statt, dass die Dissertation von mir selbständig und ohne unzulässige fremde Hilfe unter Beachtung der „Grundsätze zur Sicherung guter wissenschaftlicher Praxis an der Heinrich-Heine-Universität Düsseldorf“ erstellt worden ist.

Düsseldorf, den 10. September 2012

Kristin Bernhardt